Oxidation of Ni-8YSZ anodes in Solid Oxide Fuel Cells - An "In status operandi" measurement method

Zur Erlangung des akademischen Grades eines
Doktors der Ingenieurwissenschaften (Dr.-Ing.)
von der KIT-Fakultät für Maschinenbau des
Karlsruher Instituts für Technologie (KIT)

angenommene
Dissertation
von

M.Sc. Valentin Steenken

Tag der mündlichen Prüfung: 22.03.2019
Hauptreferent: Prof. Dr. rer. nat. Michael J. Hoffmann
Korreferent: Prof. Dr. rer. nat. Helmut Ehrenberg

Acknowledgment

This work has been supported by so many people. I would like to take this opportunity to express my thanks to all of them.

The present thesis has been developed during my time as a research associate at the department of fuel cell development of the ElringKlinger AG in collaboration with the institute for ceramics of the Karlsruhe Institute of Technology. First of all, I would like to express my sincere thanks to the holder of the chair, Prof. Dr. M.J. Hoffmann, who made this thesis possible. Thank you for your reliable support, your time and advice as well as for the extensive freedom in definition of contents and purpose of my project. Furthermore, I would like to send additional thanks to Prof. Dr. H. Ehrenberg for being co-referee of this thesis.

Special thanks go to Dr. U. Maier, head of the fuel cell department and to Dr. T. Kiefer, team leader of SOFC development. Thank you for giving me the chance to do my research within your department and for giving me freedom with my schedule for scientific work besides day-to-day business. Furthermore, I want to thank all my colleagues from the fuel cell department for the pleasant working atmosphere. For many discussions and the support over the last three years I would like to thank colleages from the SOFC team, namely (in alphabetical order) Dr. T. Bause, Dr. P. Freundt, Dr. F. Hauler, S. Heldmaier, M. Hoffmann, Dr. S. Hornauer, Dr. A. Morandi, M. Müller, J. Reichenecker, E. Reitz and F. Wipfler. I owe particular thanks to Dr. M. Pausch for his continuous help, the fruitful discussions and for the correction of this work - thank you very much!

Moreover, I want to thank G. Holstermann from the New Enerday GmbH for his support regarding the system testing.

I'd like to deeply thank my parents for their loving and continuous support at all times in my life. I also appreciate your critical words as well as your professional advice.

I would like to express my deepest gratitude to my wife Silvia. Thank you for your patience, your constant and affectionate support. I love you.

Table of contents

Nomenclature

List Of Symbols

η_c	Carnot efficiency	[%]
η_{id}	Ideal reversible thermodynamic efficiency	[%]
E_a	Activation energy	[kJ/mol]
F	Faraday constant	[C/mol]
$\triangle G$	Gibbs free energy	[J/mol]
$\triangle H$	Standard enthalpy of reaction	[J/mol]
n	Number of electrons transported	[-]
$p_{H_2,anode}$	Hydrogen partial pressure on the anode side	[bar]
k	Linear reaction rate	[1/s]
k_0	Reaction rate constant	[1/s]
k_p	Parabolic rate constant in the WAGNER-theory	[1/s]
$\Delta m_{cellmax}$	Maximum possible weight change during oxidation and reduction	[g]
$M(x)$	Molar mass	[g/mol]
m_{gain}	Measured weight gain of the cell	[g]
$m_{cellNiO}$	Mass of NiO within the cell	[g]
m_{Ni}	Atomic mass of nickel	[g/mol]
m_{NiO}	Atomic mass of nickel oxide	[g/mol]
m_O	Atomic mass of oxygen	[g/mol]
$p_{H_2O,anode}$	Water steam partial pressure on the anode side	[bar]
$p_{O_2,cathode}$	Oxygen partial pressure on the cathode side	[bar]
$p_{O_2,anode}$	Oxygen partial pressure on the anode side	[bar]
R	Gas constant (8.314)	[J/molK]
T_H	Highest process temperature within the CARNOT cycle	[K]

T_L	Lowest process temperature within the CARNOT cycle	[K]
U_0	Cell voltage	[V]
U_n	Nernst voltage	[V]
W_e	Electrical work	[J/mol]
W_m	Mechanical work	[J/mol]
x_{red}	Reduced fraction	[%]
y	Thickness of the oxide layer	[mm]

List Of Abbreviations

ASC	Anode Supported Cell
Cermet	Ceramic Metal
CPOX	Catalytic Partial Oxidation
CSC	Cathode Supported Cell
CTE	Coefficient Of Thermal Expansion
DoO	Degree Of Oxidation
EK	ElringKlinger AG
ESC	Electrolyte Supported Cell
FEM	Finite Element Analysis
LSC	$La_{1-x}Sr_xCoO_{3-\delta}$
LSCF	$La_{1-x}Sr_xCo_{1-y}Fe_yO_{3-\delta}$
OCV	Open Circuit Voltage
RedOx	Repeating Reduction And Oxidation
RT	Room temperature
Sl	Standard litre
Slpm	Standard litres per minute
SOFC	Solid Oxide Fuel Cell
TPB	Triple Phase Boundary
8YSZ	8 mol% Yttria Stabilized Zirconia

Abstract

Currently, Solid Oxide Fuel Cell (SOFC) systems do not fulfill the required lifetime for a successful product launch. The main difficulties lie in the stress-induced failure of the electrolyte due to repeating oxidation and reduction (RedOx) of the anode material.

The most common anode material is fabricated from a precursor composed of a powder mixture of ceramic nickel oxide and Yttria Stabilized Zirconia (YSZ). When hydrogen-rich fuel gas is supplied to the cell, NiO is reduced to Ni, so that the precursor is converted into a Ni-YSZ ceramic-metal-composite. The operation of a SOFC system starts with the unit heating up to its operation temperature of 800 °C and stops with the unit cooling down back to room temperature. During these start and stop periods, the fuel supply is interrupted to prevent the formation of soot. Thus, air can flow to the anode leading to oxidation of the anode material. A key factor indicating the extent of cell damage is the degree of oxidation (DoO). The simplest way to determine the DoO is to measure the weight gain caused by the oxidation. However, weight measurement of cells is only possible after destructive disassembling of the stack.

This research explains a new non-destructive method, which describes the oxidation state of SOFC cells in stacks and systems within operation. Scientific investigations into this topic are very time- and cost-consuming, because of the RedOx-induced cell damage and thus the failure of the entire stack. To simplify the research on such topics, a special test bench has been developed. This test bench facilitates testing of single stack layers, which goes hand in hand with quick and cheap cell exchange.

During initial RedOx testing, SOFC cells show a characteristic voltage curve before, during and after oxidation. Using this behavior, different measurement methods have been developed. After the successful development of the measurement methods at the single layer test bench, they have been used to investigate the oxidation behavior of stacks and systems in operation. The oxidation during an entire start- and stop cycle can be measured. Furthermore, oxidation occurring during start up is separated from oxidation during the shutdown phase. The mea-

surement shows that the start up phase has the more major contribution caused by the hot air flowing through the stack and the system when it heats up. Furthermore, the influence from system components such as oxygen diffusion through the exhaust can be separated from leakages of the stack itself by showing that the stack leakage is sufficient to destroy the stack within several start- and stop cycles. The work concludes with two possible solutions. First, the minimal cell voltage for a safe operation is determined. This determination enables the use of forming gas under economically feasible conditions, since it is used as little as possible. Furthermore, the results regarding occurring DoOs are used to create a more RedOx-stable cell within a finite element model.

Kurzfassung

Derzeit erfüllen Hochtemperaturbrennstoffzellensysteme (SOFCs) nicht die erforderliche Lebensdauer für einen erfolgreichen Marktstart. Die Hauptschwierigkeiten liegen im spannungsinduzierten Versagen des keramischen Elektrolyten durch wiederholte Oxidation und Reduktion (RedOx) des Anodenmaterials.

Das Anodenmaterial wird durch Sintern auf Basis einer Pulvermischung aus Nickeloxid und Yttrium stabilisiertem Zirkoniumoxid (YSZ) hergestellt. Bei Erstkontakt der Anode mit wasserstoffreichem Brenngas wird das enthaltene Nickeloxid zu Nickel reduziert, so dass ein metallkeramischer Verbundwerkstoff entsteht. Während des Start- und Stoppvorgangs des SOFC Systems kommt die Anode in Kontakt mit Sauerstoff, da in dieser Phase aufgrund von Rußbildung keine Brenngaszufuhr erfolgen kann. In diesen Phasen reoxidiert das Nickel. Diese sogenannten "Redoxzyklen" führen zur irreversiblen Schädigung des Elektrolyten, da die Oxidation/Reduktion mit einer Volumenänderung einhergeht, die stark abhängig vom Oxidationsgrad ist.

Die einfachste Methode zur Messung des Oxidationsgrads erfolgt gravimetrisch durch Bestimmung der durch die Oxidation verursachten Gewichtszunahme. Die Gewichtsmessung der einzelnen Zellen ist jedoch nur nach destruktiver Demontage des Brennstoffzellenstacks möglich, da die Schweiß- und Lötverbindungen zwischen den Ebenen aufgetrennt werden müssen.

Im Rahmen dieser Arbeit wird eine neue zerstörungsfreie Messmethode entwickelt, die den Oxidationszustand von SOFC-Zellen im Betrieb beschreibt und kein zusätzliches Equipment erfordert. Experimentelle Untersuchungen zu diesem Thema sind wegen der starken Zellschädigung sehr zeit- und kostenaufwändig. Daher erfolgt die Methodenentwicklung auf einem eigens für diese Arbeit aufgebauten Prüfstand auf Einzelebenenbasis. Die entwickelten Messmethoden basieren auf dem charakteristischen Verlauf der Zellspannung vor, während und nach der Oxidationsphase. Durch gezielte Variation der eingebrachten Sauerstoffmenge wird der Zusammenhang zwischen Spannungsverlauf und Oxidationsgrad herausgearbeitet.

Im Anschluss wird die Methode zur Charakterisierung des Oxidationsverhaltens von Stacks und Systemen im Betrieb genutzt. Die Oxidation während eines gesamten Start- und Stopp-Zyklus kann so gemessen werden und nach ihrer Hauptentstehungsphase (Start vs. Stoppphase) aufgelöst werden. Sowohl bei stacknahen als auch bei realen Systemtests kann gezeigt werden, dass die Startphase den größeren Beitrag an der Oxidation hat. Die Aufheizung während der Startphase erfolgt mit aufgeheizter Luft, die auf der Kathodenseite des Stacks für einen Überdruck sorgt. Durch den Vergleich reiner Stackversuche ohne Systemkomponenten mit Versuchen am Komplettsystem wird klar, dass bereits die internen Stackleckagen ausreichend sind, um den Stack innerhalb weniger Zyklen zu zerstören.
Die Arbeit schließt mit der Erarbeitung einer marktfähigen Lösung. Kern der Lösung ist der Betrieb mit Formiergas, das spannungsgeregelt dosiert wird. Durch diese Regelung kann die Menge auf ein wirtschaftlich tragfähiges Maß reduziert werden. Um die Toleranz gegenüber Systemfehlern (ohne Formiergasschutz) zu erhöhen, wird am Ende der Arbeit eine Hybridzelle vorgeschlagen, die die Vorteile von elektrolyt- und anodengestützten Zellen in sich vereint.

Chapter 1

Introduction

Our modern society is based on a reliable and economic energy supply. In times of climate change and the sustainability debate, it is crucial to change the world's energy supply to save the prosperity of future generations. In Germany, the transition from the fossil fuel and nuclear energy age to the efficient and sustainable energy age are subsumed under the heading "Energiewende". Basically the "Energiewende" consists of the sustainable supply, conversion and distribution of energy [1]:

- Use of renewable energy sources such as wind, water and sun
- Adaption of energy infrastructure regarding the different bahavior of new energy sources, in particular development of energy storage, efficient energy conversion and improvement of electricity grids
- Increasing efficiency of energy consumption of industry, private households and the mobility sector

Following this path, the German government plans to reduce the country's CO_2 emissions by 14 % (2005-2020) and even up to 95 % by 2050 [2].
In this regard, fuel cells are promising power sources for vehicles, buildings and special applications such as building site power supplies or auxiliary power units. A big advantage lies in the direct conversion from chemical to electrical energy without the indirect route via mechanical energy, which enables electrical efficiencies of up to 60 % and even up to 90 % in combined heat and power applications [3, 4]. The fuel cell principle works also the other way round. By applying an electrical current to the cell, water can be divided into hydrogen and oxygen. This

bi-directional capability makes the fuel cell a key technology in future energy business. A fuel cell combined with hydrogen storage and solar energy makes a 100 % renewable energy cycle possible. Unfortunately at the moment this ideal solution is not yet state of the art. Hydrogen infrastructure is in its infancy, so the efficient usage of conventional fuels is quite important. Against this background a special type of fuel cell, the Solid Oxide Fuel Cell (SOFC), is a very promising technology. SOFCs work at high temperatures and consist of only solid-state components. The high operation temperatures between 600 °C and 1000 °C enable the efficient usage of conventional fuels [4].

Figure 1. 1 shows a typical SOFC system working with propane.

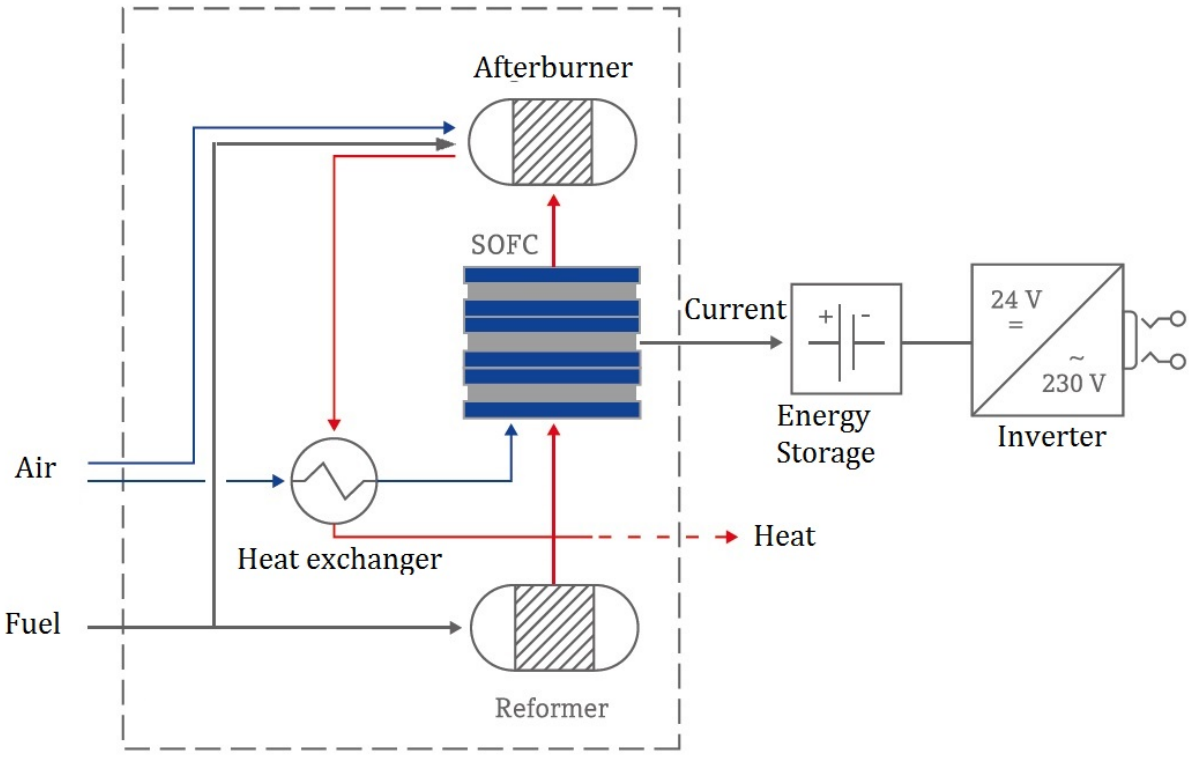

Figure 1. 1: Architecture of a SOFC-System [5]

The core of this system is the SOFC-stack, where several cells are connected in series. Inside the stack, electricity is generated from hydrogen-rich gas (reformate). Reformate consists of H_2, CH_4, CO, CO_2, H_2O and N_2 and is generated in front of the stack by catalytic partial oxidation (CPOX). Since SOFCs work only at high temperature, the system has to start up by hot air flowing over the cathode side, which is generated by direct burning of the fuel. While

starting the system, there is no reformate flowing over the anode side of the cells to prevent the formation of soot. For system shutdown fuel and air flow are stopped and the system cools down.

1.1 Problem statement and research objectives

Currently SOFC systems do not fulfill the required lifetime for a successful product launch. A life cycle of a SOFC system is characterized by constant operation combined with start and stop cycles. The latter is one of the major technical challenges for successful commercialization. The main difficulties lie in the stress-induced-failure of the electrolyte due to repeating oxidation and reduction (RedOx) of the anode material. The most common anode material is fabricated from a precursor composed of a powder mixture of ceramic nickel oxide (NiO) and Yttria Stabilized Zirconia (YSZ). When hydrogen fuel gas is supplied to the cell, NiO is reduced to Ni, so that the precursor is converted into a Ni-YSZ ceramic-metal-composite (cermet)[3]. Once the fuel flow is interrupted (start and stop-phase), oxygen will enter the anode side. This leads to oxidation since nickel is not stable in air at temperatures above 300 °C. This insufficient stability in combination with the tendency towards soot formation forms the core of the RedOx issues for SOFCs. The soot formation depends on temperature, humidity and fuel type.
A key factor indicating the extent of cell damage is the degree of oxidation (DoO), where 100 % is the initial state of the precursor and 0 % is the reduced state during operation. The simplest way to determine the DoO is to measure the weight gain during oxidation. However, weight measurement of cells is only possible after destructive disassembling of the stack.
This research aims to develop a new non-destructive method which describes the RedOx behavior of SOFC cells, stacks and systems. During oxidation and reduction a SOFC cell shows a characteristic voltage curve. The methods developed in this study are based on this characteristic. Scientific investigations into this topic are very time- and cost-consuming, because of the RedOx-induced cell damage and thus the failure of the entire stack. To simplify the research on such topics, a special test bench needs to be developed in this investigation. This test bench is supposed to facilitate testing of single stack layers, which goes hand in hand with quick and cheap cell exchange. Only method validation is done by stack testing. Using the new methods, degree and operation phase of oxidation occurring in stacks and systems has to be determined. Based on the results of this work, suitable measures against reoxidation can be taken to make the system ready for the market. Suitable options will be investigated and discussed at the end

of this work.

1.2 Basic principle of SOFCs

Fuel cells are electrochemical devices, which convert chemical to electrical energy. William Grove is regarded as the inventor of fuel cells as he constructed the first small prototype of a fuel cell in 1839. His first experiment consisted of a water container, two test tubes and a power supply with electrodes. In the first section of the experiment, water could be converted into hydrogen and oxygen while an electric current was passing through it. When the power supply was removed, a small fuel cell was generated. This fuel cell produced a small current via the consumption of H_2 and O_2. To get higher power values he connected several containers in series [6].

This experiment shows the direct conversion of chemical to electrical energy, which enables high efficiencies since the process is not subject to the CARNOT limitation. CARNOT's theorem describes the maximum of efficiency for the conversion from heat into work by a thermal heat engine. It is based on the temperature difference between the heat source and cooling medium and follows a simple rule: The higher the difference between heat source (T_H) and cooling medium (T_L), the higher the possible efficiency following equation 1.1, where W_m is the mechanical work related to the enthalpy change ($\triangle H$) [7].

$$\eta_c = \frac{W_m}{\triangle H} = 1 - \frac{T_L}{T_H} \tag{1.1}$$

However, the overall efficiency is lower due to friction, fluid - mechanical effects and generator losses for conversion into electricity. The limitation by CARNOT places huge demands on the materials used, because their temperature stability is also the limit of efficiency.

The big advantage of fuel cell technology lies in its independence of high operation temperatures, since the efficiency is given by the Gibbs free energy ($\triangle G$) and the enthalpy change of the reaction, also called 'ideal reversible thermodynamic efficiency' η_{id}:

$$\eta_{id} = \frac{W_e}{\triangle H} = \frac{nFU_0}{\triangle H} = \frac{\triangle G}{\triangle H} = 1 - \frac{T\triangle S}{\triangle H} \tag{1.2}$$

A maximum of efficiency is achieved if $\triangle G$ is completely converted into electrical work (W_e), so that $T\triangle S$ is zero as it corresponds to the reversible heat exchanged with the external environment. Following equation 1.2 the electrical work is directly related to the cell voltage U_0, where F and n are the Faraday constant and n the number of electrons involved in the

reaction, respectively. Assuming standard conditions (Concentration of reactants: 1 mol/l and T = 298 K) the cell voltage U_0 of a H_2/O_2 fuel cell is 1.48 V relative to the upper heating value of hydrogen for $\triangle H$ [8]. For different temperatures and concentrations the cell voltage under no-current conditions (OCV = Open Circuit Voltage) is described by the NERNST-equation:

$$U_n = OCV = U_0 + \frac{RT}{nF} ln \left(\frac{p_{O_2,cathode}}{p_{O_2,anode}} \right) \tag{1.3}$$

Insertion of the natural constants R and F and assuming the reaction of a SOFC (n=2, H_2O as product of the reaction) yields equation 1.4 [9].

$$U_n = OCV = U_0 + 0.0295 \cdot T \cdot ln \left(\frac{\sqrt{p_{O_2,cathode}} \cdot p_{H_2,anode}}{p_{H_2O,anode}} \right) \tag{1.4}$$

Figure 1. 2 shows the calculated OCV as a function of the steam concentration at a typical SOFC operation temperature of 800 °C in air.

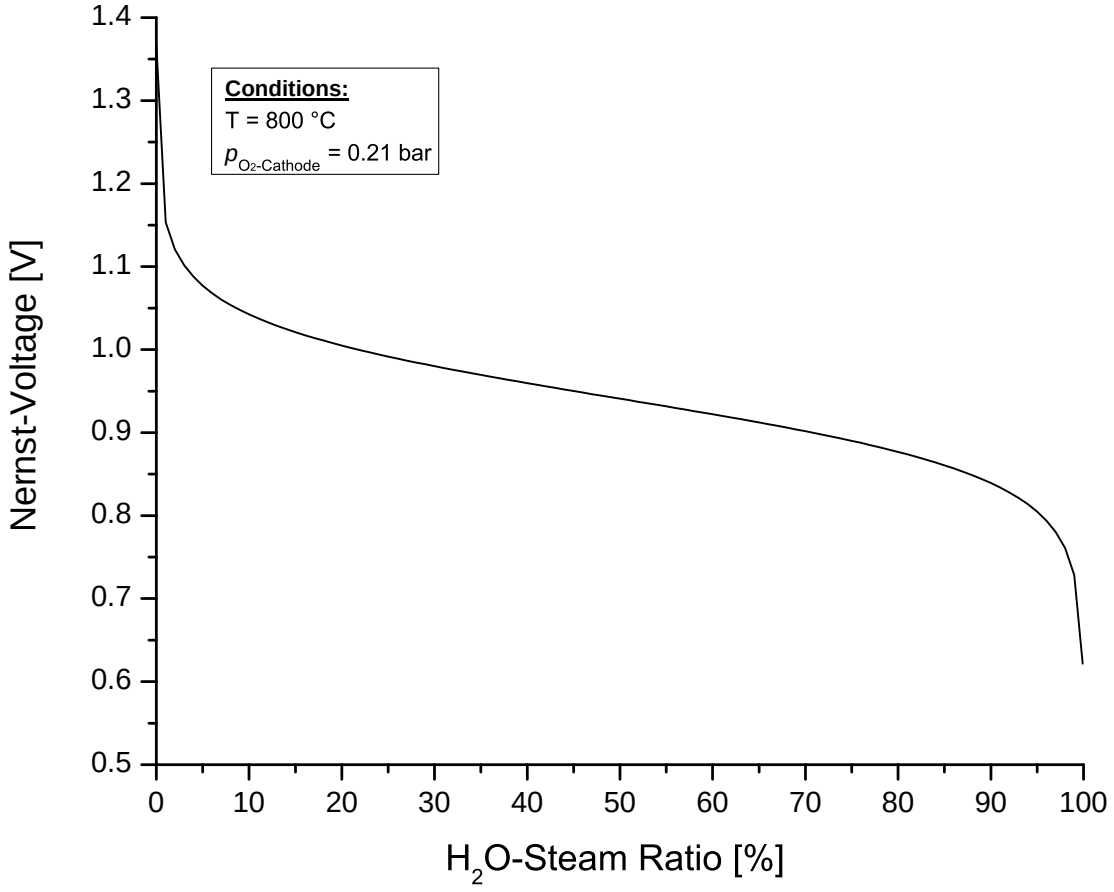

Figure 1. 2: OCV as a function of steam concentration (Anode: H_2, Cathode: Air, T = 800 °C)

Under no current conditions, there is no H_2O coming from the cell reaction, so that the cell

voltage tends towards infinity. Under real conditions a typical OCV of a SOFC is around 1.3 V, because a fuel cell system is never 100 % tight. Even if there is no current, air can infiltrate the anode side and can react directly with hydrogen. For this reason the OCV provides a suitable reference point for the tightness of the system.
Under load the cell voltage decreases with increasing current as illustrated in figure 1. 3.

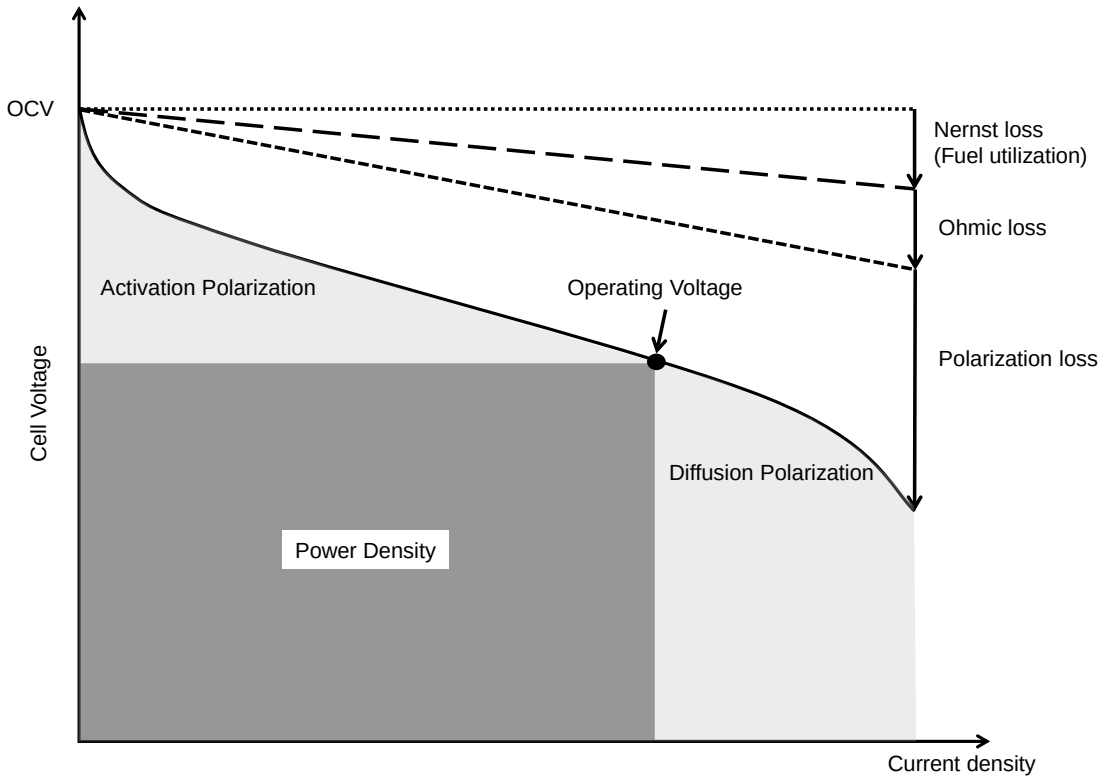

Figure 1. 3: Typical current-voltage-plot of a fuel cell

The power of an operating fuel cell is defined by the area under the current-voltage plot. Consequently, there is an optimum for the product of current density and cell voltage. It can be observed that the operating voltage is always smaller than the initial OCV due to various losses at three different current density levels:

- At low current densities the major contribution to cell voltage losses is from activation polarization, which is caused by the energy-intensive activity of breaking of old bonds and forming of new bonds at the electrodes. The effect of activation polarization can be reduced by increasing temperature, the active area of the electrodes or the use of catalysts [4, 10]. A second loss dominating at low current densities is the loss due to fuel utilization

following equation 1.4. Following NERNST the influence of water steam on the cell voltage is higher at low steam concentration.

- At medium current densities the ohmic resistance dominates the plot characteristic. Ohmic losses are caused by the resistance of all conductive parts. In addition to that, the ionic conduction of the electrolyte leads to further losses.
- At high current densities, the cell resistance is controlled by mass transport and diffusion processes as indicated by a rapid voltage decrease [4].

Figure 1. 4 shows the various ways that fuel cell technology works in practice.

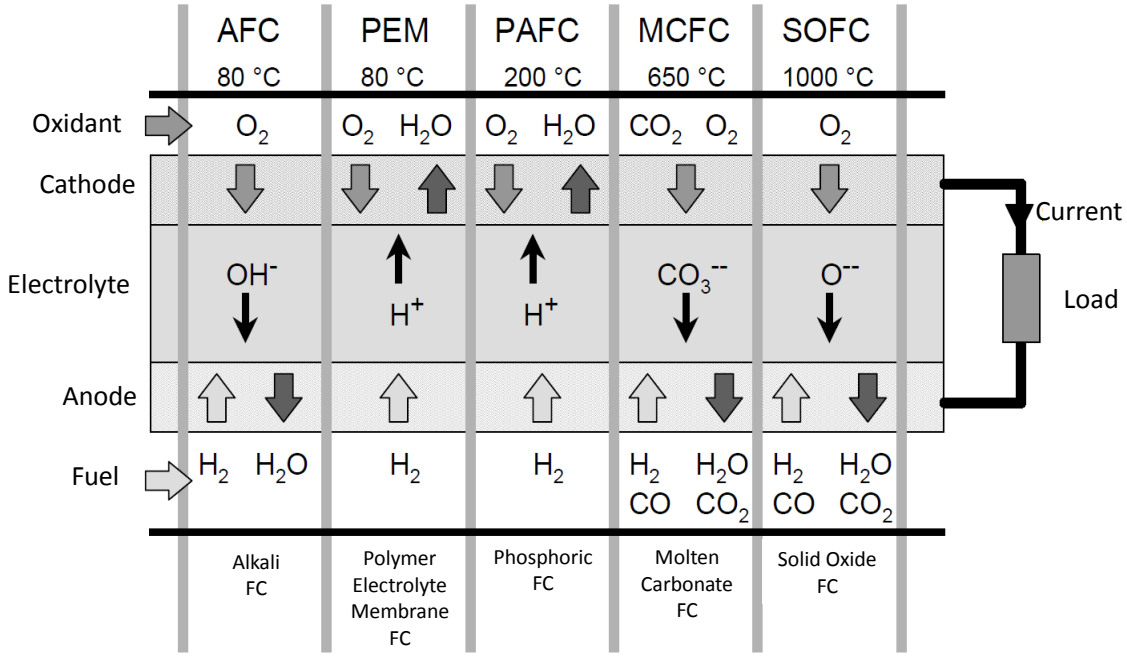

Figure 1. 4: Fuel cell types [11]

Fuel cells can be classified by temperature (low and high) and by the electrolyte. Whereas low temperature fuel cells have high power densities and low demands on the temperature stability of the materials used, high temperature fuel cells can be operated by hydrocarbon fuel such as methane [11]. This makes them especially interesting for mobile applications without hydrogen infrastructure. Depending on the fuel cell type, different reactions take place at the electrodes, explained more in detail for SOFCs, this work is about.

The SOFC is a complete solid state fuel cell with an ionic-conducting dense ceramic electrolyte and porous electrodes. The operating principle is illustrated in figure 1. 5.

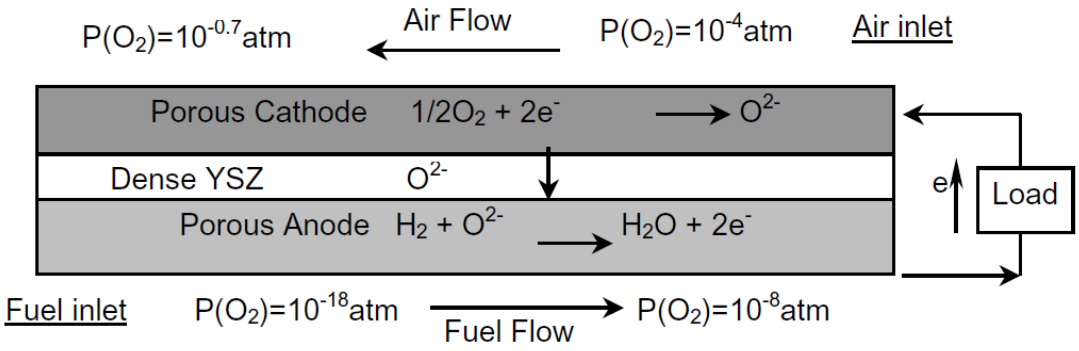

Figure 1. 5: Working principle of SOFC powered by hydrogen [12]

As shown in equation 1.4 there is an electric potential between the electrodes. If the circuit is closed, electrons flow to the cathode side (oxygen electrode). There, oxygen reacts with two electrons to become oxygen ions that diffuse through the electrolyte. Arriving at the anode side (fuel electrode), fuel is oxidized to water by releasing two electrons that flow back to the cathode. These electrochemical reactions take place at the interface between gas, electrolyte and electrode - also called triple phase boundary (TPB). Its size decides the reaction rate.
As SOFCs excel regarding their fuel flexibility, they are mostly operated by reformate consisting of CO and CH_4 according to equation 1.5 and 1.7 [12].

$$CO + O^{2-} \rightarrow CO_2 + 2e^- \tag{1.5}$$

$$CO + H_2O \rightarrow CO_2 + H_2 \tag{1.6}$$

$$CH_4 + 4O^{2-} \rightarrow 2H_2O + CO_2 + 8e^- \tag{1.7}$$

Instead of the direct electrochemical use of CO, it can be oxidized with water to form CO_2 and H_2 (Equation 1.6) - the so-called water-gas shift reaction [13]. The use of carbonaceous fuels can lead to the formation of soot and thus to a high degradation of the anode microstructure. Sufficiently high temperatures in combination with humidity can prevent this process.

1.3 Configuration of SOFC cells and stacks

The core of every SOFC system consists of anode, cathode and electrolyte. To resist the high thermo-mechanical loads, one of the layers must provide sufficient mechanical properties to

support the entire cell. In planar fuel cells, this task is assumed by the thickest layer, thus there are cathode, anode and electrolyte supported cells. Depending on the cell type, there is a big difference in RedOx tolerance [14]. For this reason this topic is further discussed in chapter 2.
To achieve good power values, cells have to be arranged in series. Over many years of experience two stacking arrangements have proven their worth, the tubular and the planar design.
The tubular design stands out with its self-sealing structure, whereas the planar design enables low fabrication costs and higher power densities. For this reason ElringKlinger (EK) has centered itself on the latter. Outstanding know-how in high temperature sealing of planar designed SOFCs is what EK is distinguished for in planar technology. Over many years of experience the OCV could increased up to values of 1.3 V, which indicates a very high sealing quality, referring to figure 1. 2 and equation 1.4.
Fuel and air flow in planar stacks can be arranged in cross-, co- and counter flow as illustrated in figure 1. 6.

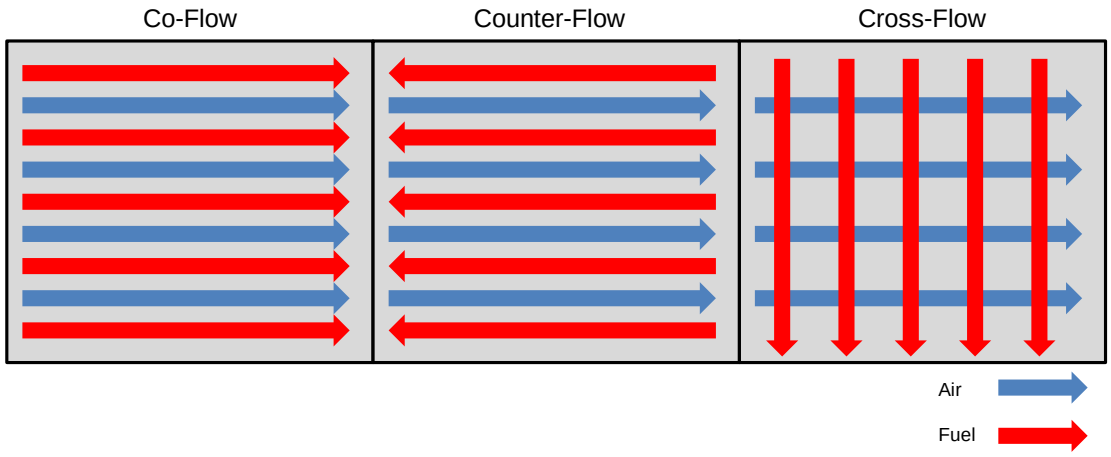

Figure 1. 6: Schematic drawing of co-, counter- and cross flow

Especially for operation with reformate, temperature-, current density- and thus humidity distribution strongly depend on the flow type. This has a significant influence on the soot formation temperature and thus also on the extent of RedOx-induced degradation. EK has experience in co- and counter flow. Figure 1. 7 a) shows the way from a single cell via a repeating unit up to the complete stack [15].

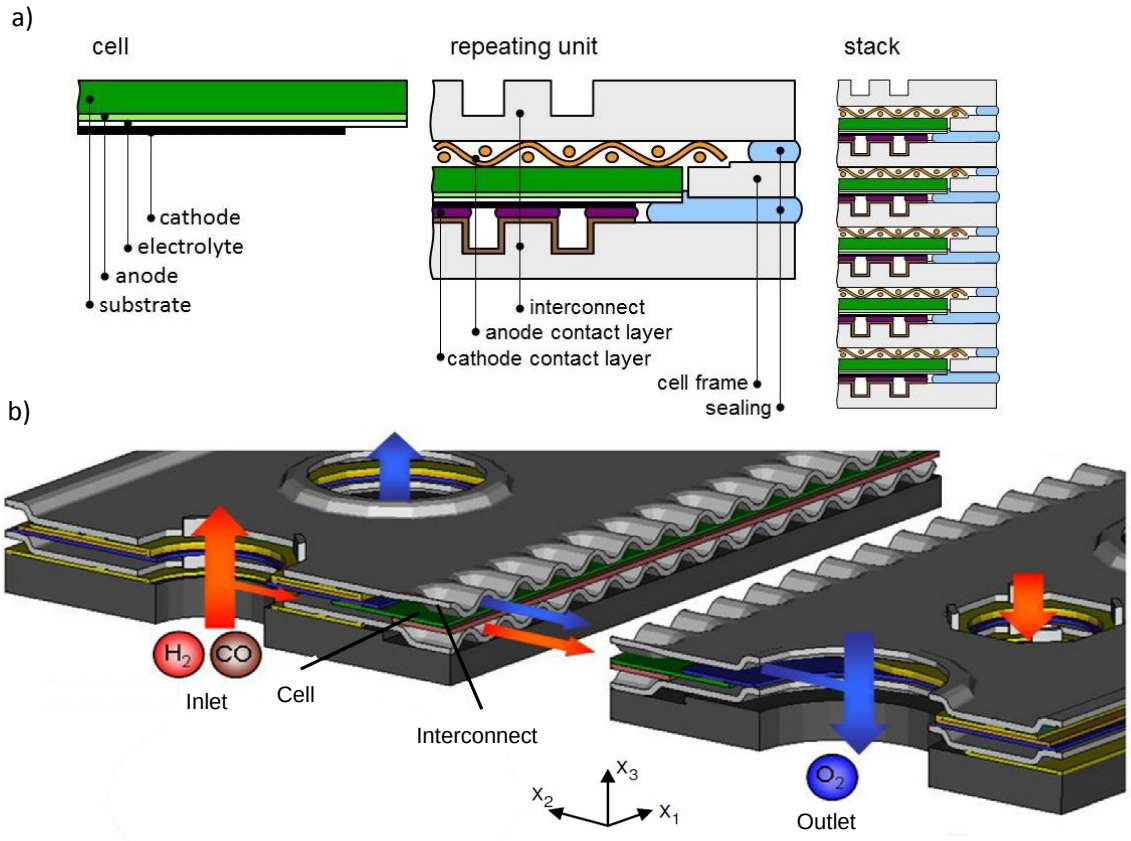

Figure 1. 7: a) Schematic drawing from the single cell via repeating unit up to the complete stack b) Section through in the first layer of the EK planar design [16, 15]

First, the cells are integrated into a high temperature steel frame by brazing. For a good gas supply as well as for the electrical contact each cell is surrounded by an interconnect. To reduce the contact resistance to a minimum there is always a contact element between interconnect and cell. Electric insulation between the interconnects is mandatory to avoid short circuits. At EK this task is assumed by the sealing, consisting of glass braze at one side of the interconnect. At the other side of the interconnect the connection is ensured by laser welding. Figure 1. 7 b) shows a section through the first layer of the EK planar design [16]. The interconnect is formed in a wavelike structure, where each wave trough provides an electrical contact. The design enables cheap processing by stamping and forming. Referring to the EK design, the following leakage sources can lead to cell oxidation by oxygen on the anode side:

- Point defects/cracks in the thin electrolyte
- Defects in the fusion zone between cell and frame part
- Defects in the sealing of the stack layers (glass braze, welding zone)

1.4 Materials - requirements and selection

The high operation temperatures place huge demands on the materials of anode, cathode, electrolyte, interconnect and sealing. Particularly worth mentioning for all materials is the compatibility regarding their thermo-mechanical properties such as thermal expansion and elastic moduli to prevent damages such as cracking or delamination. All parts must withstand the big temperature changes from room to operation temperature. Of course, low fabrication cost, high (fatigue) strength and toughness are fundamental requirements [6].

For planar stack arrangements an interconnect is used. The interconnect ensures electric connection between the layers with minimal ohmic losses. Furthermore, the interconnect acts as manifold for the reactants and prevents gas mixing. At typical operation temperatures of up to 800 °C heat-resistant steels can be used. To match the thermal expansion of the other components, only steels with a ferritic microstructure are of interest. Depending on the temperature they have a coefficient of thermal expansion (CTE) of around 10-12 x 10^{-6}/K, which is achieved by alloying with Cr as ferrite former [17, 18]. To ensure a low contact resistance between cell and interconnect, the oxide layer consisting of Cr_2O_3 has to be of high conductivity. Hence, low contents of Al and Si (< 1 %) are required to prevent the formation of poor conductive Al_2O_3 and SiO_2 layers [19]. Typical steels are Crofer22 APU®, Crofer 22 H® and 1.4509 - the last one is outstanding for its low price. For further optimization these steels can be additionally coated to prevent Cr-evaporation and thus poising and degradation of the cathode [19].

Successful stacking and operation only works with a tight seal. The stack layers as well as the connection between cell and frame sheet have to be sealed. The most advanced materials consist of glass-ceramics based on the system Ba-Ca-Al-Si-O. Research at EK is based on this system, which is already used for the sealing between the layers, whereas the sealing between cell and frame sheet works with a metallic braze. Unfortunately this braze tends to form pores due to the dual gas atmosphere. For this reason EK focuses on the development of a glass ceramic cell sealing [20]. If a non bonded connection is required (e.g. for stack-/cell testing), compressive seals are used.

The oxygen ions, transported through the electrolyte, are produced at the cathode by reducing O_2 to $2O^{2-}$. For high reaction rates, the surface area should be as high as possible. For this reason the microstructure is porous, which is, however, limited by the electrical conductivity [6]. State of the art cathodes are doped perovskites based on lanthanum: $La_{1-x}Sr_xCoO_{3-\delta}$ (LSC), $La_{1-x}Sr_xCo_{1-y}Fe_yO_{3-\delta}$ (LSCF) and $La_{1-x}Sr_xMnO_3$ (LSM) [21].

Transportation of the oxygen ions is ensured by the electrolyte. This requires good ionic conduction to minimize the cell impedance. Simultaneous electric conductivity is forbidden, because the current has to flow outside the cell to be useful for electric energy generation. Furthermore, the electrolyte must be constructed in such a way, that the fuel is separated from the oxidant [6]. The most common electrolyte material is stabilized zirconia oxide (ZrO_2), because of its high ionic conductivity at elevated temperatures. The structure of ZrO_2 strongly depends on the temperature and can be monoclinic (RT-1170 °C), tetragonal (1170-2370 °C) and cubic (2370-2690 °C), but only the latter is of interest due to its high ionic conductivity [22]. Doping with lower valent oxides such as Sc_2O_3, CaO or Y_2O_3 enables good conductivity even at temperatures under 1000 °C [23]. For SOFC-electrolytes the most common doping material is Y_2O_3, which is added in a concentration of 8 mol%, abbreviated as 8YSZ (Yttria Stabilized Zirconia) [24].

The main purpose of the anode is to oxidize the fuel and combine it with the ions coming from the cathode. At the anode, recombination takes place and water is produced. For this reason the fuel must be able to penetrate the anode and evaporated water has to leave. Since the material must be electrically conductive and of low cost, a metal seems to be the logical material of choice [12]. Nickel was found to match all requirements [25]. However, nickel has a higher CTE (18 x 10^{-6}/K) than the YSZ-electrolyte (10.5 x 10^{-6}/K) [26]. Moreover, nickel has a tendency towards agglomeration at operation temperature as well as during the fabrication process. Agglomeration leads to a reduced TPB and thus to a lower cell performance. An addition of 8YSZ solves that problem as it reduces the CTE significantly [27] and prevents Ni agglomeration [28]. In addition to that, 8YSZ provides ionic conductivity, so that the ions coming from the cathode, can flow fast to react with the fuel immediately [29]. For this reason a Ni-YSZ cermet (cermet = ceramic metal) is the most common material in today's SOFC applications [30, 27]. Unfortunately Ni and YSZ are essentially immiscible even at the higher temperatures, so the manufacturing process is based on producing green samples with subsequent sintering. After sintering, NiO is reduced by hydrogen to pure Ni, so that the final cermet material is produced [27]. The reduction process as well as the use of pore formers ensures the sufficient porosity of around 30-40 vol.-% [31]. The porosity and the Ni-YSZ ratio have a strong influence on the electric conductivity of the anode material, as shown in figure 1. 8 a) [32, 33].

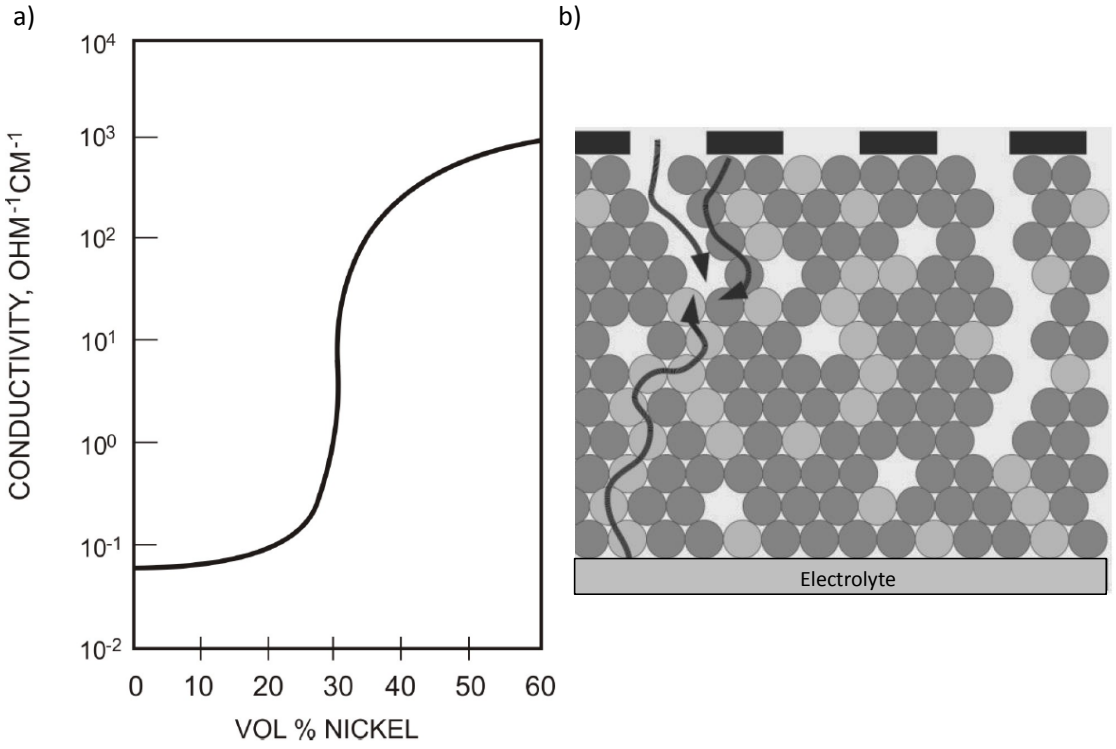

Figure 1. 8: a) Conductivity of Ni/8YSZ cermet as a function of nickel content (T=1273 K) [32, 33] b) Schematic drawing of TPB with conductive paths (arrows), dark gray: nickel, light gray: YSZ, white: Gas [34]

The conductivity follows a S-shaped curve, which has its turning point around 30 vol.-% Ni. Typically, the mixture for manufacturing the anode has around 60 wt.-% NiO, which is equal to ca. 43 vol.-% nickel. This amount of nickel is the optimum between electric/ionic conductivity and the best match of the CTE of anode and electrolyte. The S-shaped curve can be explained by the percolation theory, which describes the behavior of connected clusters and is schematically drawn in figure 1. 8 b [34]. The percolation depends not only on Ni-content and porosity, but also on many other variables such as pore size, size distribution and the particle size ratio between YSZ and Ni [35].

Since the electrode materials in SOFC applications have to satisfy challenging and contradictory requirements, for instance high porosity and electric conductivity at the same time, state of the art cells follow a multilayer structure concept [36]. Figure 1. 9 shows the standard cell with LSCF-cathode, which is used as current standard at EK and thus also in this research.

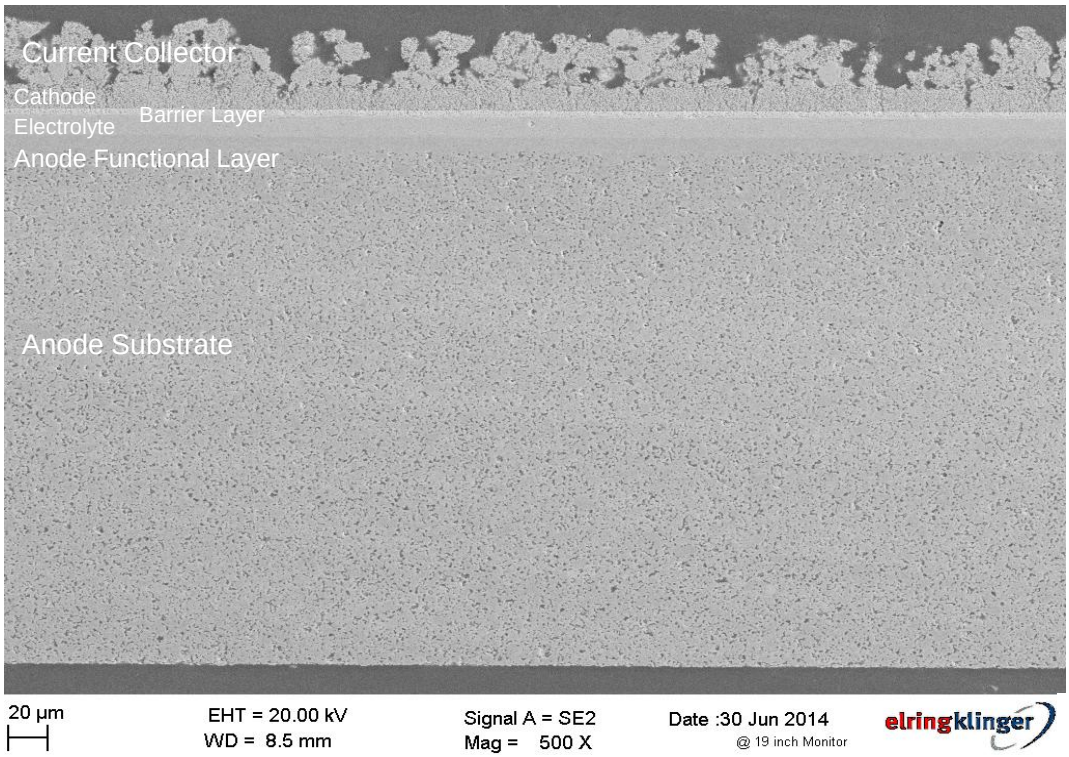

Figure 1. 9: Current standard cell design at EK with LSCF-cathode [37]

The electrodes are divided into a functional layer, where the electrochemical reaction takes place, and into a substrate (anode) and current collector (cathode). In addition to that, a barrier layer is located between cathode and electrolyte to prevent unwanted interactions. This layer ensures high performance and long term stability [38].

Chapter 2

RedOx cycling of Ni/YSZ anodes

As previously mentioned, state of the art anodes are based on nickel and 8YSZ. Nickel is not stable against oxidation in air above 300 °C [36]. For this reason repetitive reduction and oxidation cycles (RedOx cycles) occur during system operation. Since this cycling comes with a volume change, the process is detrimental for the cell. The cell damage strongly depends on the degree of oxidation (DoO) and thus on the amount of oxygen coming to the anode side [36]. This chapter reviews the principle of RedOx as well as the research performed over the last few years by different scientists. It starts with a detailed description of the reduction and oxidation process including the voltage behavior, which the methods developed in this research are based on (2.1). Following mechanical and electrochemical degradation phenomena are presented (2.2). Finally, possible solutions are discussed 2.3.

2.1 RedOx - process description

Figure 2. 1 gives an overview of the reducing and oxidizing steps during a typical RedOx cycle of the anode material [39]. The initial anode material consists of NiO/8YSZ. When fuel is supplied to the cell, NiO is reduced to Ni increasing the porosity due to the volume change from NiO to Ni. During long-term operation, nickel agglomeration can occur mainly depending on water content and temperature - driven by minimizing the free surface energy [40]. If the oxygen activity on the anode side rises above the equilibrium condition between Ni and NiO, the anode oxidizes. Even though the anode can be re-reduced, the initial structure cannot be restored, which leads to a complete failure over time [41].

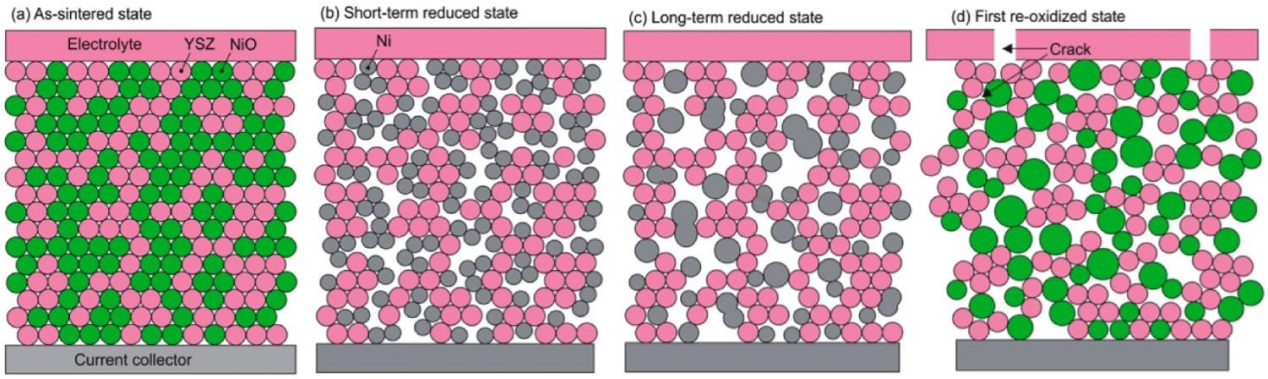

Figure 2. 1: Microstructural changes from initial processing to the first re-oxidized state [39, 14]

The initial as well as all repetitive reduction steps follow equation 2.1 [14].

$$NiO + H_2 \rightarrow Ni + H_2O \tag{2.1}$$

The reduction of NiO starts with the nucleation of metallic clusters. Once these clusters exist, they grow at a linear reaction rate k following equation 2.2 at constant temperature, where x_{red} and t are the degree of conversion and the time, respectively [42].

$$x_{red} = k \cdot t \tag{2.2}$$

As the NiO is almost reduced, the reaction rate deviates from the linear characteristic, because the diffusion paths get longer through the porous nickel. At higher temperatures the access of the reactants is further restricted by agglomeration of the nickel particles. The same rule applies to the comparison between pure NiO and the NiO/8YSZ cermet, where the 8YSZ causes longer diffusion paths. Using the ARRHENIUS equation 2.3, the activation energy E_a for the reduction of pure NiO could be determined to be 85-90 kJmol^{-1}, where T is the absolute temperature in K and k_0 the reaction rate constant [43, 44, 41]

$$k = k_0 \cdot exp\left(-\frac{E_a}{RT}\right) \tag{2.3}$$

The activation energy of NiO/8YSZ reduction is around 95 kJmol^{-1}, determined at 600-800 °C for a fully dense sample [45].

Of course, there is a mass change $\Delta\, m_{cellmax}$ during the reduction process. Its maximum can be calculated by the quotient of the atomic masses of NiO m_{NiO} and O m_O related to the weight of the NiO content of the cell $m_{cellNiO}$ before reduction as shown in equation 2.4.

$$\Delta m_{cellmax} = \left(\frac{m_O}{m_{NiO}}\right) \cdot m_{cellNiO} \tag{2.4}$$

If the scaled value for Δ $m_{cellmax}$ is smaller than the calculated one, the cell is not fully reduced. If it is higher, there must be an error in the calculation. A probable error can come from a incorrect value for the NiO content of the cell, which is not easy to determine, since the weight of cathode and electrolyte as well as the NiO/8YSZ ratio of the anode must be known. To avoid these challenges, an experimental determination is possible. This works with weight measurement before and after reduction as well as sufficiently long exposing times, assuming a 100 % reduction. If Δ $m_{cellmax}$ is successfully determined this way, the quantity of hydrogen m_{H_2} needed for reduction can be calculated from the molar mass ratio (known from the periodic system) according to equation 2.5 [46].

$$\frac{M(H_2)}{M(O)} = \frac{2.0158\frac{g}{mol}}{15.999\frac{g}{mol}} = 0.12599 \Rightarrow m_{H_2} = \Delta m_{cellmax} \cdot 0.12599 \tag{2.5}$$

If the cell is oxidized again, the maximum possible weight gain corresponds to Δ $m_{cellmax}$. The quotient from Δ $m_{cellmax}$ and the actual weight gain m_{gain} is called degree of oxidation referred to in equation 2.6.

$$DoO = \frac{m_{gain}}{\Delta m_{cellmax}} \tag{2.6}$$

Oxidation of the cell can occur for various reasons [14]:

- Under high load in combination with high fuel utilization or bad flow distribution the oxygen partial pressure increases up to the equilibrium value for NiO/Ni [47]
- Damage of the sealing system (cell-framesheet, layer sealing) referring to chapter 1 [48]
- To reduce cost and system complexity, shutdown and start up without protective gas or an emergency stop of the system

In current research activities the last point is the most challenging. For a structured approach there must be made a distinction between oxygen coming from the system setup and the stack itself:

Since no state of the art sealing system suitable for SOFCs is entirely perfect, there will always be a flow of some oxygen to the anode side. Moreover, the electrolyte can have some defects as well. In the case of a shutdown the amount of oxygen is limited, because the external oxygen supply is turned off. However, at start up the stack is heated up by hot air, which leads to overpressure at the cathode side.

The system setup causes additional oxygen sources. Referring to figure 1. 1 oxygen can flow from the afterburner back to the stack during start up. During shutdown oxygen can flow/diffuse

through the exhaust pipe back to the stack. It has to be mentioned that the flow rate of oxygen is probably higher during start up. However, the start up time is clearly shorter than the cool down, because the system is embedded in an insulated box. This leads to the question of whether the start up- or the shutdown period is more detrimental to the cell.
In general, oxidation of the Ni/8YSZ cermet is divided between thermochemical and electrochemical oxidation. Both mechanisms are schematically drawn in figure 2. 2

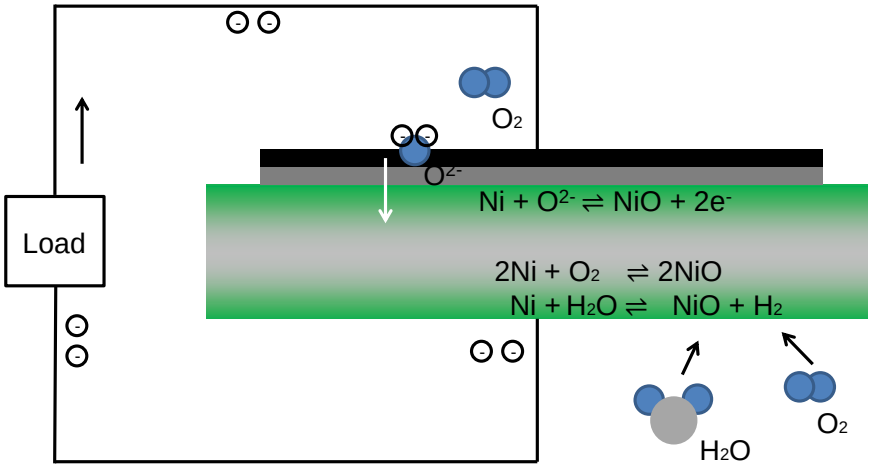

Figure 2. 2: Schematic drawing of oxidation processes taking place at the SOFC anode

The thermochemical oxidation shown in equation 2.7 is driven by molecular oxygen. Moreover, there can be oxidation caused by high water content due to high fuel utilization according to 2.8.

$$2Ni + O_2 \leftrightharpoons 2NiO \tag{2.7}$$

$$Ni + H_2O \leftrightharpoons NiO + H_2 \tag{2.8}$$

The electrochemical oxidation according to equation 2.9 takes place at the electrode-electrolyte interface [49].

$$Ni + O^{2-} \leftrightharpoons NiO + 2e^- \tag{2.9}$$

The oxidation is driven by the oxygen ions flowing through the electrolyte. Arriving at the anode they react with Ni to NiO by releasing two electrons that flow through an external circuit back to the cathode. Closing the loop, oxygen reacts with two electrons arriving to become oxygen ions. Electrochemical oxidation takes place, if the fuel supply is too low or completely turned off, while the external circuit is closed. If it is opened, there is a voltage between the electrodes,

also called RedOx potential. The RedOx potential can be calculated from equation 2.10 [14].

$$OCV_{RedOx} = \frac{1}{2F}\left(\frac{Rln(p_{O_2,cathode})}{2}T - \Delta G^0_{Ni/Ni0}(T)\right) \tag{2.10}$$

Figure 2. 3 shows the calculated potential between 300 °C and 1000 °C based on data from [50]. Based on equation 1.4 (cell voltage under hydrogen) and equation 2.10 the voltage behavior

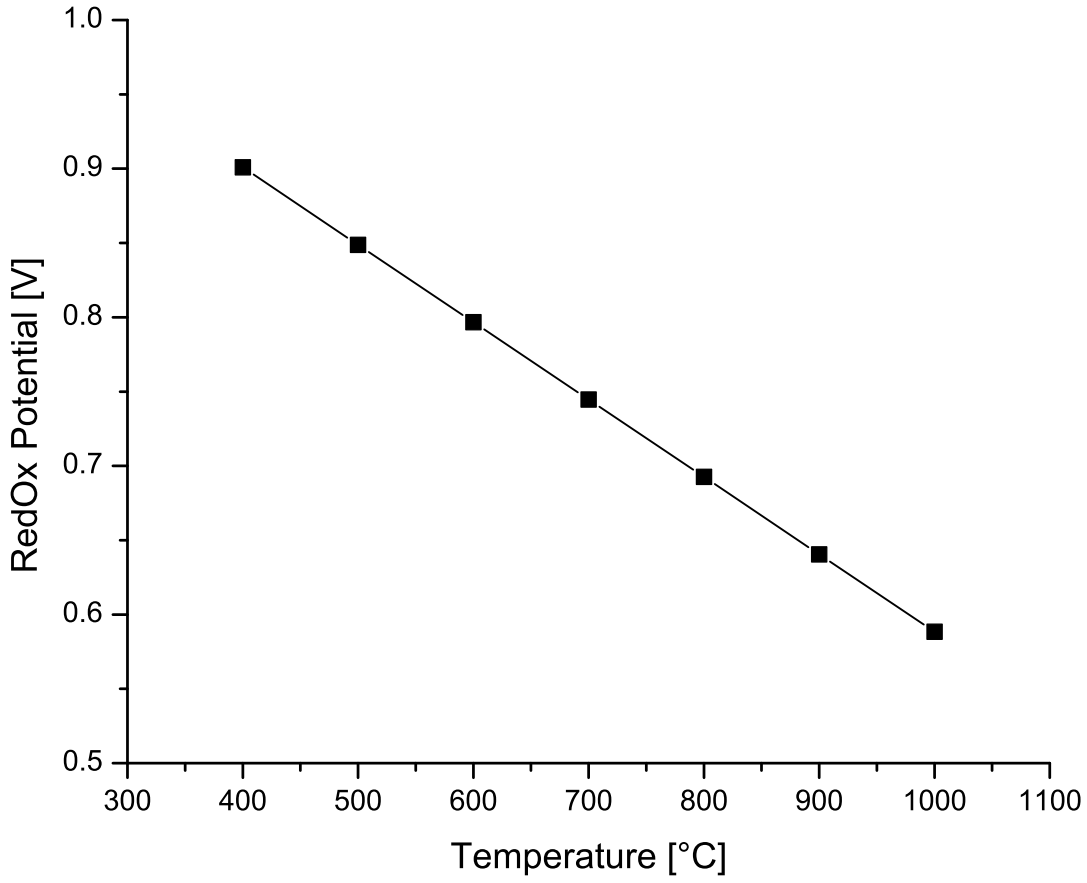

Figure 2. 3: RedOx potential as a function of temperature

during an isotherm RedOx cycle can be drawn. Figure 2. 4 shows the voltage curve from a complete cycle based on experimental data of this work.

At the beginning the fuel supply is turned off. Since the system is not completely tight, oxygen flows to the anode area and "burns" directly to water. Furthermore, there can be a low parasitic current, which consumes the fuel. For this reason the water content rises over time and thus the OCV falls according to equation 1.4 and figure 1. 2 (Large drop - linear - large drop) When the hydrogen is fully utilized, oxidation begins and thus the voltage has to be at the value for the calculated RedOx potential. Once hydrogen is supplied to the cell, reduction takes place.

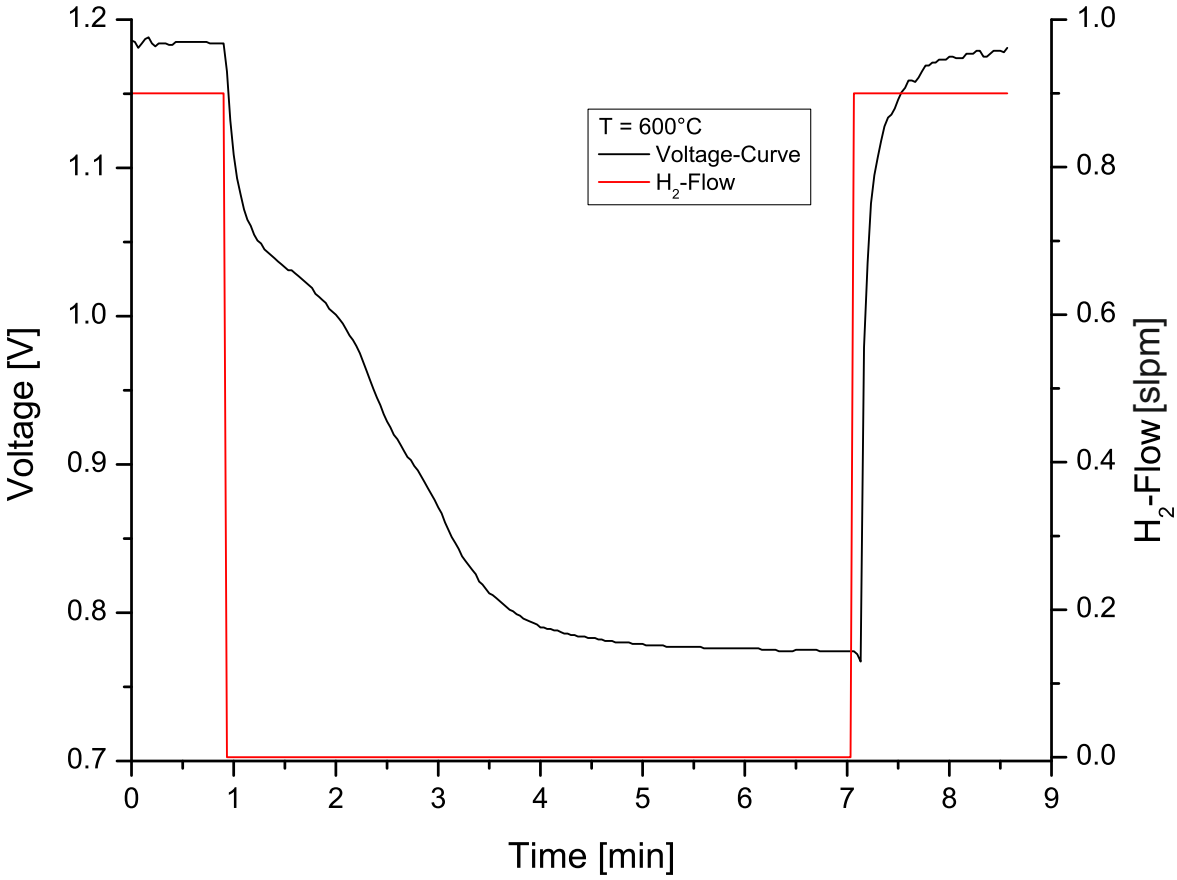

Figure 2. 4: RedOx cycle at 600 °C, Fuel supply turned off, while oxygen is flowing at the cathode side.

If the cell is fully reduced as well as dried of any water (product of the reduction process), the voltage corresponds to the initial value - assuming no cell damage due to the oxidation. This potential as well as equation 2.9/2.10 imply that Ni can not only act as a catalyst but also as a reactant, which is, however, detrimental to the cell structure. In order to prove the electrochemical oxidation, the so-called non-fuel current experiment can be conducted [51]. Figure 2. 5 shows a current-time plot of this experiment. During the experiment the fuel is shut off, while oxygen still flows at the cathode side. Then, the current is increased, so the voltage becomes lower as the calculated RedOx potential. Subsequently, the voltage is held at 0.335 V, while the current behavior is observed. In [51] no explanation for the current drop is given, but it can be assumed that it is due to decreasing reaction kinetics and the limited amount of nickel. A value for the DoO during this experiment is not reported.

As reaction kinetics of nickel oxidation are quite crucial for the cell damage during start up

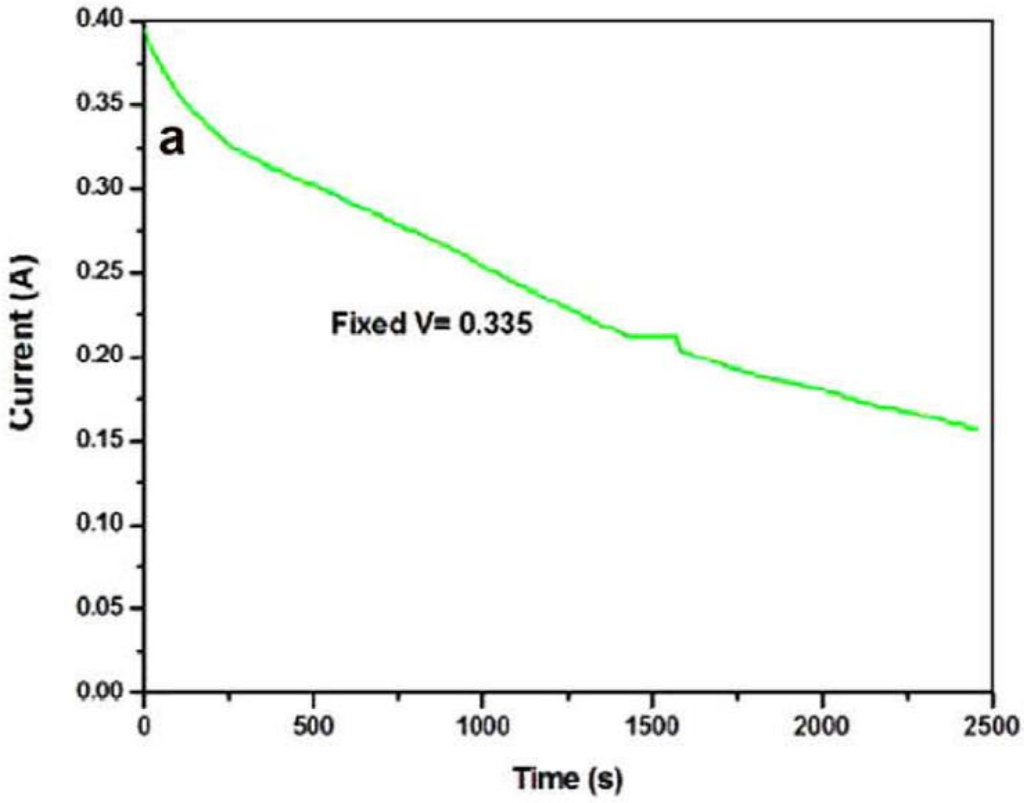

Figure 2. 5: Non-fuel current experiment conducted with a fixed voltage of 0.335 V at a temperature of 800 °C [51].

and shutdown, a brief summary should be given in the following section:
As the nickel oxidation begins, a thin oxide layer is formed on the Ni surface. At the beginning the process follows logarithmic laws. While the layer becomes thicker, the characteristic becomes parabolic (WAGNER-theory) according to equation 2.11, where y is the thickness of the oxide layer and k_p and t are the parabolic rate constant and the time, respectively [52].

$$y^2 = k_p \cdot t \tag{2.11}$$

In the typical temperature region of SOFC operation (300-800 °C), the activation energy of nickel oxidation could be determined to 144-150 kJmol^{-1} [41, 53, 54]. Nickel oxidation also depends on the oxygen partial pressure according to equation 2.12 [14], which implies that a low partial pressure reduces the growth rate.

$$k_p \propto (p_{O_2})^{1/6} \tag{2.12}$$

In comparison to the oxidation behavior of pure nickel, Ni/8YSZ cermets oxidize at lower temperatures and higher rates, respectively. Since 8YSZ is able to transport oxygen ions, it

supports the oxidation process [55, 14, 36]. Figure 2. 6 shows the oxidation behavior of Ni/8YSZ half-cells conducted between 400 °C and 800 °C with 1.2 slpm air flow rate conducted by [36]. Based on these results, the activation energy was determined to 114 ± 4 kJmol^{-1}, which is lower

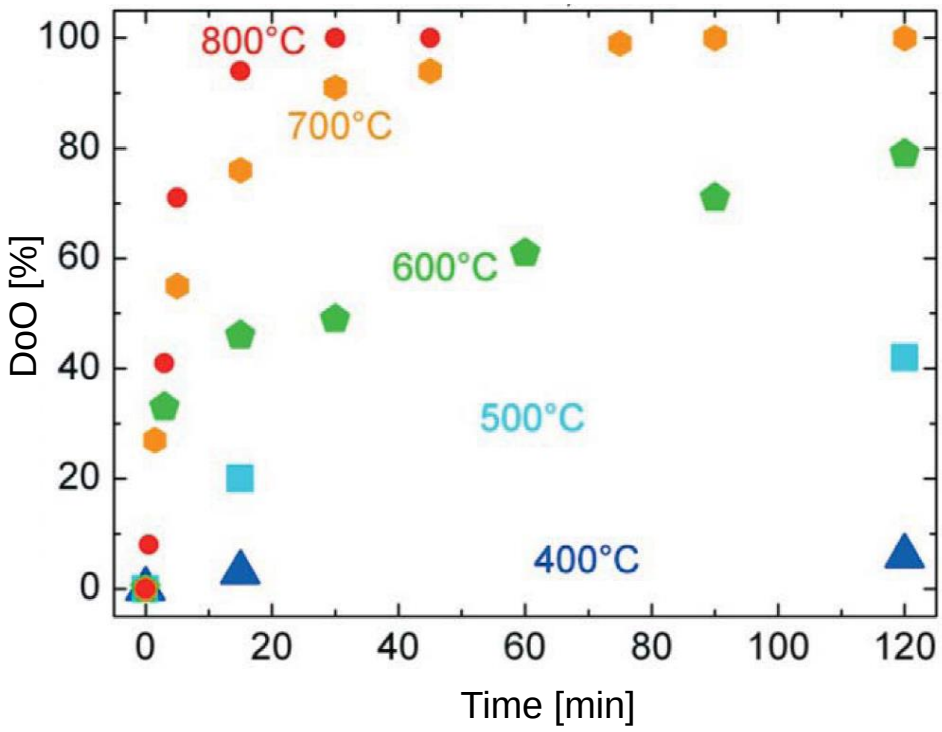

Figure 2. 6: DoO as a function of time and temperature. Experiments were conducted with half-cells (Ni/8YSZ) with an air flow rate of 1.2 slpm air by [36]

than the activation energy for nickel oxidation, corresponding very well with the explanation given before. According to this data, nickel oxidation has to be taken into account over 400 °C.

2.2 RedOx-induced cell degradation

RedOx-induced cell degradation can be divided into a smooth performance decrease and an abrupt failure of the entire cell, the latter one being the key issue for EK stack development. For this reason this section focuses on a detailed description of the mechanical damage behavior. Nevertheless, a brief summary of microstructural changes inducing lower power density should be given[14]:

- 8YSZ network with higher porosity, coarser pores, and lower conductivity of the anode

material [39, 56]

- Cracks in the nickel network and thus a lower amount of conductive pathways [57]
- Decrease of the triple phase boundary [49]
- Decrease of gas diffusion [34]

The mechanical failure of cells is induced by dimensional changes of the anode cermet during RedOx. The dimensional changes come from the volume change from Ni to NiO, which is around 70 % [58]. For Ni/8YSZ the strain is clearly lower, but still detrimental to the cell. Figure 2. 7 shows the relation between the DoO and the strain of a Ni/8YSZ cermet [59]. The

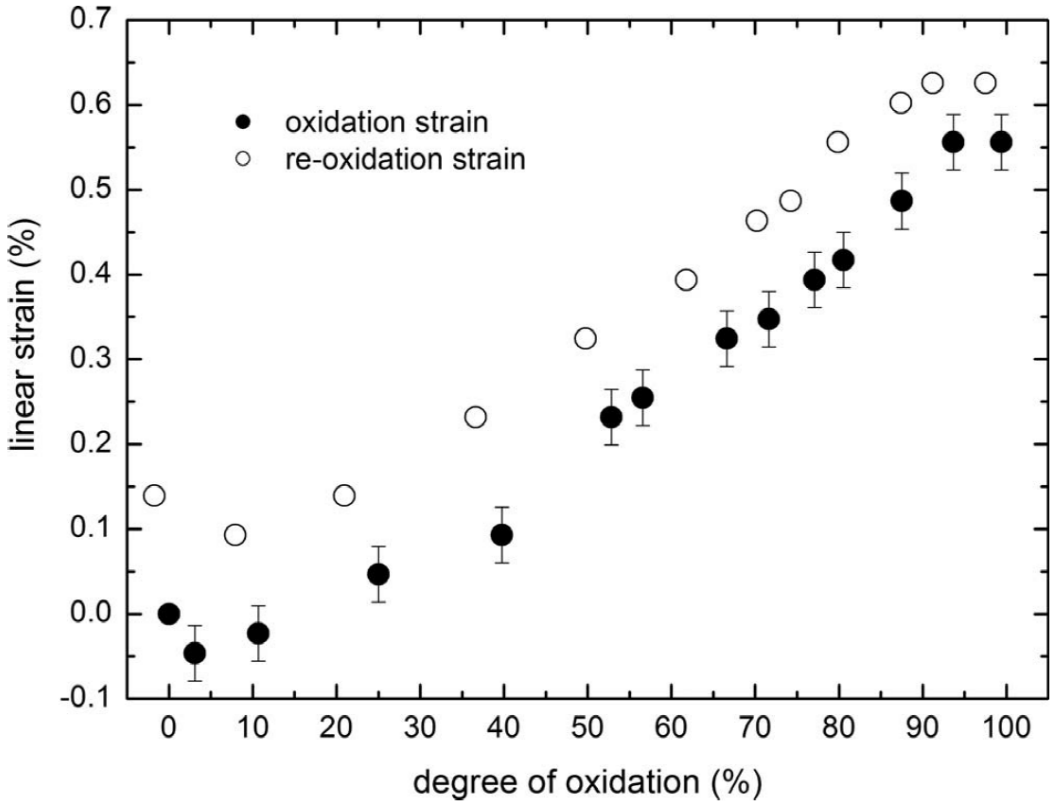

Figure 2. 7: Expansion strain of anode substrates as a function of DoO [59].

first complete oxidation causes a strain of 0.5 % and closely matches results from [60] (0.3-0.4 %) and [61] (0.6 %). As can been seen from the figure, successive RedOx cycles cause accumulated expansion strain putting the electrolyte under tension. The expansion comes from intergranular pores, which lead to a sponge-like microstructure, also known as closed porosity [62, 41]. Once the fracture stress of 8YSZ-electrolyte material (180-220 MPa) is exceeded, the electrolyte cracks

[57]. Conveniently, after fabrication there are residual compressive stresses at the electrolyte as a consequence of a difference in CTE of anode and electrolyte [63]. The stresses within the electrolyte depend not only on the DoO, but also on the cell design referred to in figure 2. 8. To resist the thermomechanical loads, one of the cell layers must provide sufficient mechanical

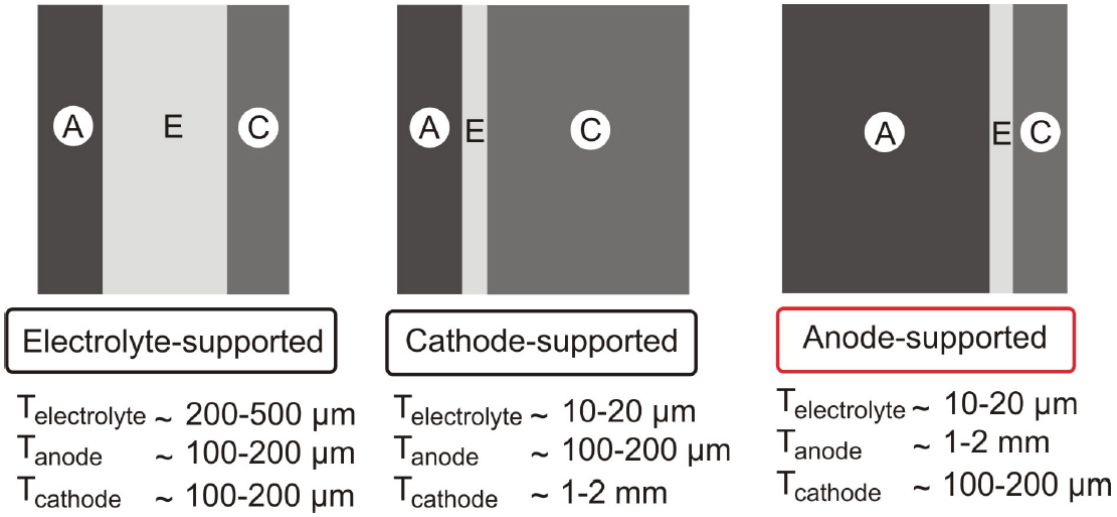

Figure 2. 8: Different ways of fabrication: Anode/Cathode/Electrolyte supported with an example of different thickness ratios [64]

properties to support the entire cell. This task is assumed by the thickest layer, so there are electrolyte (ESC), cathode (CSC) and anode supported cells (ASC). The latter is used for EK-stacks, which have an electrolyte thickness of 10 μm, anode thickness of 290 μm and cathode thickness of 60 μm. The advantage of ASCs lies in the high power densities due to their thin electrolyte. However, ESCs are more stable concerning RedOx compared to ASCs. Since in the case of ASCs the thick layer expands (whereas the thin layer has to withstand this expansion), the tensile stresses occurring in the electrolyte are fundamentally higher for ASCs [60]. Once the electrolyte cracks, the problem becomes worse, because of additional oxygen flowing through the leaking electrolyte. Figure 2. 9 gives an impression of the impact of RedOx on anode and electrolyte. Figure 2. 9a) shows a RedOx-induced crack in the electrolyte captured by SEM imaging [49]. 2. 9b) shows a layer of a stack, which was operated under oxidizing conditions during start up and stop as part of this research. The color of the anode material shines through the electrolyte. Next to the cracks it appears green (oxidized), while reduced areas appear in dark gray. At this point it should be mentioned that the color of oxidized cermet depends on the temperature during oxidation. With decreasing temperature the green changes smoothly

to grey color. This behavior of oxidation temperature-dependent color was observed in this research and fits to the appearance of RedOx samples of [36], where no explanation can be found. In [65] the color change is explained by the non-stoichiometry of the oxidation reaction. On the one hand this makes it difficult to differ between oxidized and reduced areas, but on the other hand a distinction between low and high temperature oxidation can be made.

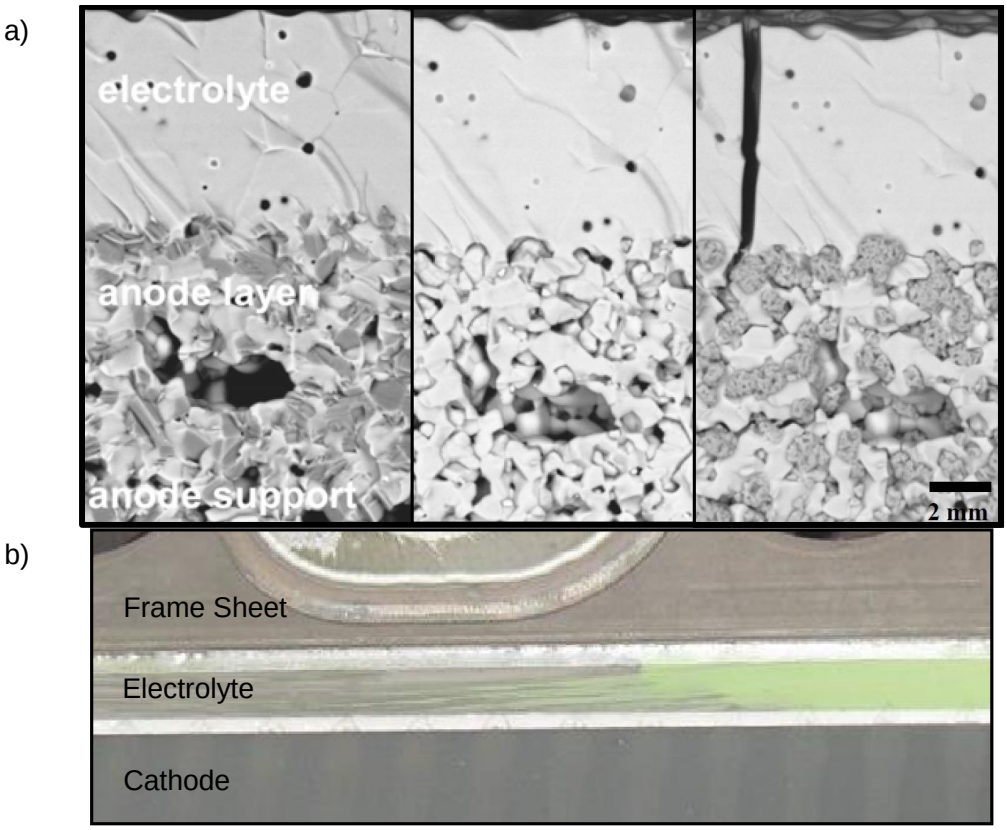

Figure 2. 9: a) Scanning electron microscope (SEM) picture showing microstructural changes in the anode cermet. Starting with the new manufactured cell before reduction on the left, reduced state in the middle and re-oxidized state with crack in the electrolyte [49] b) Photo of a stack layer operated without protective gas during start up and stop in this research

2.3 RedOx solutions

Since the RedOx-induced failure of SOFCs is a big issue, the scientific community has endeavored to find a solution over the last few years. Research conducted up to now can be divided into solutions at cell, stack and system level according to 2. 10. Some results were quite promising, so they are included in state of the art anodes such as the gradation of nickel content [66], a

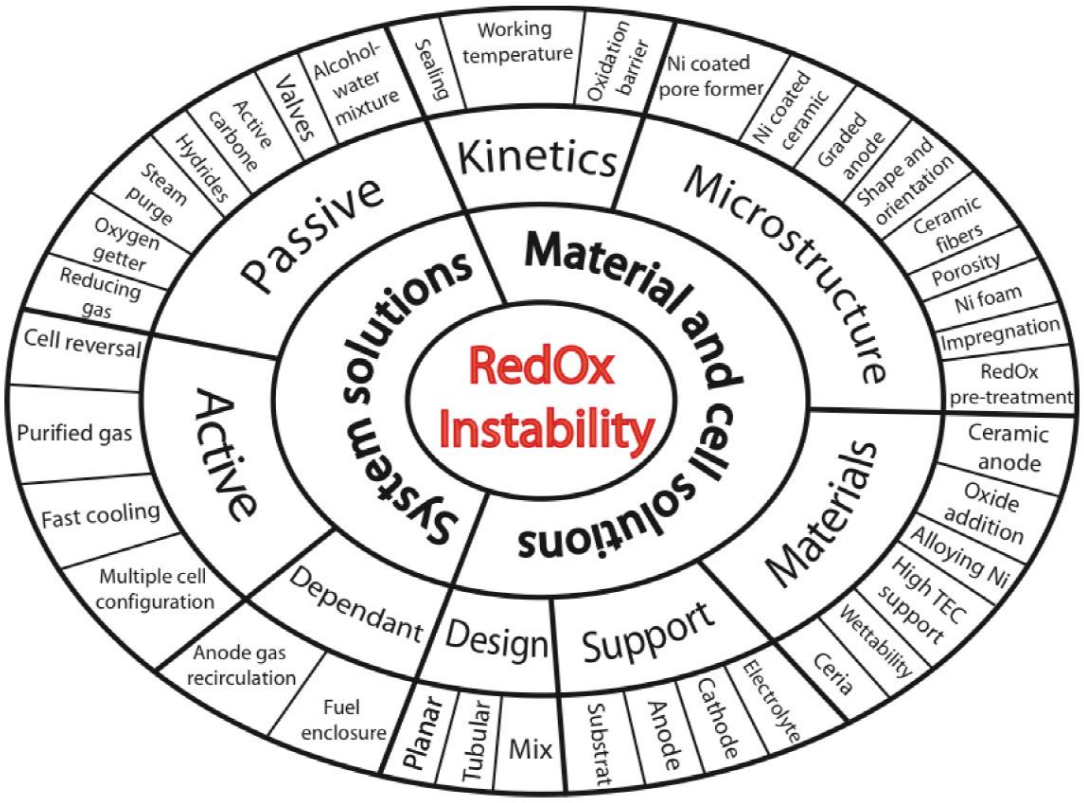

Figure 2. 10: Summary of the solutions and influencing factors for anode RedOx instability [14]

low ratio of fine to coarse 8YSZ particles [67] or the influence of the porosity on the speed of oxidation under same conditions (The lower the porosity, the lower the speed of oxidation) [36]. However, there is no final solution for a marketable product for the following reasons:

- Many of the measures increase the RedOx stability, but do not completely prevent reoxidation. For a marketable product absolutely no RedOx is acceptable. The market has strict requirements regarding degradation, where there is no room for additional degradation due to RedOx. Nevertheless, the advances in RedOx stability are quite important, because it improves the stability regarding incidents like an emergency stop
- Measures that are unreasonably costly
- Measures that decrease the power density
- **Limited effect of some measures, because the oxygen source is not correctly located. For example the usage of an oxygen getter in the exhaust pipe, while the oxygen still comes through a bad cell sealing**

Chapter 3

RedOx behavior in operation - development of new measuring methods

This chapter forms the core of the present research as it presents the development of new measurement methods, which are able to describe the RedOx behavior of cells, stacks and systems. It refers directly to the item in bold on the previous page. The successful application of the methods developed in combination with different stack and system tests will determine whether the start up or the shutdown phase is the major contributor to RedOx-induced degradation. Moreover, the influence of the system setup on the oxidation will be investigated. The determination of a DoO (not only for SOFCs) is not a new problem. Thus, there is already a range of methods in existence such as gravimetric determination (weight before and after oxidation), determination of the porosity gain, analysis of SEM-pictures by phase characterization, density determination or chemisorption [36]. However, none of the methods can be used within operation and thus without destructive disassembling of stacks and systems. The second problem is that it is quite difficult to make a difference between start-up and shutdown oxidation. In a standard test run without forming gas (mixture of 5 % H_2/95 % N_2 always used in this work) the cells oxidize during start up. At operation they are reduced by the fuel. During the shutdown phase oxidation takes place again. Consequently, afterwards only the oxidation due to shutdown can be measured. If only the start up oxidation is of interest, the stack must be shutdown without operation and without reducing or oxidizing atmosphere which is almost impossible.

The methods developed in this work are based on the voltage characteristic during a RedOx cycle according to figure 3. 1 and described in detail in chapter 2.1. During initial experiments

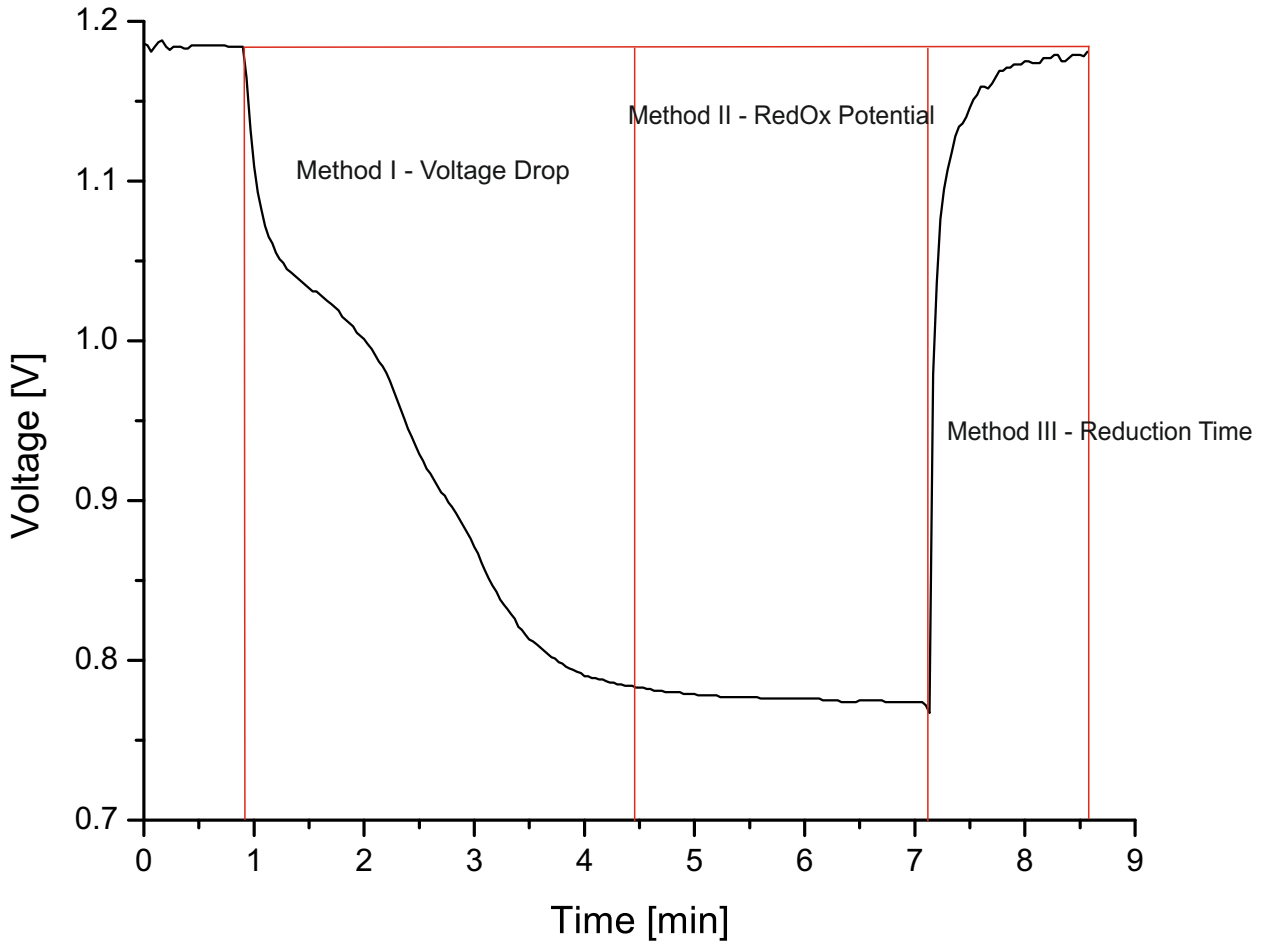

Figure 3. 1: Voltage characteristic during a RedOx cycle and relation to the measurement methods developed in this work.

it was found that the voltage behavior significantly depends on the amount of air flowing to the anode and thus on the DoO of the cell. From this observation three methods could be developed, which are named after the phase of the cycle, so there is the voltage drop, the RedOx potential, and the reduction time method.

Since research on the RedOx topic is very material- and cost-consuming, the fundamental method development has to be conducted with single layers of the stack. As there was no test equipment at the beginning of this work, a special test bench was developed, which is presented in the first section of this chapter, followed by the measurement methods that were developed (chapter 3.2 - 3.4). To make sure the methods do not only work for single layers, chapter 4 validates the methods by stack testing. Chapter 5 deals with the actual measurement of stack's and system's RedOx behavior.

3.1 The single layer test bench

This section deals with the construction of a test rig for single layers, where the method development of this work takes place. The test rig aims the electrochemical characterization of single layers with the same size as original stack layers. The single layers consist of the cell soldered to the frame sheet as they are used for the actual stack design. For convenient testing

Figure 3. 2: Test rig consisting of the test bench with hot box in the middle at the EK testing laboratory.

a quick and non-destructive cell change must be possible, thus sealing by welding or soldering is no option. Operation at around 800 °C must be possible, which requires heating options as well as high temperature insulation.

Figure 3. 2 shows the test rig at the EK testing laboratory. Basically the test rig consists of a hot box (in the center of the picture) and the actual test bench. The hot box includes two steel plates consisting of heating elements, gas distribution and temperature measurement for

anode and cathode side of the single layer according to figure 3. 3 on the right. The temperature

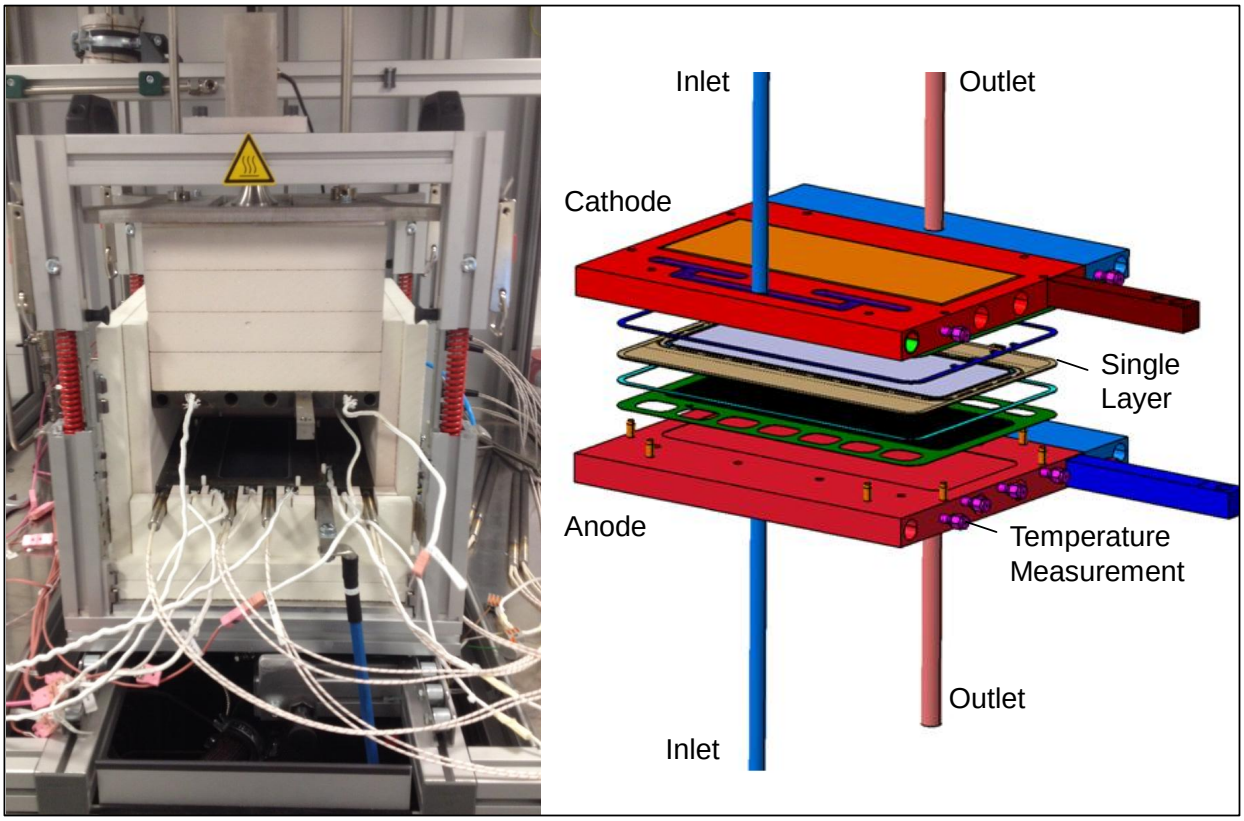

Figure 3. 3: Left: Hot box in the open position, Right: Exploded view of the steel plates housing the single layer.

measurement includes both gas temperatures at the in- and outlet and three material test points under the cell, where the one in the middle is the input value for the temperature control. For electrical current collection, a stack interconnect plate is assembled on both sides by welding in combination with a nickel grid at the anode side and a platinum grid at the cathode side. Whereas the nickel grid matches the stack design, the platinum grid replaces the cathode contact paste, because a paste is only for single use and also difficult to remove. The electrical insulation between anode and cathode side as well as the sealing is ensured by mica gaskets. This type of gasket is only tight under compression, which is ensured by four springs integrated into the frame of the hot box pressing the steel plates together. To ensure good contact between contact grid and the cell, it is very important, that the design comes with an exact height adjustment. The biggest risk for a good adjustment lies in the unknown compression behavior of the mica seals. For this reason, compression tests with the mica sealing material were conducted at the

Jülich Research Centre (Forschungszentrum Jülich) to support this work [68]. In addition to that, a contact force can be applied to the cell area. The contact force can be adjusted by a screw and is supervised by a force sensor to guarantee the same testing conditions for all cells. A test run always begins with the assembly of the cell into the hot box. Therefore the upper part of the hot box can be lifted up (figure 3. 3), so the single layer tested before can easily be removed as well as the mica gaskets, which are only for single use. As soon as the new layer and the gaskets are put into the box, it is closed.

Safe operation of the hot box is provided by the test bench surrounding the box. In the event of the housing possibly leaking, hydrogen can be exhausted. Moreover, temperature monitoring with included emergency shutdown in combination with smoke and gas sensors ensures a safe operation. In addition to the safety devices, the test bench supplies different gases, controls the temperature and records all important values measured. The test bench is supervised by a computer, where controlling is either based on a R-I flow sheet of the test bench (simplified version is shown in figure 3. 4) or automatically by a programmed test sequence. The special

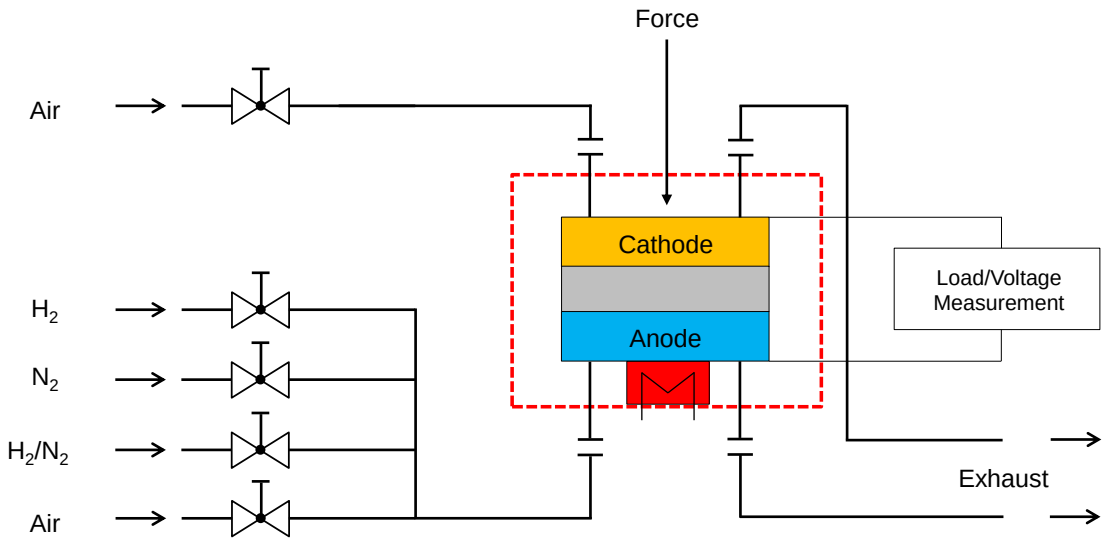

Figure 3. 4: Simplified R-I flow sheet of the test bench.

feature of this test bench is the option to supply air also at the anode side for specific RedOx testing. With the mass flow controllers the exact amount of every gas can be adjusted. In this

work every test sequence begins with heating up and reduction of the cell. The reduction begins as soon as the temperature rises to 800 °C and works by a mixture of N_2/H_2. During heating and reduction air is supplied to the cathode side. After this procedure the cell is ready for different tests such as power density measurement by current-voltage plots, long term degradation tests or RedOx testing. Targeted oxidation can be adjusted by the amount of air flowing to the anode. This amount depends on the value set at the mass flow controller (anode) and the air flow at the cathode. Even if there is no air flow at all, there is oxidation, since the mica gaskets are never entirely tight. In general, an oxidation test can be performed at different temperatures as well as during the heating up and cooling down period.

3.2 Voltage Drop Method

This section describes the first measuring method based on the voltage drop from OCV to the RedOx potential. Consequently, at the beginning of the measurement the cell is fully reduced and hydrogen/forming gas must be supplied to the anode. The objective of the voltage drop measurements is to find out if there is a correlation between this drop and the amount of air flowing to the anode. Figure 3. 5 shows the first voltage drop experiment conducted on the single layer test bench. Every test is started by closing the forming gas valve. Afterwards different conditions are set influencing the drop down curves. Test 1 and 2 show the drop down at 620 °C and 700 °C, while all anode gases are turned off and 5 slpm air are supplied to the cathode. At both temperatures the RedOx potential is reached after around 300 seconds. The measured values for the RedOx potential decrease with rising temperature match the calculated values very well (Equation 2.10/Figure 2. 3). The drop characteristic follows the NERNST equation, since at the very beginning the air flow to the anode leads to rising water content. In the case of test 1 and 2 the air can come from the cathode as well as through the mica gaskets. Test 3 is conducted at 700 °C without air at the cathode side, assuming less air flowing to the anode and thus a slower voltage drop down. However, the voltage drop down behaves differently than expected, because it falls a little faster. An explanation can be found from the calculated OCV, where 0.21 bars is assumed for the oxygen partial pressure. Small defects in the electrolyte do not only let air flow to the anode, but also causes hydrogen to flow to the cathode, dropping the oxygen partial pressure. Depending on the type of defect and pressure/flow conditions, one of the effects dominates the drop down. For example a test run with an old, leaking stack showed a drop down to a voltage of zero, when the air supply was shut down and while hydrogen was still

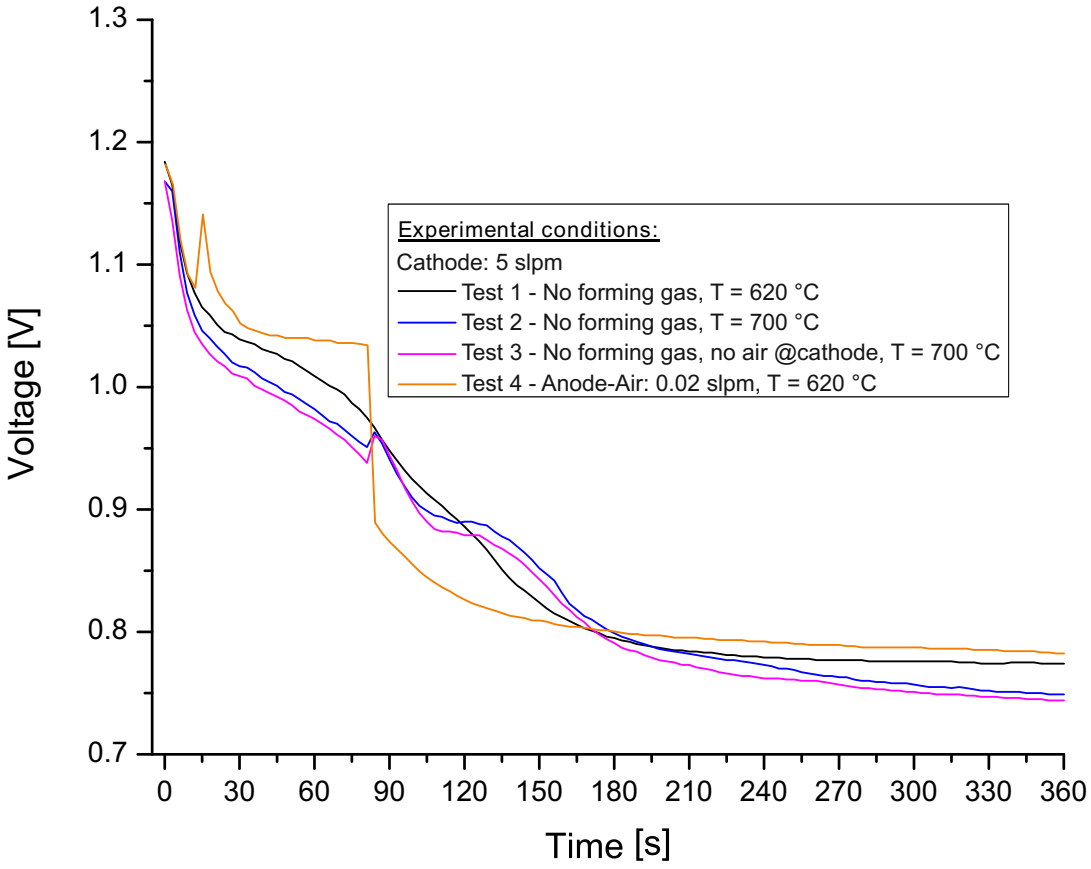

Figure 3. 5: Voltage drop down of the single layer after fuel shutdown in different conditions.

supplied to the anode. Since tests 1 to 3 did not lead to significantly different behavior, test 4 was conducted with additional air at the anode by opening the valve to 0.02 slpm. However, at the beginning the drop down is very slow, because the air pushes the remaining forming gas out of the pipes. For the first 90 seconds forming gas is still supplied to the cell this way, distorting the drop down behavior. At 90 seconds, air arrives at the cell leading to a sudden voltage drop. Summarizing the first testing at the single layer test bench, it is very tricky to simulate realistic leaking conditions, particularly for a short period of time where the drop down takes place. For this reason, an additional stack test was conducted as illustrated in figure 3. 6. The test is based on a used stack consisting of partially leaking layers, which is very convienent, because it shows the difference in drop down behavior very well. At the beginning of the test, the stack was operated at 627 °C with air at the cathode side during the drop down. Before the drop down every layer started at a different OCV indicating a different state of tightness. The drop down behavior follows the rule - the lower the OCV, the faster the drop, and the higher the leakage. For example layer 1 (black curve) starts at 1.25 V and needs 210 seconds for its drop

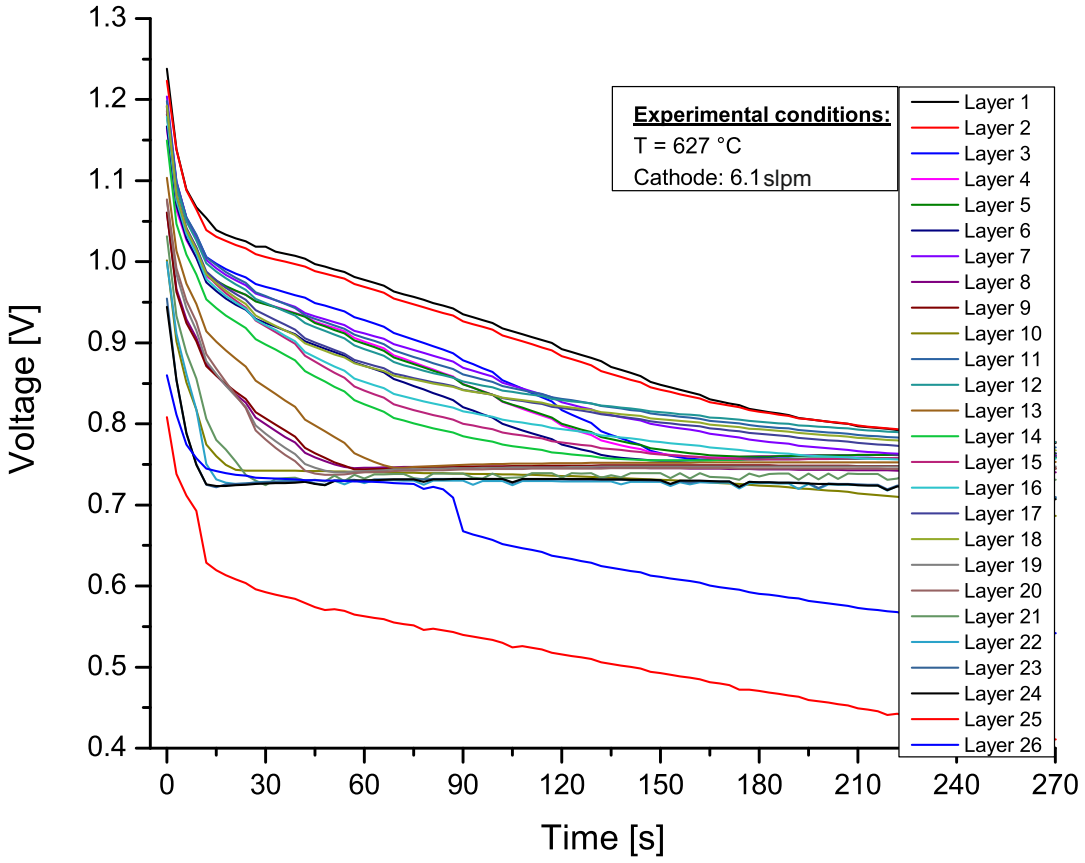

Figure 3. 6: Voltage drop down of stack layers after fuel shutdown at 627°C.

down to the RedOx potential, while layer 14 (green curve) starts at 1.15 V and needs around 160 seconds. The damage of layer 25 and 26 was very high, so that their OCV was almost at the value for the RedOx potential and falls below the potential respectively, which is discussed within the next section.

To conclude, the voltage drop method characterizes to what extent a layer/stack leaks. However, the voltage drop is quite short even for tight layers. Additional air flowing to the cell after the drop down is not captured by this method, but leads to further oxidation. Additional air comes from external sources such as the system exhaust pipe. Consequently, the air has to pass a longer way. Arriving at the anode, the voltage has already fallen to the RedOx potential. Moreover, the development of a new method should always come with a benefit. In this case, there is no additional information compared to the OCV value, which is well-known a leading criterion for tightness. However, the results presented here give a good introduction into the electrochemical behavior during RedOx as they throw up new questions such as the drop down below the RedOx potential.

3.3 RedOx Potential Method

The section deals with the question brought up in the previous section, why and when the voltage falls below the RedOx potential and if there is a possibility to use the drop down for a description of the DoO. Figure 3. 7 shows the voltage curve during an isotherm oxidation at 620 °C with additional air flow at the anode side and no air at the cathode side. The initial fall from OCV to the RedOx potential is well-known from section 3.2. The voltage stays at

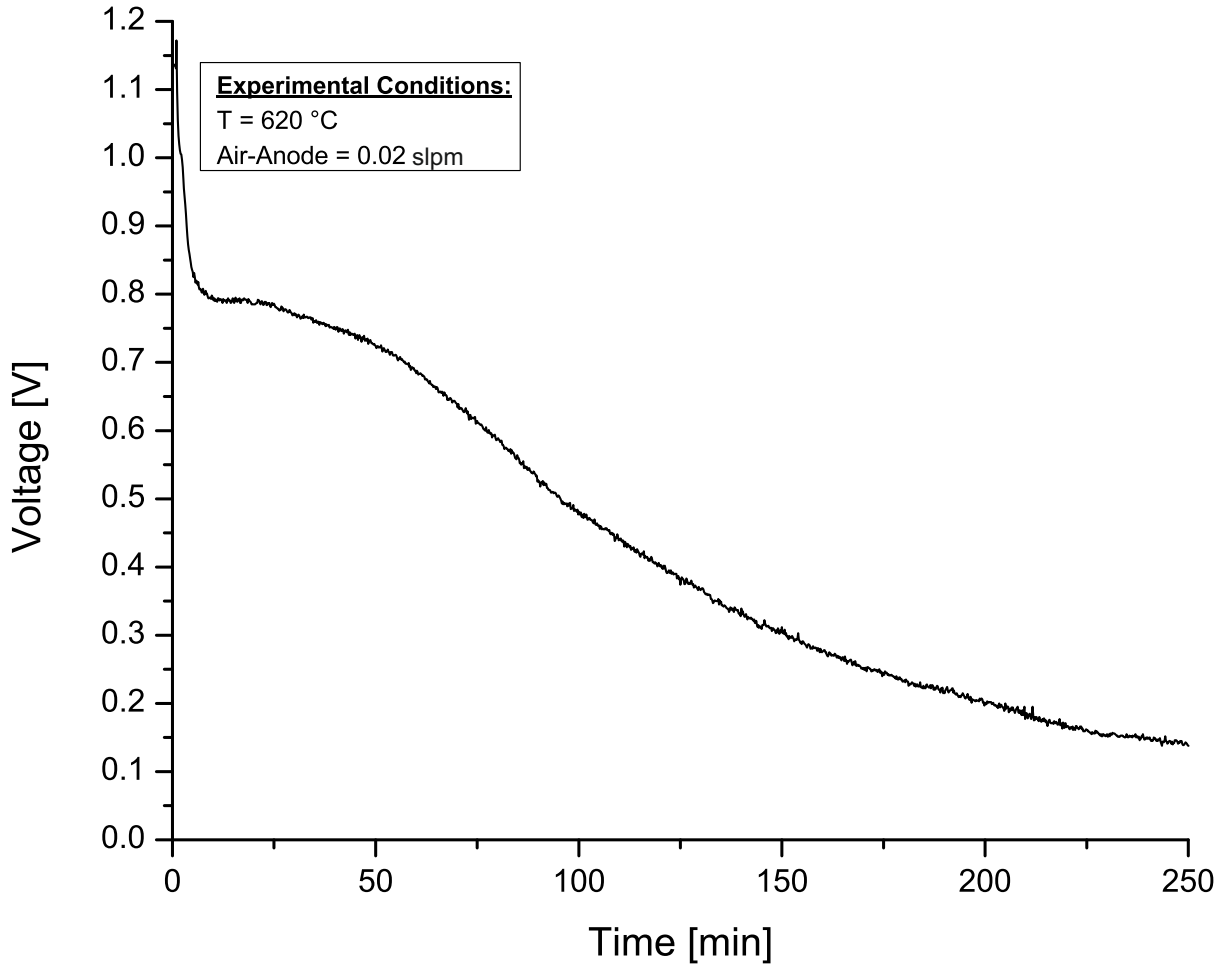

Figure 3. 7: Voltage characteristic of the single layer as a function of time during oxidation at 620 °C.

the RedOx potential for around 25 minutes and drops down almost to zero within four hours. The voltage drop investigated in the last section was caused by rising water content. Obviously the voltage drop below the RedOx potential must be associated with a change in the oxidation state, because the DoO is the only thing changing during several hours of air being supplied to the anode. If this assumption is right, the voltage must depend on the air flow as investigated by the following experiments. Figure 3. 8 shows the voltage behavior during three hours of isotherm

oxidation at 700 °C without air at the cathode, but with different air flows at the anode side. At

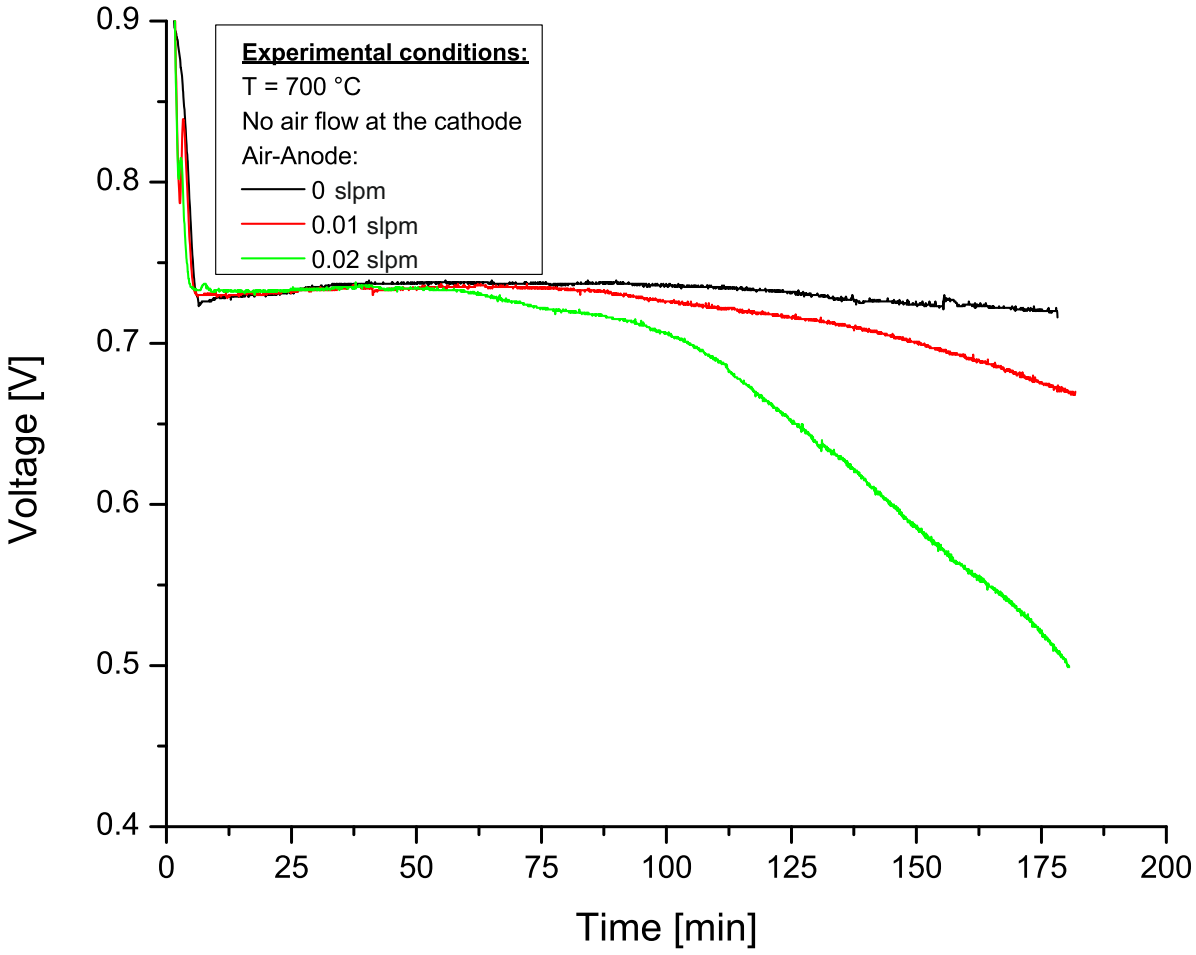

Figure 3. 8: Voltage characteristic of the single layer as a function of time during oxidation at 700 °C at different anode air flows.

the beginning all curves go down to the RedOx potential as observed before. After one hour of oxidation, the curve shape depends on the air flow - the higher the air flow, the faster the voltage drop down. This relation is very important, since it enables the comparison of the oxidation behavior of different stacks and systems. To give an example, the following situation should be assumed: There are two stacks of the same sealing quality (indicated by equal OCV values) built in two different SOFC systems with different exhaust pipes, reformers etc. the voltage drop down can be compared and thus the better system setup concerning the amount of oxidation can be chosen. Furthermore, different drop downs can be related to degradation rates and to a maximum number of RedOx cycles. Once a well-known stack should be integrated into a new system, the drop down times give a first indication of the expected lifetime. Normally, oxidation takes place during the start up and the shutdown period. Consequently, this method comes with

no additional measuring effort, but consists only of analysis of the voltage curves during these two periods. As the previous experiment was only isotherm, oxidation tests during start up and cool down must also be conducted. Figure 3. 9 shows the curve shape for shutdown oxidation with different air flows at the anode side. Oxidation starts at 700 °C and takes three hours,

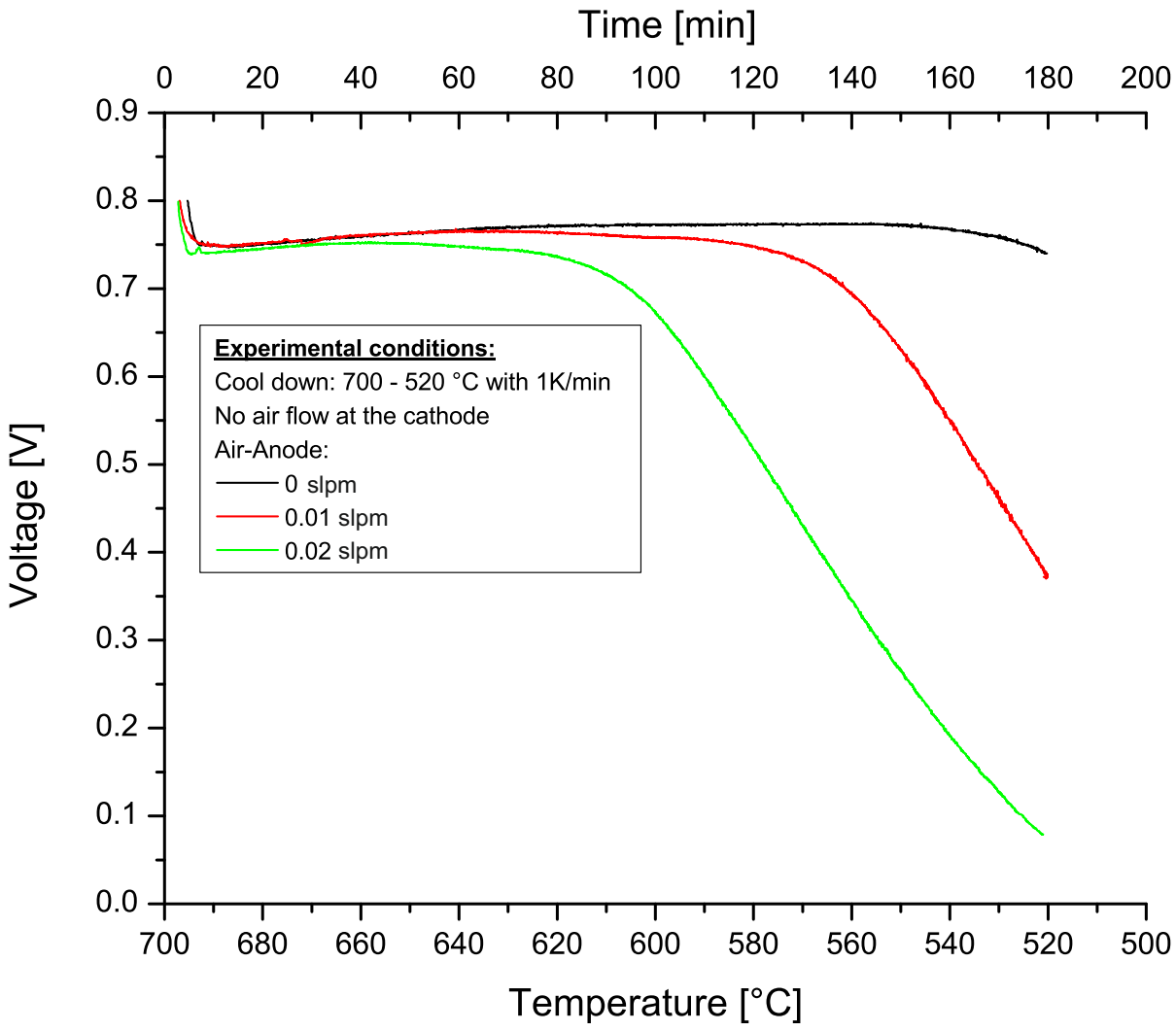

Figure 3. 9: Voltage characteristic of the single layer as a function of time during oxidation and cool down from 700 °C at different anode air flows.

while the temperature is ramped down by 1 K/min. The general drop down characteristic is similar to the isotherm experiment, which makes the method work for shutdown investigations. At the beginning of the experiment, the voltage rises with falling temperature. This effect is well known from the calculation of the RedOx potential behavior by equation 2.10 described before. However, the subsequent drop down is faster compared to the isotherm experiment. Moreover, the oxidation kinetics becomes slower with falling temperature, so the drop down cannot be

caused by a higher DoO. So, the voltage drop down seems not only to depend on the oxidation state, but also on the temperature. For this reason it is very important to always compare the voltage drop down at the same temperature. To complete the method development, figure 3. 10 shows the oxidation behavior during start up. For this experiment a fully reduced single layer

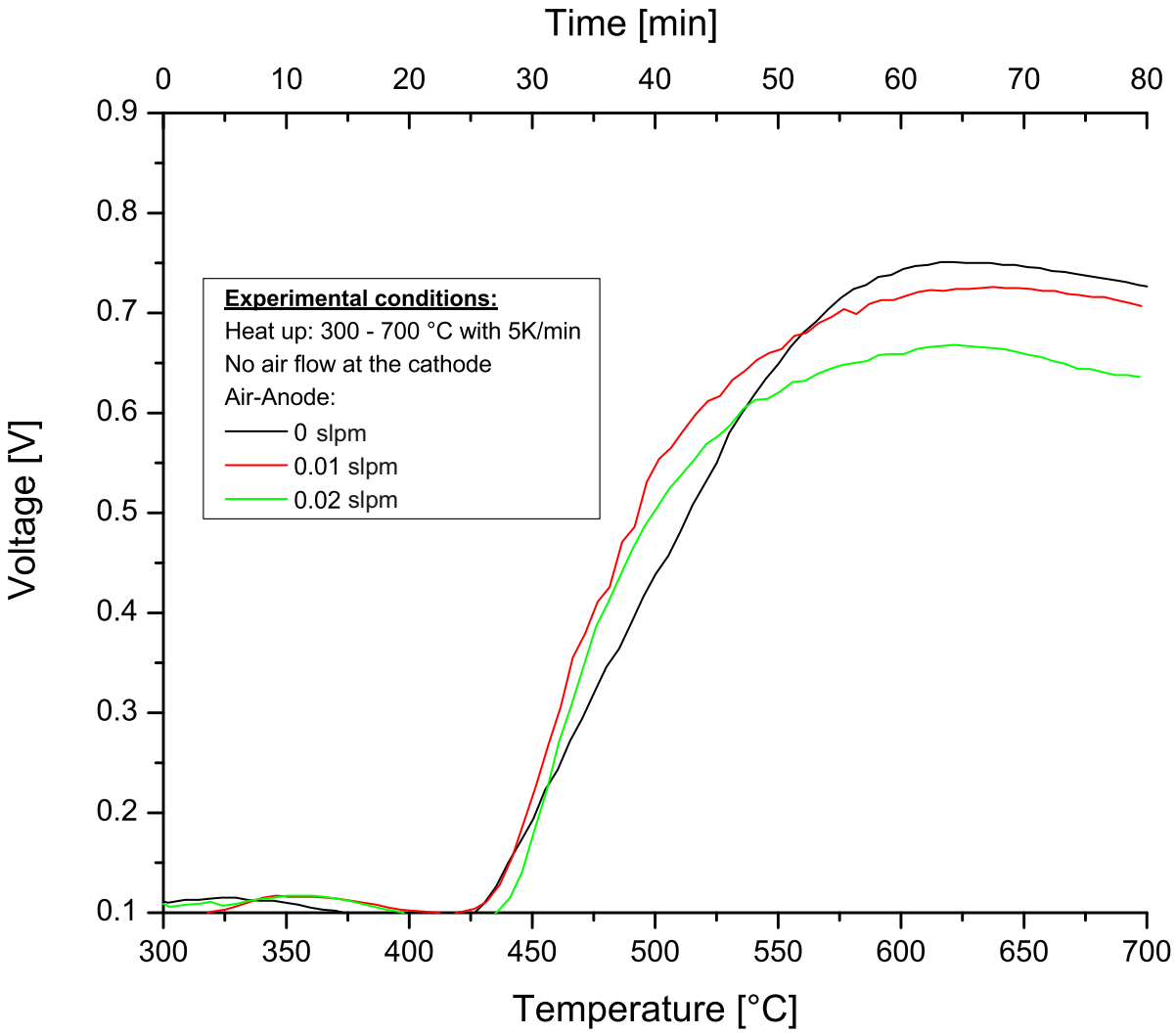

Figure 3. 10: Voltage characteristic of the single layer as a function of time during oxidation and heat up to 700 °C at different anode air flows.

was heated up from 300 °C to 700 °C by 5 K/min again, with different values for the air flow at the anode side. All curves begin their rise at 425 °C, which correlates well to the beginning of significant oxidation kinetics (cf. figure 2. 6). The increase of all voltage curves is approximately the same, whereas all curves reach a different maximum depending on the air flow - the higher the air flow, the lower the maximum.

Even if all information for a successful application of this new measuring method is given by

the previous experiments, there is still the question of where the voltage drop down comes from and why it depends on the DoO as well as on temperature.

The water pump model

In order to gain an understanding of this, a model can be built, which is based on the previous experiments as well as on the basics of electrochemical oxidation according to chapter 2.1. The model can be easily explained by figure 3.11 illustrating a water pump. The height of the tank

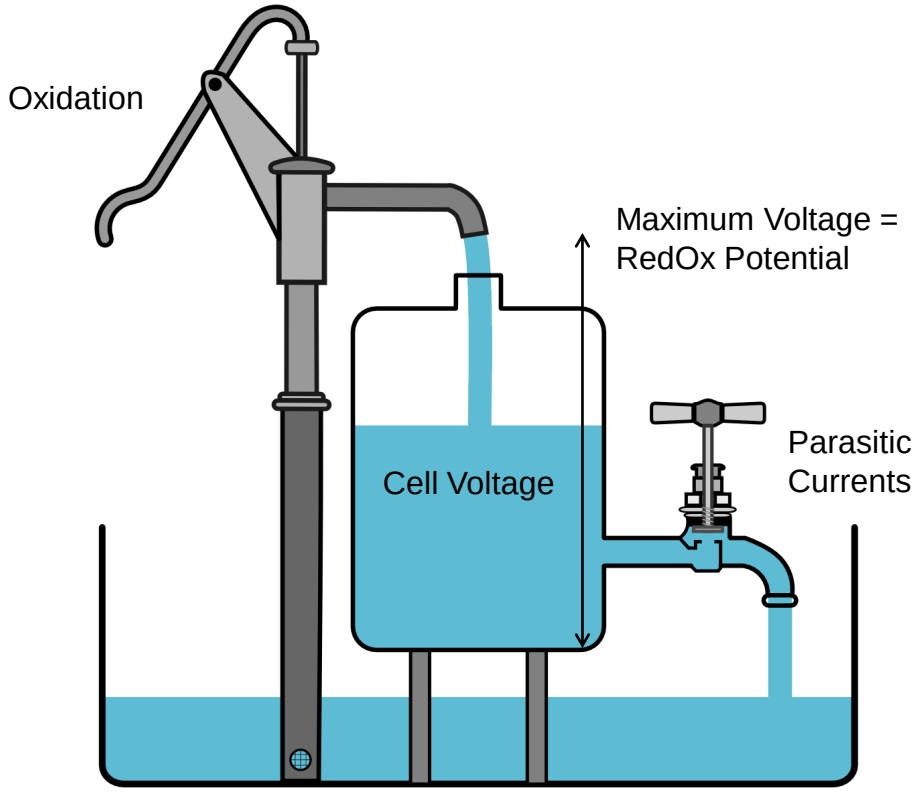

Figure 3.11: The relation between oxidation speed and actual cell voltage behavior illustrated as a water pump model. Amount of water = cell voltage, Pump = speed of oxidation, Water tap = parasitic current [69].

and the pump represents the maximum of voltage according to the calculated RedOx potential. The actual amount of water in the tank stands for the cell voltage measured. Since no cell and stack configuration is entirely perfect, there is always a small parasitic current represented by the water tap in the diagram. Just as the open water tap lowers the amount of water in the tank, the parasitic current lowers the cell voltage. In the model the tank is refilled by a water

pump according to the oxidation 'producing' electrons at the anode side by electrochemical oxidation (figure 2. 2). As long as the electrochemical oxidation produces more or just as many electrons as consumed by the parasitic current, the voltage measured is equal to the RedOx potential. Once the oxidation speed falls under a certain level, the voltage drops down. With rising DoO the oxidation speed slows down as a consequence of growing oxide layers on the nickel particles. Consequently, the voltage drops faster with rising oxidation time and air flow at the anode, as both increase the DoO. At this point it is important to understand that oxygen at the cathode side is needed for electrochemical oxidation, while the oxygen at the anode side oxidizes the nickel without contributing anything to the voltage. For an ideal high voltage curve, only electrochemical oxidation should occur.

Another factor influencing the voltage curve is the temperature - a lower temperature also causes a faster voltage drop. At first glance, this behavior seems to be strange, because the DoO increases more slowly and thus there is a thinner oxide layer. However, lower temperatures lead to slower diffusion, eliminating the effect of a thinner layer. Moreover, the ionic conductivity of the electrolyte - needed for electrochemical oxidation - is reduced. Another possible effect can come from the increase of homogeneity of the oxidation. As described by Ettler, the oxidation becomes more homogeneous with lower temperatures [36], because the oxidation kinetics become slower. So the oxygen is not consumed by the first nickel particles getting in contact with them, but can diffuse deeper into the cell. This way, at higher temperatures the anode substrate can form a type of protective layer, where all the oxygen is captured and thus hindered from flowing to the anode functional layer, where the electrochemical oxidation takes place (cf. figure 1. 9). The relation from air flow to temperature defines whether this effect plays a role or not.

Check of the water pump model

In order to check the water pump model, the following experiments at the single layer test rig should be presented. The check works with target influencing of the water tap (parasitic current) and the refueling of the water tank (speed of oxidation). The target influencing checks whether the observed behavior of the cell voltage fits the presented model.

Figure 3. 12 shows the first part of an experiment conducting further research on the temperature dependence (speed of oxidation) of the voltage drop below the RedOx potential. The graph shows the voltage curves of isotherm oxidation at 550 °C, 650 °C and 750 °C without additional air at both electrodes as a function of time. As already known from the comparison

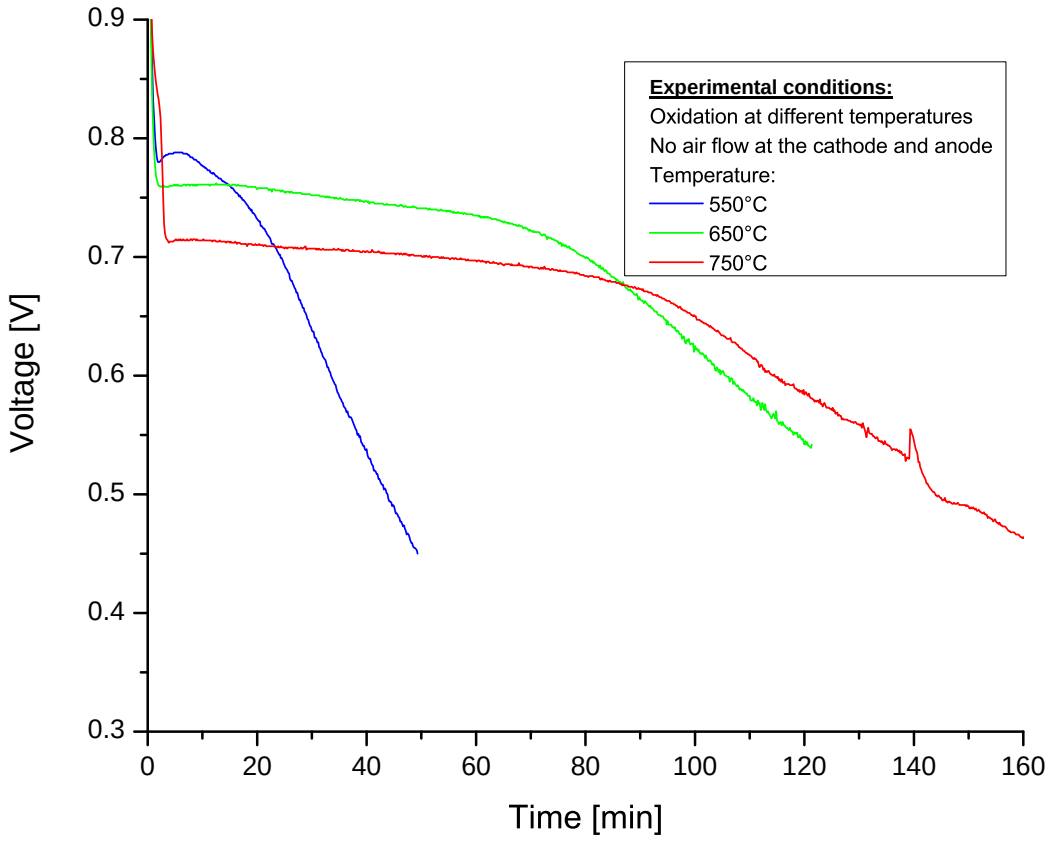

Figure 3. 12: Voltage characteristic of the single layer as a function of time during oxidation at different temperatures without additional air flow at the anode.

between cool down and isotherm oxidation curves before, the drop down is faster for lower temperatures and the curves start at a higher RedOx potential. The most exciting part comes with the temperature increase during oxidation in the second part of the experiment illustrated in figure 3. 13. The continuous lines still represent the voltage, whereas the dotted lines in the same color show the temperature of oxidation. After there was a large drop down at both temperatures, the test rig was heated up by 100 °C. Once the temperature increased, the voltages began to increase simultaneously. Looking at the blue lines (550 °C - Test 1) the voltage curve almost matches the curve of the isotherm oxidation at 650 °C. Consequently, in this case, the homogeneity of the oxidation is not responsible for the faster drop down, but only the kinetic of oxidation, which rises with the temperature.

In the following, the behavior of the voltage plots should be double-checked by discussing them in the background of occurring DoOs. The difference in DoO cannot be that big, because the

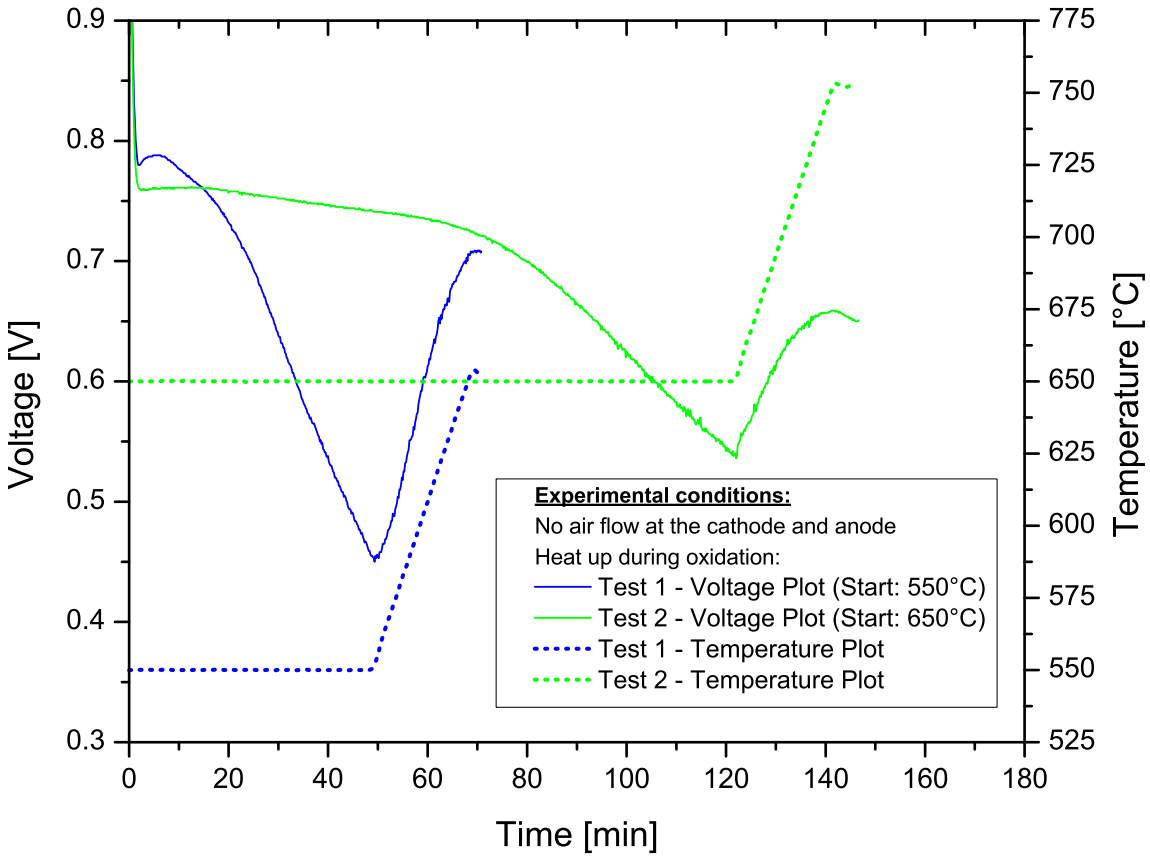

Figure 3. 13: Second part of the previous experiment: After isotherm oxidation the temperature is increased by 100 °C. Dotted lines = Temperature curve, Continuous lines = Voltage vs. Time.

voltage after 70 minutes of isotherm oxidation at 650 °C is even a little higher compared to the voltage after 50 minutes oxidation at 550 °C with subsequent heating to 650 °C. This is in good agreement with additional oxidation tests conducted as part of this work:
In those tests the DoO was measured to be around 6.5 % after 30 minutes at 700 °C and 5.5 % after 30 minutes at 500 °C without additional air at the anode. The DoO was determined by weight measurement. By measuring the weight before and after reduction of several single layers, the weight of oxygen was found to be 3.74 ± 0.04 g. For DoO determination, the single layer's weight was measured after oxidation. The small difference in DoO at different temperatures comes from the low amount of oxygen compared to tests by Ettler (cf. figure 2. 6) [36]. As long as there is less oxygen than the cell can consume in relation to the temperature-dependent oxidation kinetics, the temperature has no influence on the DoO - however, the homogeneity of oxidation can change.

Following the postulated water pump model, the characteristic of the voltage curves during oxidation is decisively influenced by the height of parasitic currents and the speed of the electrochemical oxidation, which in turn is influenced by the thermochemical oxidation at the anode side. At this point, the influence of the parasitic current is investigated. Here, no fuel current experiments provide the possibility to change the parasitic current and thus the electrochemical oxidation. Changing these parameters should affect the voltage curves in the way described - the higher the parasitic current, the faster the drop. The key factor of these experiments is the current applied to the cell without fuel at the anode, but during oxidation, simulating different parasitic currents.

Figure 3. 14 shows the first of these experiments, which essentially corresponds to the one before investigating isotherm oxidation. The experiment starts by shutting down the fuel flow

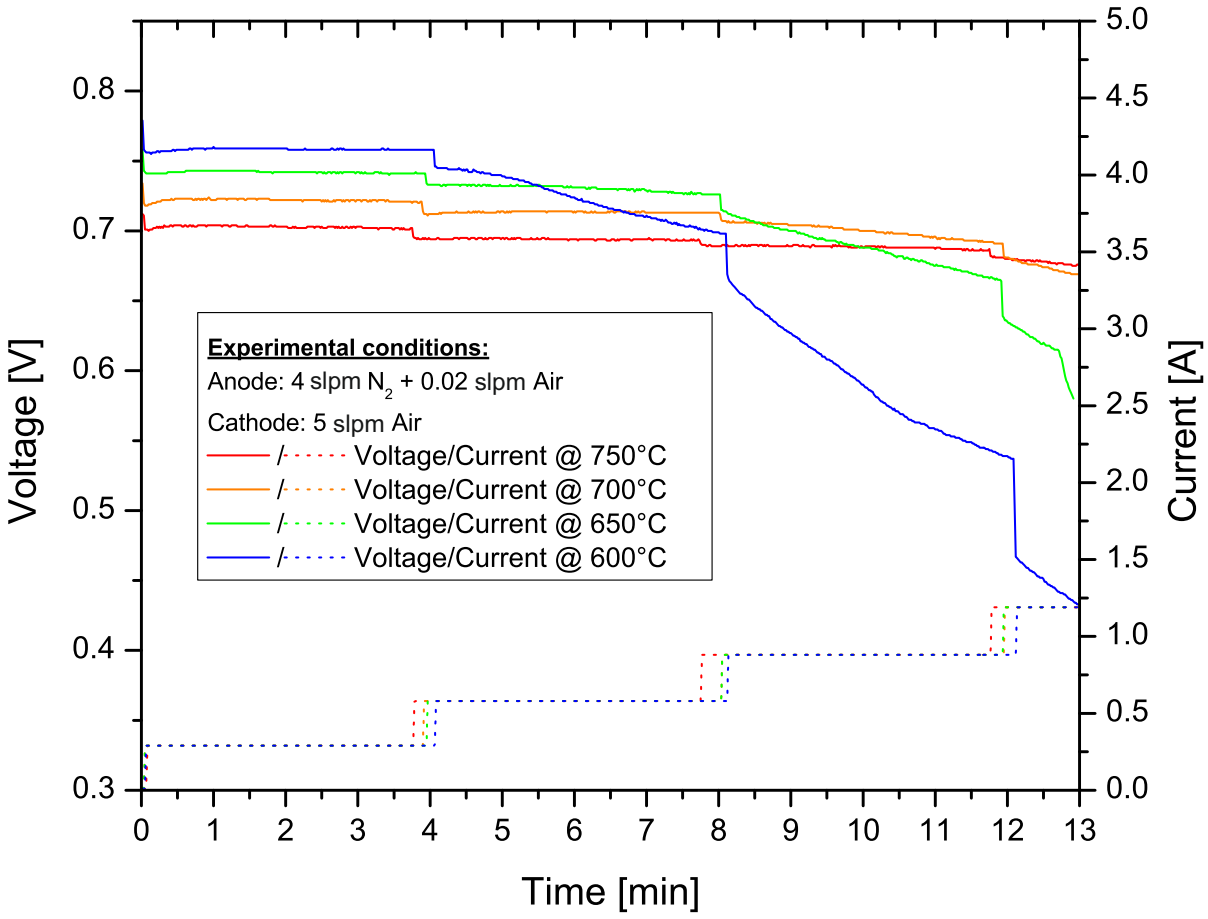

Figure 3. 14: No fuel current experiment at different temperatures showing cell voltage of the single layer vs. time simulating a high parasitic current during isothermal oxidation, Dotted lines = Current steps, Continuous lines = Voltage vs. Time.

and supplying air to both sides of the single layer. Once the voltage is constant near the RedOx potential, a small current is applied to the cell. Starting with 0.3 A, the current is raised every

four minutes by 0.3 A illustrated by the dotted line in the graph. At 0.3 A, the voltage curves stay constant indicating that the electrochemical oxidation can generate at least the current flowing through the external circuit - the water level in the tank does not change. Taking the current to the next level of 0.6 A, the first voltage curve begin its drop downwards. As expected, it is the one at the lowest temperature. All other curves remain at a constant level. At the third current level of 0.9 A, the drop down becomes worse, because the curves at 650 °C and 700 °C also begin to drop. At 1.2 A even the voltage curve at 750 °C drops down. To sum up, the curves represent the expected behavior - the faster drop down compared to the previous experiments is a result of the high 'parasitic' current simulated by the external load.

Next, the influence of the electrochemical oxidation should be investigated. According to the water pump model, a decrease of the electrochemical oxidation speed is responsible for the voltage drop down. Furthermore, the model indicates that anode air is responsible for the decrease in speed, since this consumes the nickel particles, which are then not available for the electrochemical oxidation. In the following, again no fuel current experiments were conducted at the single layer test rig are shown in figures 3. 15, 3. 16 and 3. 17.

They offer the possibility to influence the electrochemical oxidation directly by the variation of the air flow at the cathode side. If the theory behind the water pump model is correct, a higher air flow will lead to a slower voltage drop down. The no fuel current experiments are a bit different to the previous ones, as there is no constant current. Once the RedOx potential is reached after fuel shutdown, the current is continuously increased the same as in regular current-voltage plots. When the voltage drops down to 0.2 V, the experiments are stopped. This way a kind of 'oxidation power' can be measured indicating the speed of the electrochemical oxidation. The first graph shows that curves at 600 °C, 650 °C, 700 °C, 750 °C and 800 °C without any air on both sides. The speed of voltage drop down gets slower with rising temperature. However, the increase becomes slower with each temperature step. From 750 °C to 800 °C, there is not even an increase of oxidation-power. This behavior makes sense, because there is not enough oxygen at the cathode making a further increase of oxidation speed possible. In this case, air is only coming through some leakages and from the outlet pipe. Assuming a 100 % tight system, it can be expected that the voltage drops down immediately, since without oxygen no oxidation can happen. The next graph shows exactly the same experiment, but with 1 slpm air at the cathode side. As expected, the maximum oxidation power is increased significantly from a maximum current of 6 A to 8.5 A. Particularly worth mentioning is the lower oxidation power at 600 °C. But there is an explanation for this behavior as well: In the first experiment

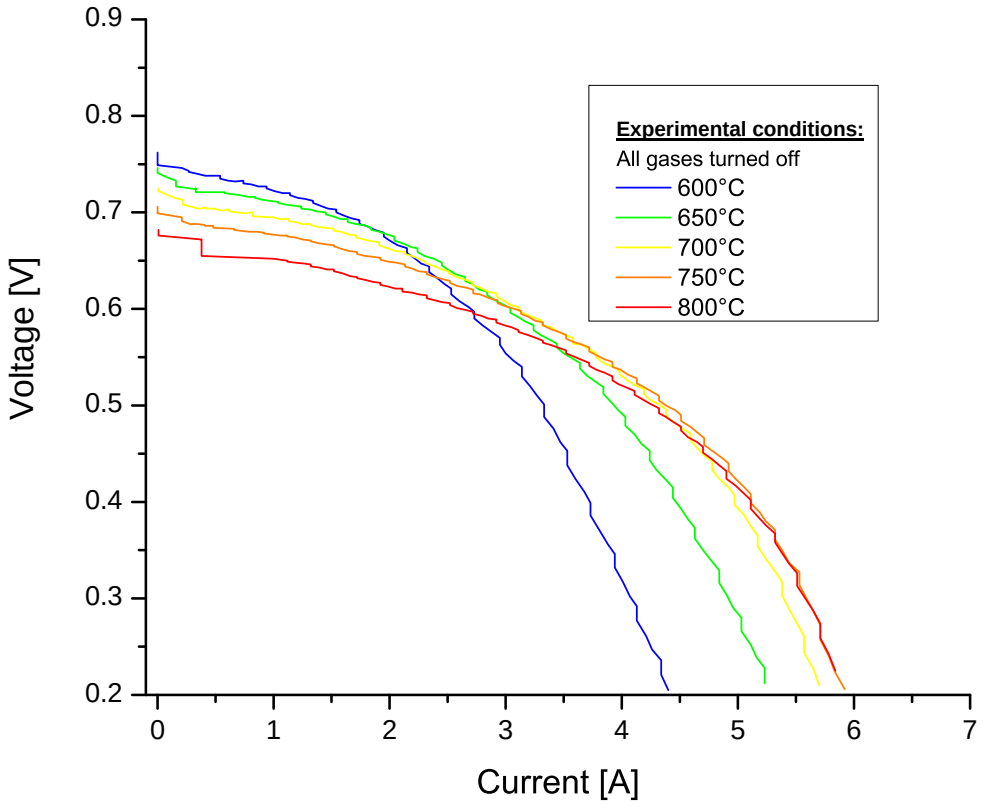

Figure 3. 15: No fuel current experiment: Voltage vs. current at different temperatures without any additional cathode air.

without any gases, the leaking oxygen is already sufficient for the oxidation kinetics at this temperature. Consequently, additional air has no enhancing effect on the speed of oxidation. However, it reduces the temperature in the immediate vicinity of the cell, also indicated by a lower gas inlet temperature measured. This is also in good agreement with the last experiment, where the air flow is increased to 5 slpm. As might be expected, the oxidation power at 800 °C is increased from 8.5 A to 10 A at 0.2 V, while the curve at 600 °C shows a small decrease from 3.7 A to 3.5 A. Figure 3. 18 shows the direct comparison between the experiment without air and with 5 slpm. The blue lines stand for the lowest and the red lines for the highest temperature, respectively.

The rule that 'the higher the air flow at the cathode at high temperatures, the higher the voltage curve' is not necessarily directly transferable to oxidation tests without an external current. Without an external current, in most cases there is enough oxygen at the cathode side due to leakages. By raising the cathode air flow, more air can also flow to the anode due to small defects in the sealing as well as in the electrolyte. Consequently, in this case a higher air

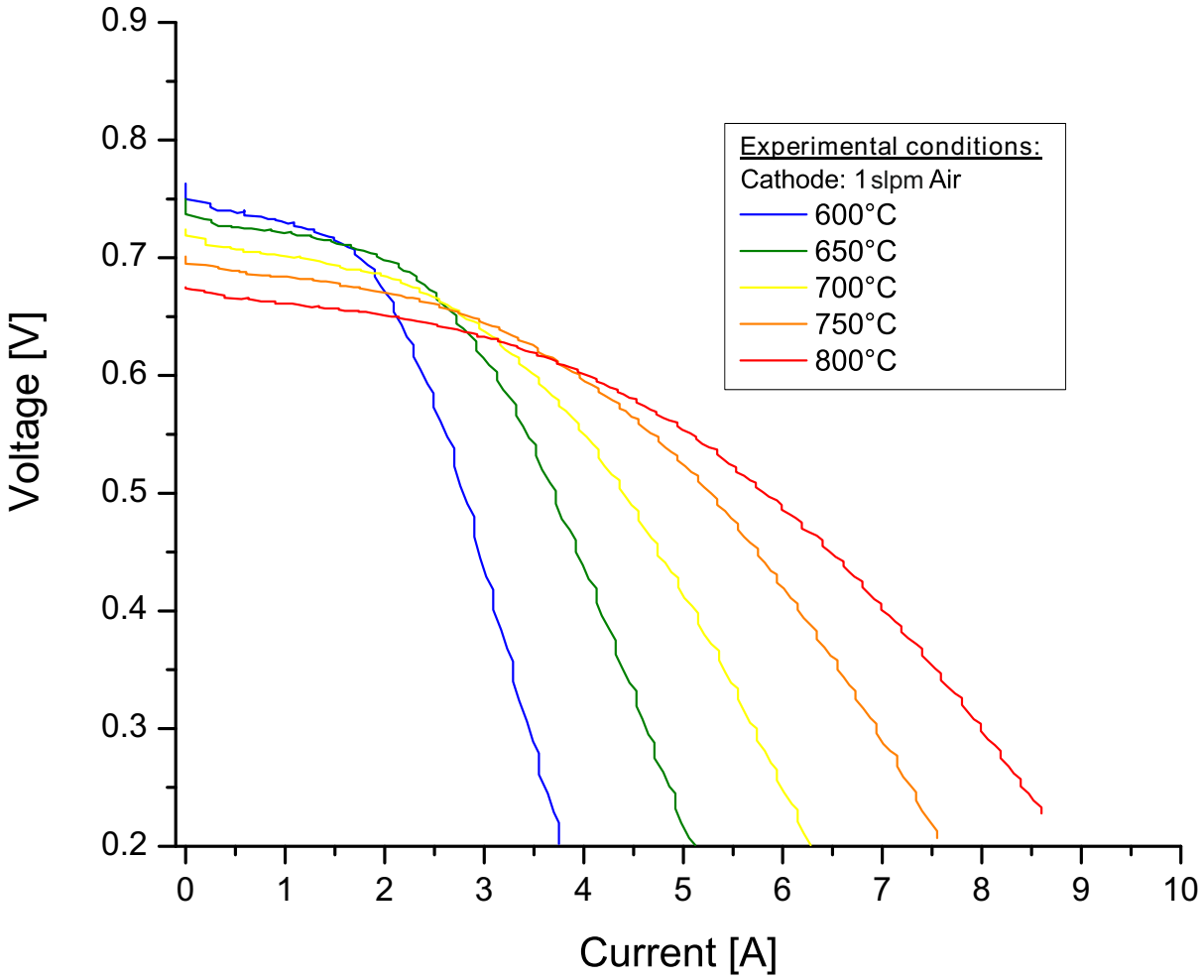

Figure 3. 16: No fuel current experiment: Voltage vs. current at different temperatures with 1 slpm cathode air.

flow can lead to a faster voltage drop down. In the following, a short summary of the voltage behavior during oxidation should make it easier to keep the most important points in mind:

- The higher the temperature, the lower the RedOx potential
- The higher the temperature, the higher the voltage level during oxidation related to the RedOx potential
- The higher the amount of air at the anode, the faster the drop down
- Without air in the system, there is no oxidation and thus a complete voltage drop down
- The higher the parasitic current, the faster the drop down

To conclude, the RedOx potential method can be used to compare different systems concerning

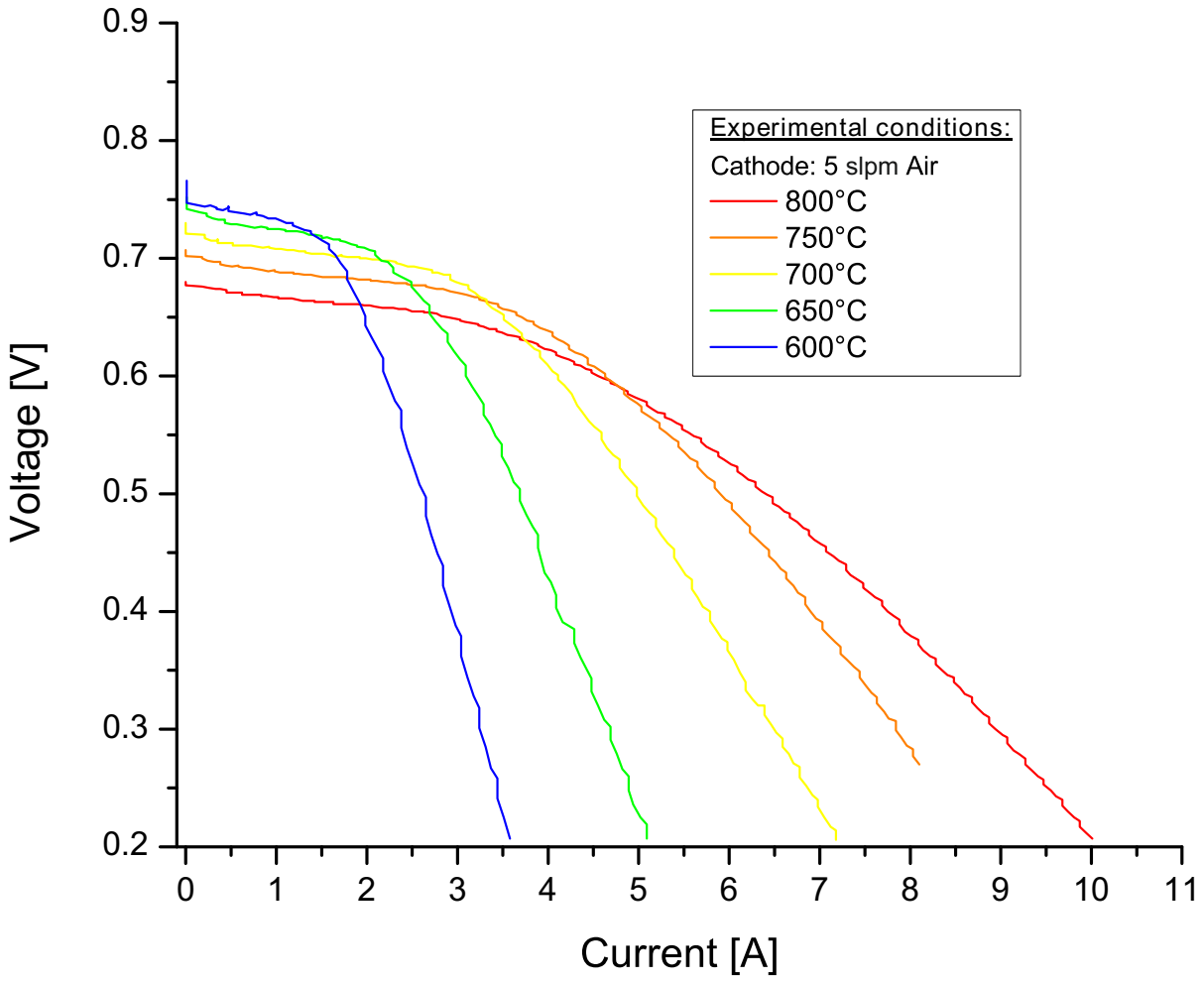

Figure 3. 17: No fuel current experiment: Voltage vs. current at different temperatures with 5 slpm cathode air.

their oxidation behavior during start up and shutdown. A big advantage lies in the simple measurement procedure. Every start up and shutdown without forming gas generates characteristic voltage plots as shown before. For this reason, the measurement comes without any additional effort. However, this method does not bring quantitative results such as an exact value for the DoO. If this is needed, there is the option to construct calibration curves, where a voltage level is directly referred to a DoO. Moreover, a database can be created providing the information of which voltage plot during start up and shutdown of different system setups leads to which lifetime. At this point it should be noted that it is important to compare only stacks with the same electric insulation material in order to keep the parasitic currents at the same level. To get closer to a direct measurement of the DoO, the reduction time method can be developed and is presented in the next section.

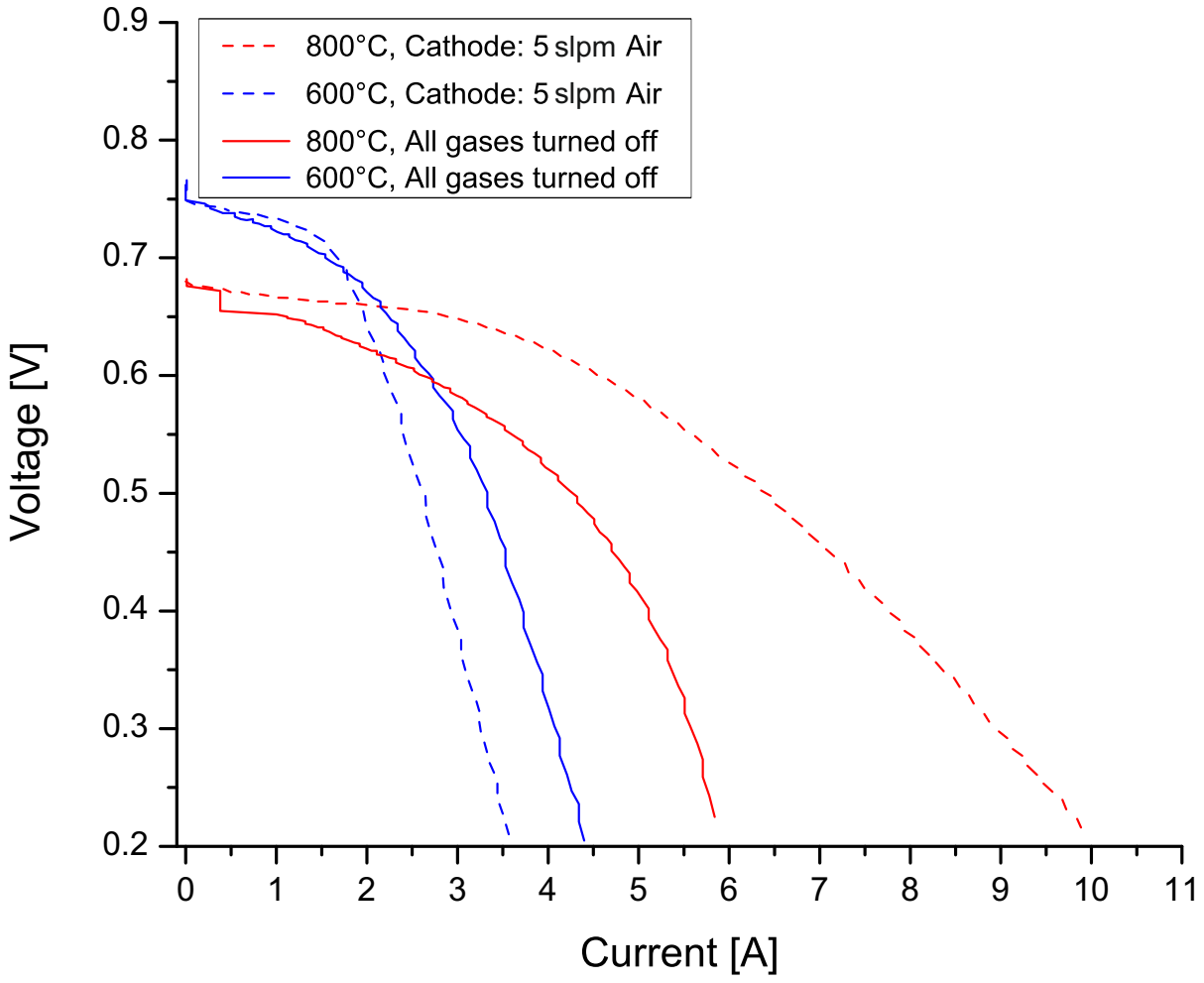

Figure 3. 18: Comparison of the 'oxidation power' as a function of the cathode air and temperature.

3.4 Reduction Time Method

Every RedOx cycle ends with the resupply of fuel leading to a reduction of the anode cermet following equation 2.1. Only the nickel particles oxidized before can be reduced - thus the higher the DoO, the more reduction takes place. As a consequence, the voltage rises from the value during oxidation to OCV value. In order to achieve the original OCV value, three conditions must be satisfied:

1. A fully reduced anode material
2. A 100 % dry cell, since the reduction produces water, which affects the OCV according to the NERNST-equation
3. There is no cell degradation in terms of tightness.

Assuming a constant flow of hydrogen, the time of reduction and the associated voltage rise to OCV strongly depends on the DoO. Figure 3. 19 shows the relation between oxidation time and voltage rise during reduction. The first part of the experiment conducted at the single layer

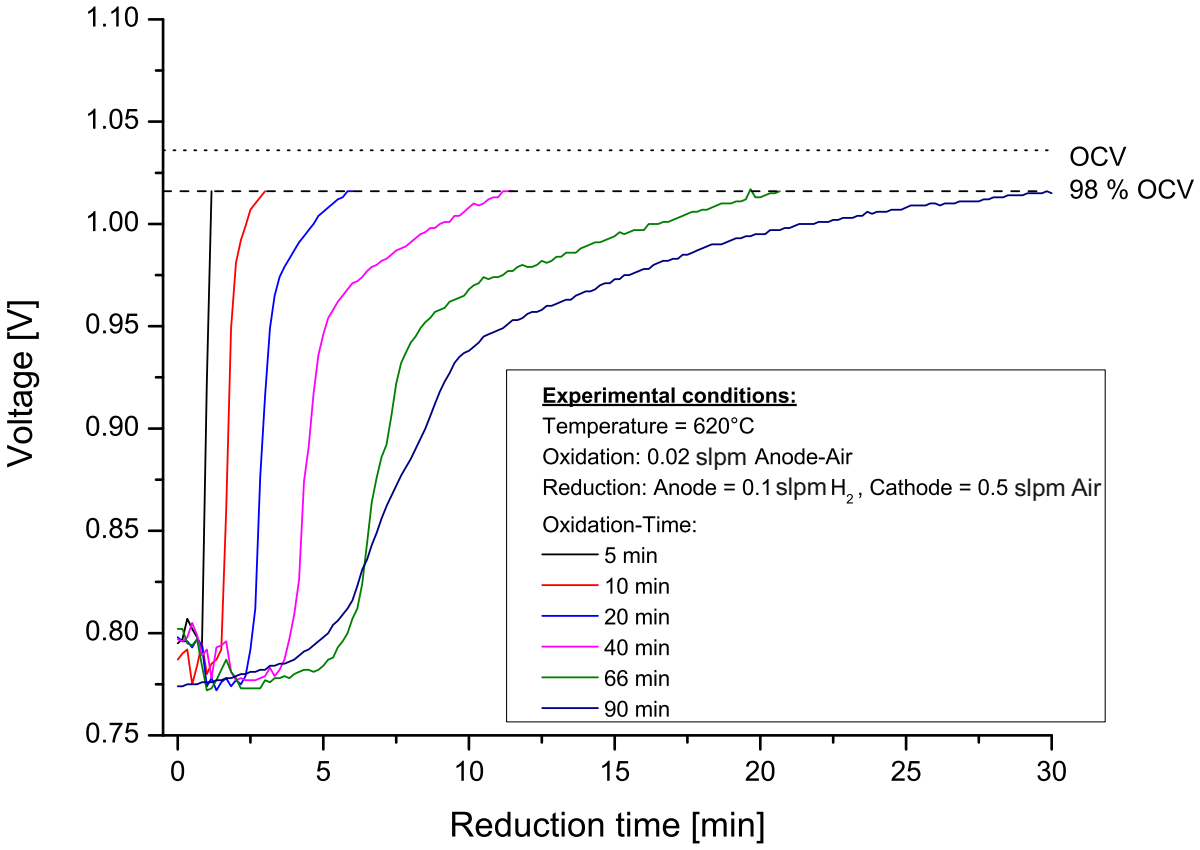

Figure 3. 19: Voltage curves during reduction from an oxidized state with different DoOs.

test bench consists of oxidation with 0.02 slpm air at 620 °C for different time periods from 5 to 90 minutes. After each period of oxidation the single layer is reduced by supplying 0.1 slpm hydrogen to the anode side, while the voltage is plotted versus the time. The different colors of the voltage plots in the graph are related to the oxidation time before. This experiment validates the relation between the amount of oxidation and the reduction time.

Figure 3. 20 shows this relation by plotting the reduction against the oxidation time. For this step the reduction time must be defined. The actual reduction time is the time between the resupply of the fuel and the point in time when the voltage reaches the original OCV. The problem here is that the original OCV is not reached for all experiments - sometimes it takes several hours, but only because some of the percentages are missing, which makes the measurement useless. Other experiments of this thesis, where cells were operated under wet - and

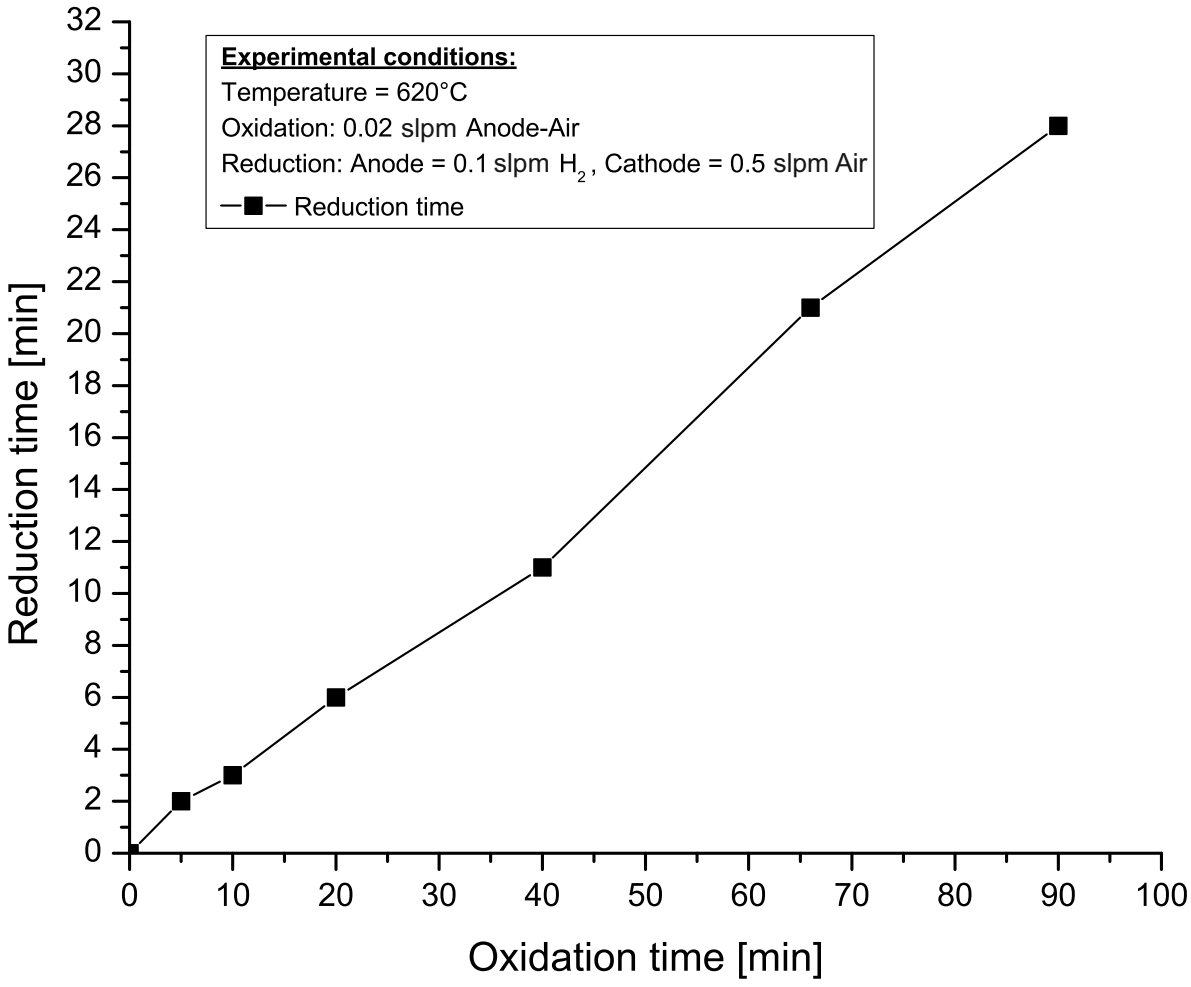

Figure 3. 20: Time of reduction measured between the starting point of the resupply of the fuel and 98 % of the original OCV value related to the voltage curves before.

subsequently under dry hydrogen - showed a similar behavior. The last percentages to the original OCV take a lot of time indicating that just a few remaining water molecules at the anode hinder the voltage coming back to its original value. To exclude this effect, the reduction time is defined to be at 98 % of the original OCV. This definition is applied to all subsequent experiments in this work. It should be mentioned that it is not decisive about whether the value is defined to be at 98, 96 or 99 %, but is only to compare results based on the same definition for the reduction time.

The oxidation/reduction time ratio in this experiment shows proportional behavior. This appears to be plausible, because the air flow is quite small compared to experiments with deviating behavior according to figure 2. 6 [36]. The proportional behavior indicates that the oxidation is limited by the amount of oxygen and not by the oxidation kinetics due to a growing oxide

layer and/or temperature.

Figure 3. 21 shows the reduction versus oxidation time for three different air flows at the anode side at 700 °C and without air at the cathode. The dark line without additional anode air shows

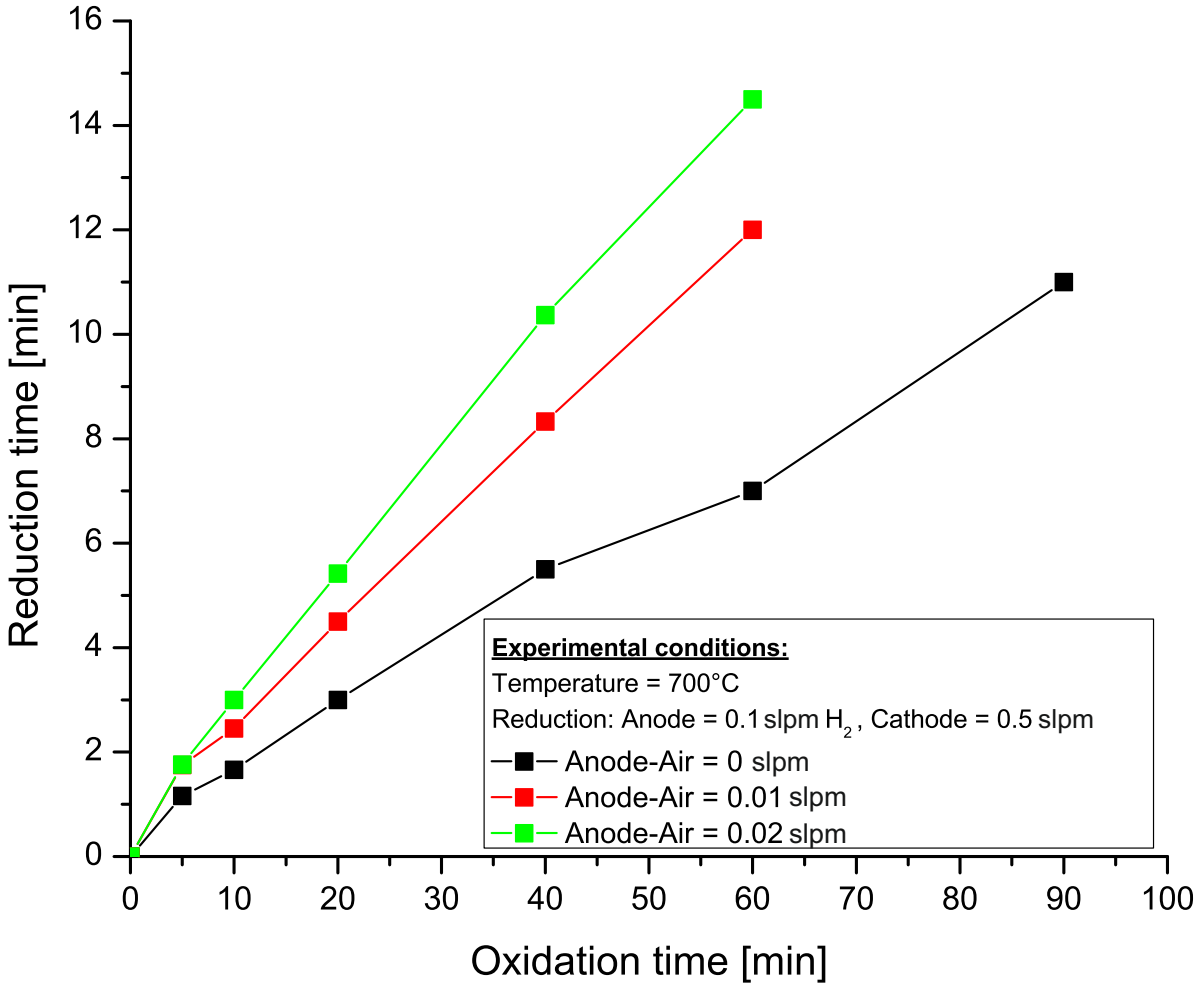

Figure 3. 21: Time of reduction as a function of additional air at the anode side.

the lowest reduction time. Here, oxidation takes place only due to the leakages. By increasing the air flow at the anode to 0.01 slpm (red line) the reduction times are almost doubled just like from 0.01 slpm to 0.02 slpm (green line). All lines show proportional behavior, which is in good agreement with the previous experiment. This makes sense, because increasing the temperature from 620 °C to 700 °C supports the oxidation kinetics, so that the amount of air is still the limiting factor for oxidation and not the speed of reaction. To sum up, the time of reduction enables the possibility of capturing the state of oxidation in a quantitative way. However, the reduction time is a new parameter for oxidation and thus not well known in the scientific community as opposed to the DoO. This causes problems for sharing and comparing RedOx

experiments from different scientists or even results in the future, where voltage measurement is no option. Consequently, the reduction time must be linked to the DoO, which is possible by using equation 2.5 from chapter 2.1. This equation connects the amount of hydrogen needed for reduction with the amount of oxygen which is reduced from the cell. The amount of hydrogen results from the hydrogen flow (in this case 0.1 slpm) and the time of reduction. From this, the amount of oxygen can be calculated. That value, related to the maximum possible value for oxygen in the cell gives the calculated DoO. This calculation is based on the assumption that the hydrogen is completely used for the reduction and nothing passes through the cell unused. To match this assumption, it is important to work with low hydrogen flows. In all following reduction time experiments the single layer is reduced by 0.1 slpm. For comparison only - at normal operation the hydrogen flow is between 0.5 slpm and 0.9 slpm. However, even if no hydrogen is wasted by passing through the cell unused and flowing through the exhaust, the hydrogen is partly consumed by leakages. This means, the calculated DoO is always equal or higher than the true DoO and never below. Thus, the reduction method comes with its own, built-in safety margin.

Developing or using a quantitative measurement method always means discussing measurement accuracy and reproducibility. Checking this is only possible if the value to be measured is constant for several measurements. In this case, exactly the same state of oxidation must be reproduced, which is unfortunately impossible to ensure, due to small changes in the tightness from test to test. These changes come from the flexible mica gaskets. Although the changes are very small, they still affect the reduction time. As shown in the next section - validation on stack level - a 1 % change of the OCV leads to a change of two minutes in the reduction time (figure 4. 5). On stack level, the sealing quality by soldering and welding is very constant. For this reason measurement accuracy and reproducibility is proven in the next chapter.

Nevertheless, the link between the DoO and the reduction time should be checked for plausibility at this point. For this reason the DoO is calculated for the three air flows after 60 minutes of oxidation, illustrated by the black line in figure 3. 22 showing the calculated DoO versus the air flow on the anode. Without additional air, the DoO is at 14 %. As already mentioned in chapter 3.3, the DoO measured by weight at the same conditions is around 6.5 % after 30 minutes at 700 °C. Extrapolating this to an oxidation time of one hour results in a DoO of 13 %. This is in good agreement with the results measured by the reduction time. The second way to check for plausibility is to use the additional air flow. In the same way that the DoO can be calculated from the amount of hydrogen, the DoO can also be calculated from the amount of air passing

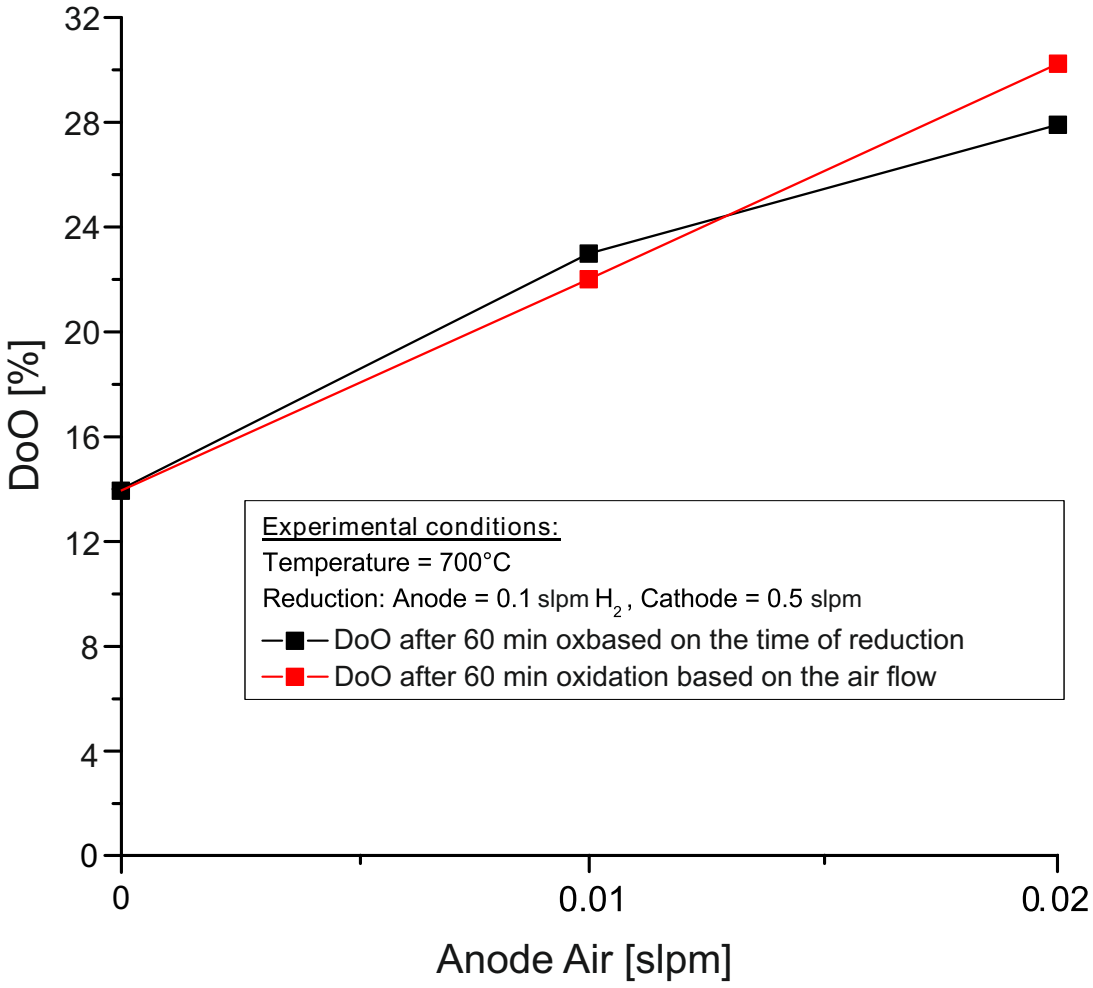

Figure 3. 22: Plausibility check of the reduction time method: Red line: Calculated DoO based on the amount of additional air. Black line: DoO measured and converted by the reduction time method.

the anode in one hour. However, only the additional air is known, but not the amount of leaking air. But the difference in the DoO between zero anode air flow, 0.01 slpm and 0.02 slpm air flow can be calculated very easily. This calculation is represented by the red line, which copies the start value from the black line for the reason mentioned before. Following a difference of 0.01 slpm in the air flow means an addition of 8 % in the DoO for the present cell. Although two ways for the calculation of the DoO are used here, the results are very similar, making the plausibility check successful.

In the following, a brief summary is given to keep the most important things in mind:

- The reduction time method is based on the simple relation: The higher the DoO is, the

more time is needed for reduction

- The time of reduction is a quantitative value, which can be converted to the DoO by using the stoichiometry of the chemical reaction
- The true DoO is equal or lower than the calculated DoO
- The biggest advantage of the method: Quantitative measurement of the DoO without disassembly of stack and systems, More precise than the RedOx potential method
- The biggest drawback: Additional measurement effort compared to the RedOx potential method because of additional periods of reduction with low hydrogen flow within the cycle

Chapter 4

Validation of the developed methods

Based on the results of the method development in the previous chapter, the reduction time method is proven to be the best one followed by the RedOx potential and the voltage drop method. For this reason the reduction time method will be used for the measurement of the DoO for applications discussed in the next chapter, while the RedOx potential will be used to get some additional information or to doublecheck the results coming from the reduction time. The voltage drop method is not used. Since the results of the method development come from the single layer test bench, there is the need for validation of those methods on stack level, which will be presented in this chapter.

Stack testing can be conducted in various ways. In general, a distinction can be drawn between system testing, close-to-system testing and general testing. General testing is done for stack development such as qualification of new cells, contact pastes or design improvements and is done in an oven, which heats up the stack. This kind of testing is optimized for a quick change of the stack as well as for repetitive testing conditions. However, this kind of testing is far away from system operation conditions. Since the RedOx behavior strongly depends on the temperature state of the stack as well as on the amount of air flowing to the stack, general testing is not a useful option. For this reason validation is conducted by close-to-system testing, which is illustrated in figure 4. 1. The system closeness is achieved by using the insulating box in the middle of the picture. In the final system this box surrounds the stack and all hot system components such as the burner and reformer. In the case of close-to-system testing only the stack is inside, because the air is pre-heated electrically and the fuel consists of H2/N2 instead of propane and its reformate, respectively. The box is located on a test rig supplying the gases/air as well as temperature, pressure, cell voltage and power measurement. Furthermore, the test

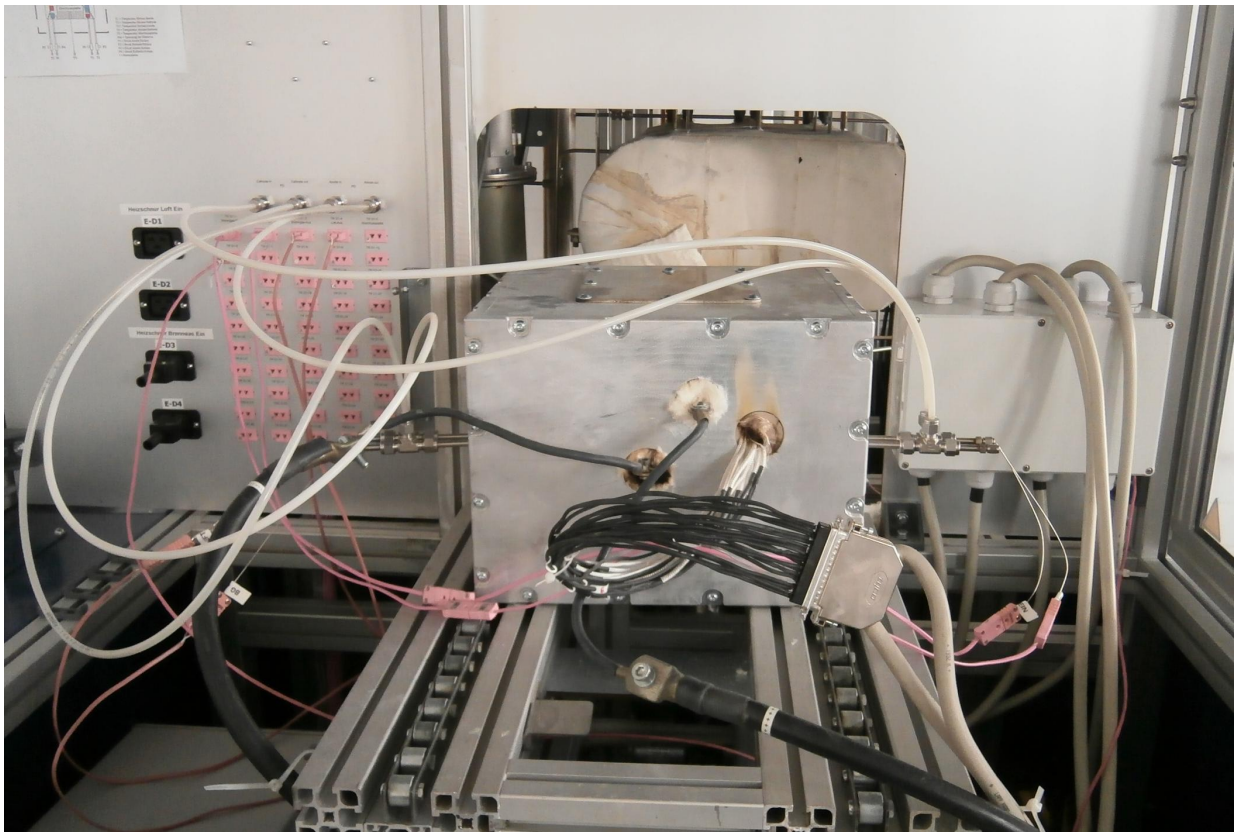

Figure 4. 1: Close-to-system testing: Insulating box with stack inside on the test rig including temperature, pressure and cell voltage measurement.

rig is capable of programed test runs, which is very helpful, especially for cyclic testing.
By using that box, cool down and heat up times are close to the system. Furthermore, the heat up by hot air flowing over the cathode is very important for a system close behavior, because the overpressure at the cathode side has a high influence on the RedOx behavior. Besides close-to-system testing, 'real' system testing is also part of this thesis, presented in chapter 5. For these tests, the reformer and gas burners are part of the insulating box.

4.1 Validation of the RedOx Potential Method

The validation starts with the RedOx potential method. The procedure for validation differs a little from the method development, since stack testing is very expensive and time-consuming. Instead of measuring the voltage drop down again for different values for the anode air, an old leaky stack is compared with the single layer as well as with a new tight stack. Figure 4. 2 shows

the first test with the leaky stack, where the cell voltage is plotted against time after shutting down the fuel supply. During the oxidation, air is still supplied to the cathode. The dotted line

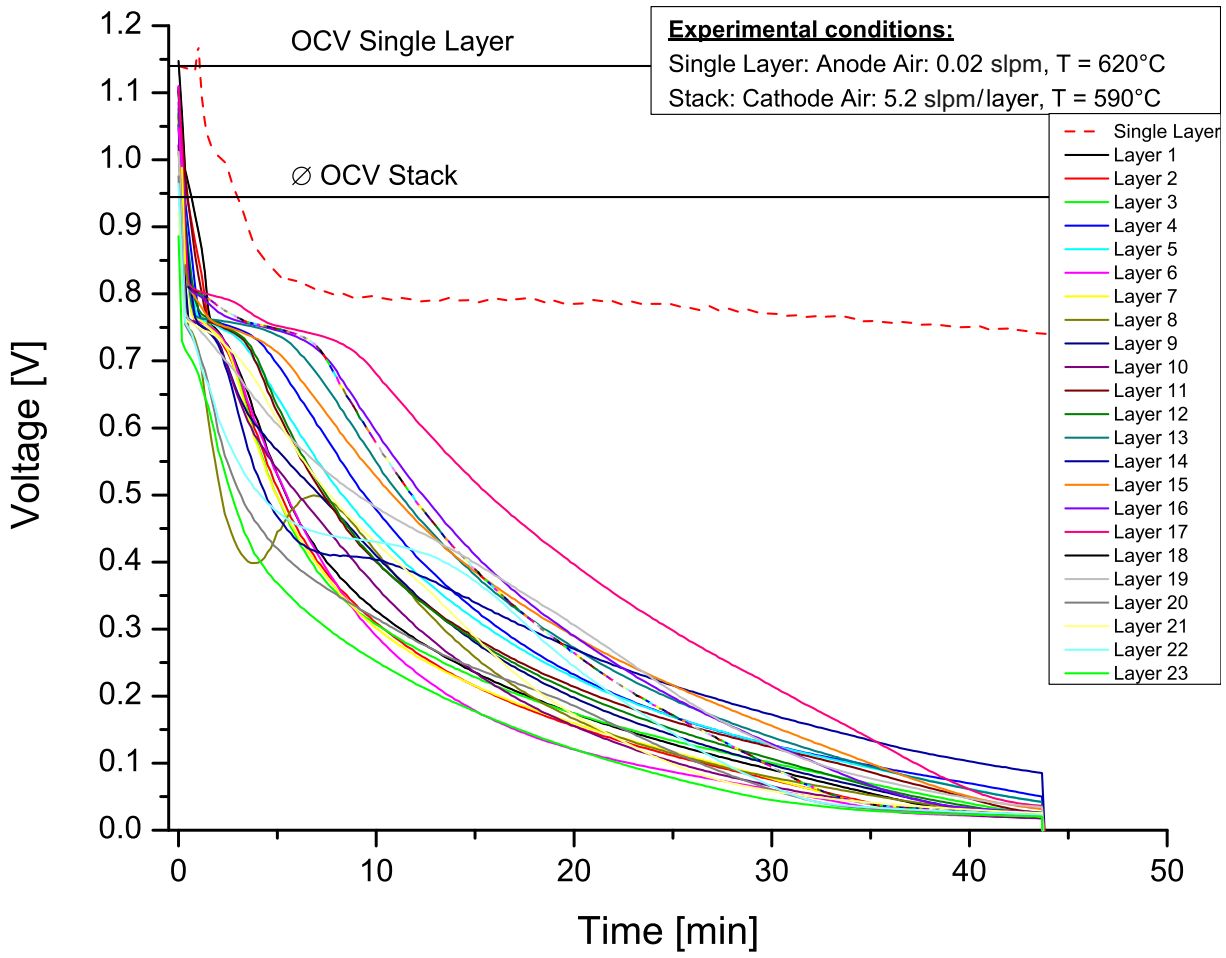

Figure 4. 2: Voltage curves of leaky stack layers compared to the voltage behavior of a tight single layer during oxidation as a function of time.

represents the voltage curve of the single layer testing from the previous chapter, where the air flow is at 0.02 slpm. The horizontal lines stand for the average OCV of the stack and the single layer, proving the stack is really leaky. As expected, the drop down of the stack layers is much faster compared to the single layer. Furthermore, it can be seen from the graph that the drop down is basically sorted by the tightness. For example, the green line on the left side of the graphic has an OCV close to 0.9 V and one of the fastest drop downs. In comparison to that, the pink line with an OCV of over 1.1 V has the slowest drop down. Of course, both tests were conducted at similar temperatures (Stack = 590 °C, Single Layer 620 °C) so as not to distort the results. Worth mentioning is the cell voltage of layer 8 (dark green line), which has a pronounced maximum in opposite to all the other voltage curves. The most probable reason

is a decrease of the parasitic current. Indicated by the low OCV value of only 0.85 V, layer 8 is the one with the highest leakage within the stack. When the hydrogen supply is stopped, the temperature around this layer decreases due to the stop of the internal leakage caused fire. This temperature decrease can lead to small deformations in the region of layer 8 leading to a change in the insulation resistance. However, this is only the most probable reason and could not be proved.

Figure 4. 3 shows the completely different behavior of a new, tight stack. Now, the average OCV

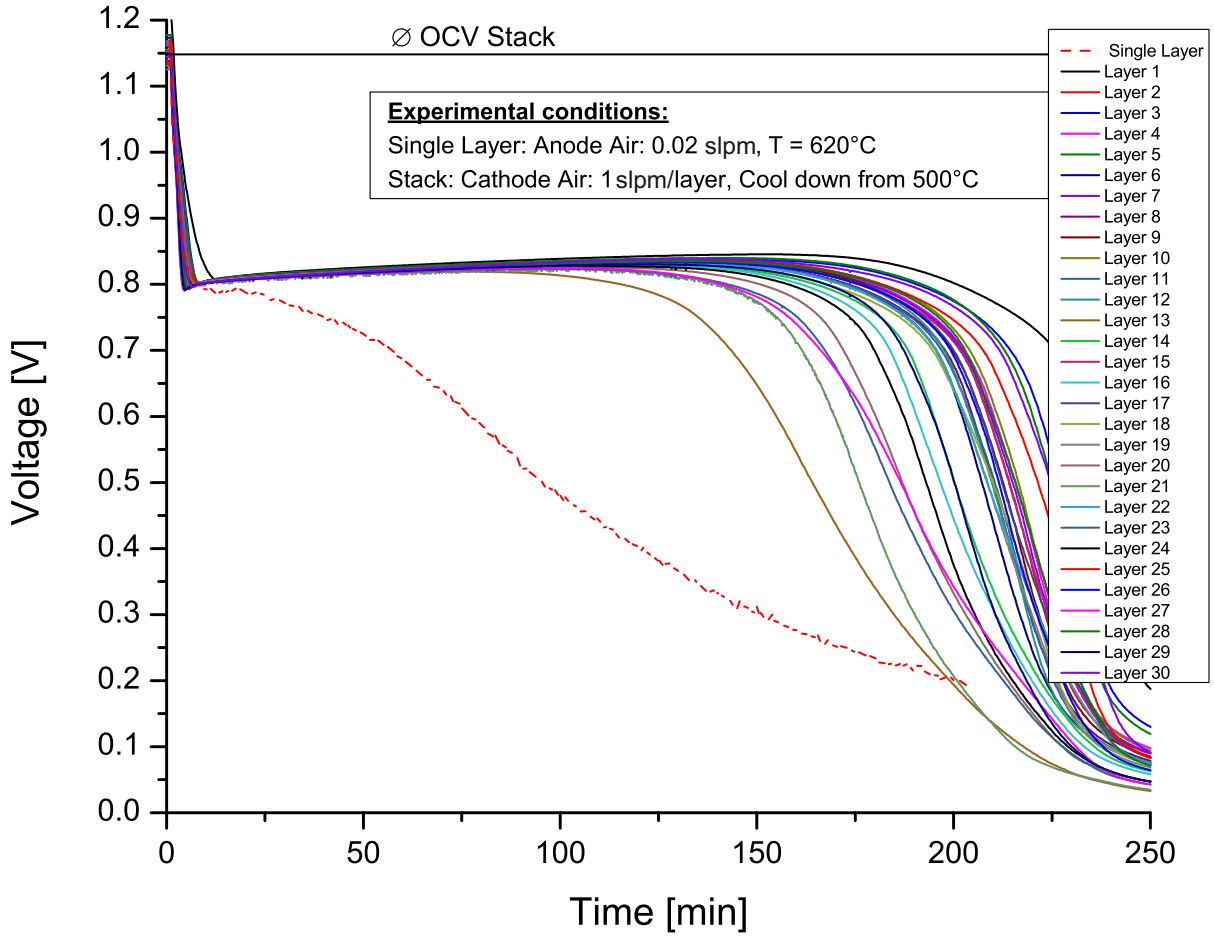

Figure 4. 3: Voltage curves of tight stack layers compared to the voltage behavior of a tight single layer during oxidation as a function of time.

is 1.15 V compared to 0.95 V before for the leaky stack. The conditions are a little different to the previous stack, but rather worse. The temperature is lower at 500 °C and decreases during the oxidation. As known a low and/or falling temperature leads to a faster drop down. On the other hand, the cathode air flow is lower. The reason for the difference is due to the fact that this stack test was not only conducted for validation purposes. Either way, the drop down is

clearly slower, even slower compared to the single layer test. Furthermore, the time point of drop fits the limiting temperature for nickel oxidation, which is well known to be at 400 °C.

4.2 Validation of the Reduction Time Method

Method validating is continued by the reduction time method on stack level. The simple way for validation would be to repeat the experiments from the method development chapter with different air flows and oxidation times by subsequent measurement of the reduction time. However, this procedure is far away from real stack operation as investigated in the next chapter (application of the methods). Normally, oxidation takes place during start up and shutdown and not during isotherm operation. For this reason the method is extended to be able to differ between shutdown and start up oxidation.

Consequently, the following stack test was conducted:

A new tight stack was operated and shutdown under safe conditions by supplying forming gas to the anode. Following, the stack was heated up to 500 °C by hot air at the cathode side under oxidizing conditions. While the heating up was continued, at 500 °C the stack was reduced by 0.5 slpm forming gas. Figure 4. 4 shows the average stack voltage curve (red line) during the time of that reduction. After several hours of operation the stack was cooled down, while the forming gas was turned off at 500 °C, so that the stack was in oxidizing conditions between 400 °C and 500 °C. Following, the stack was started up as it was before, but also reduced, by passing the 500 °C temperature line. The voltage curve during reduction (green line) now respresents the accumulated oxidation of shutdown and start up. The reduction time of the start up oxidation is 3 minutes, while the time for the entire cycle is 11 minutes. These values can be converted into a DoO of 1.5 % and 5.5 % respectively, so that the DoO coming from the shutdown period is at 4 %. To accept these results as plausible, it is important to understand the oxidation conditions during the cycle. First, the start up period between 400 °C and 500 °C takes 20 minutes, while the shutdown oxidation in this temperature range lasts 150 minutes (factor 7.5). However, the DoO is only higher by a factor of 2.6 (4 % after shutdown to 1.5 % after start). This can be explained by the difference in air flow at the cathode. During start up there is an air flow by 5 slpm/layer to heat up the stack, while during shutdown there is only a flow of 1 slpm/layer. It should be noted that the air cannot be completely turned off for safety reasons regarding the air preheaters. For this reason the oxidation rate is higher during start up, but nevertheless the difference in time has the greater influence. To check the reproducibility of

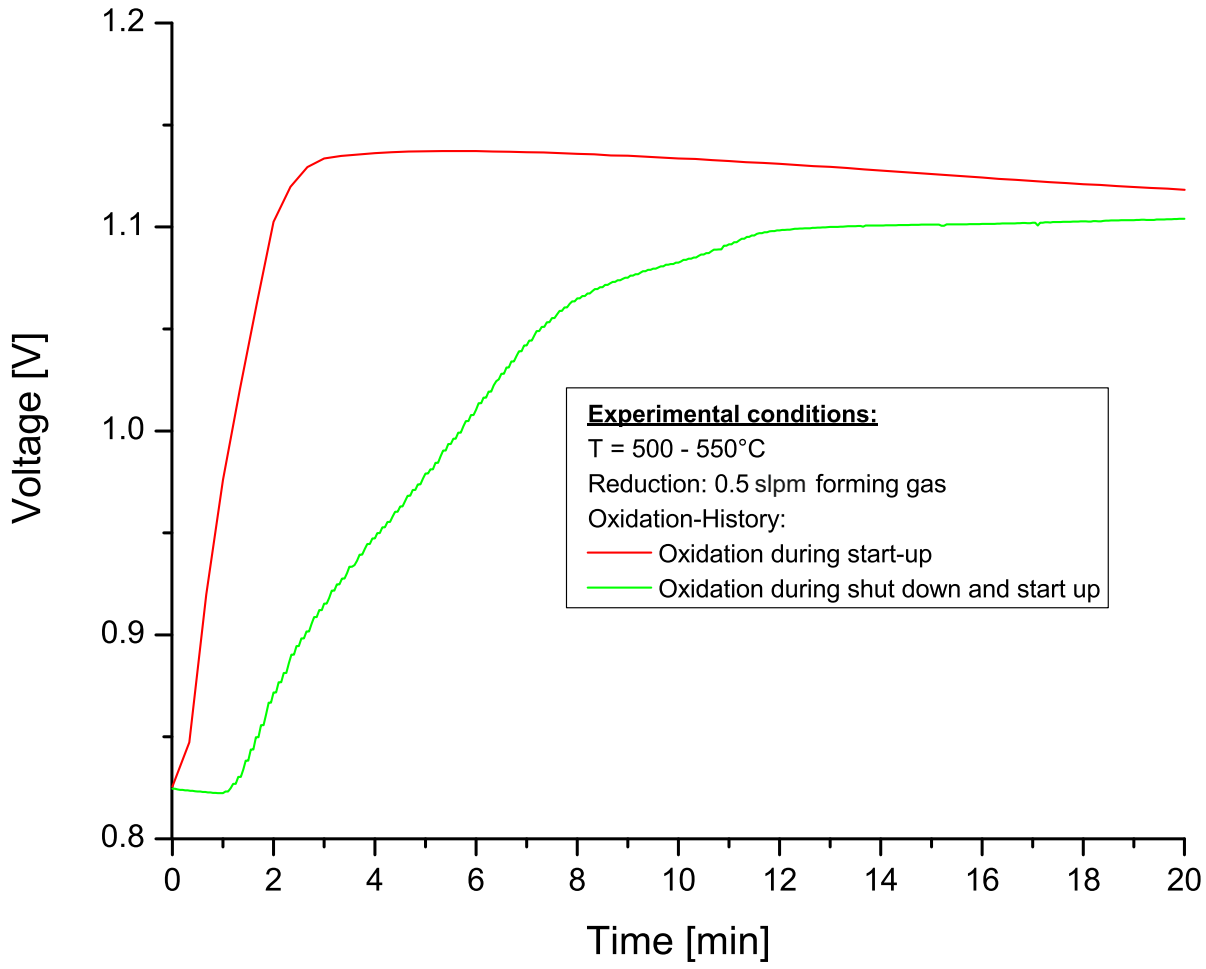

Figure 4. 4: Average cell voltage during reduction from two different states of oxidation: Red line = Only start up oxidation, Green line = Start up and cool down oxidation.

the method, the stack was cycled several times. Figure 4. 5 shows the average reduction times of all stack layers as well as the average OCV as a function of the cycle number. The first two reduction times are the ones already discussed. The graph shows the very high reproducibility of the measurement method, where there is actually no change in time with rising cycle number. By passing cycle 10, there is a sudden decrease in reduction time, which does not make any sense at first glance, because such a result indicates the stack tightness has risen by passing several RedOx cycles. However, the OCV values makes it clear: there is no doubt that the tightness actually improved in this cycle for unknown reasons. The change in OCV is quite small, only well visible by the detailed scale from 1.08 V to 1.12 V. That fact shows the high sensitivity of the reduction time, which in combination with the excellent reproducibility is evidence for the high level of quality that the reduction time method provides.

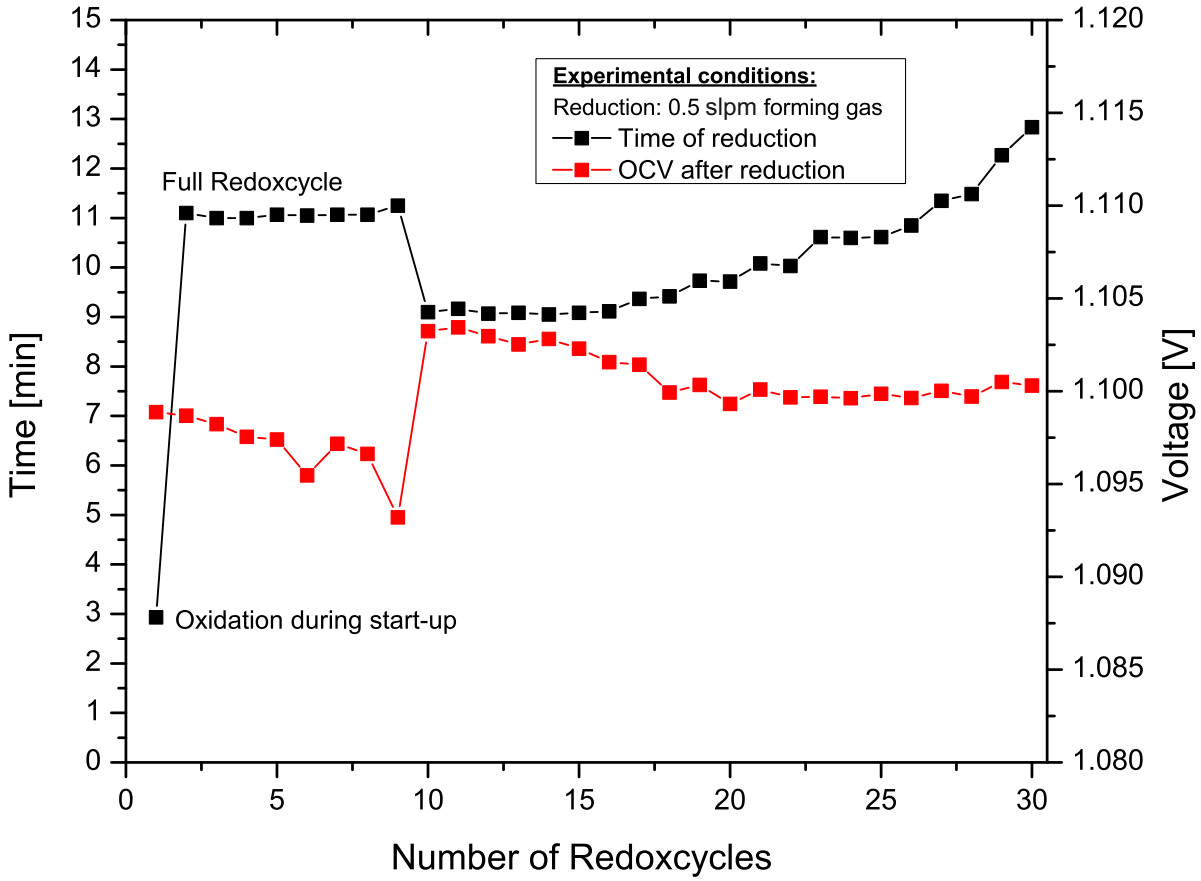

Figure 4. 5: Time of reduction and OCV values as a function of the cycle number.

By passing the next RedOx cycles, the reduction time increases while the OCV decreases, indicating the degradation of cell tightness. After 30 cycles, the test was stopped to prevent the complete destruction of the stack. Within the last cycle, the oxidized state was frozen after a complete cycle to measure the DoO by weight, making the validation 100 % complete. For this reason, the stack was cooled down and started up to 500 °C without forming gas by subsequent cool down from 500 °C with nitrogen, to prevent further oxidation during shutdown. Forming gas is no option at this point, because the cells would be reduced then. The overall DoO, which is expected, consists of the last reduction time (13 minutes) with an addition due to the cool down with nitrogen. The additional cool down oxidation is not known, but probably lies between 0 % (perfect protective effect) and 4 % DoO (no protection), so that the assumed DoO is around 6.5 and 11 %. In the worst-case scenario, the nitrogen could spread the oxygen coming through leakages, leading to higher DoO than 11 %, but it is not known if this is the case or not.

For the gravimetric determination of the DoO, the cells were disassembled from the stack and divided into different pieces - one piece from the gas inlet, one from the middle and one from the gas outlet. Afterwards the cells were oxidized for 24 h at 800 °C. The weight before and after the oxidation was measured. From previous testing with those cells, the maximum of relative weight gain is known. By comparing these values with the lesser weight gain of the cell pieces from the stack, the DoO of the cell pieces can be calculated. Figure 4. 6 shows the overall DoO for four stack layers as well as the local DoOs at inlet, outlet and in the middle of the four layers. The overall DoO of the four cells are between 12.5 % and 15 %, which is a

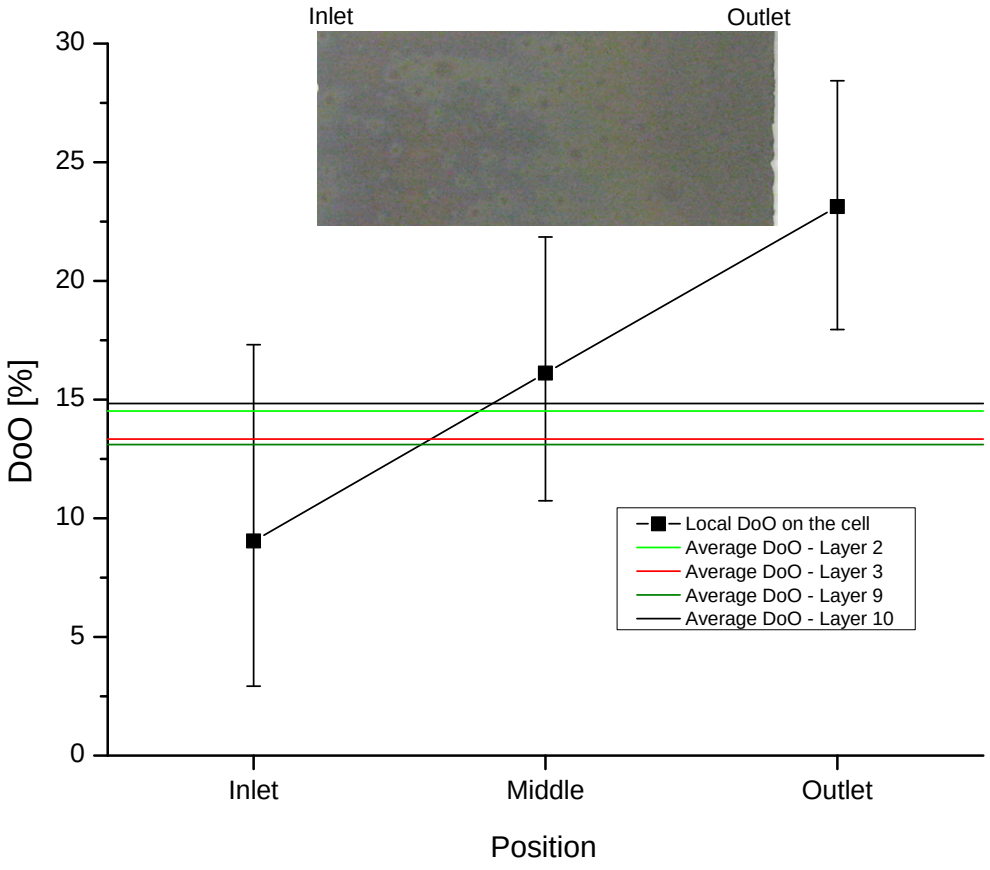

Figure 4. 6: Gravimetric determination of the local and global DoOs of the RedOx cycled stack.

little higher than the calculated value of 11 %. On the top of the graphic the appearance of the oxidized cell of the stack is illustrated. The gray scale of the oxidation proves that this is low temperature oxidation as explained in the introductory chapters. Furthermore, the appearance from left to right confirms the results from the local gravimetric DoO measurements. The rising

DoO from inlet to outlet is a result of the higher stresses due to higher temperatures during operation. For this reason the mechanical degradation is higher there, which is well known from several stacks investigated before at EK. For degradation the high local values for the DoO are the biggest problems, because they cause high local strains. The combination of high thermal stresses at the outlet, followed by tightness degradation and thus higher DoOs with accompanying strains/additional stresses completes the vicious circle.

Chapter 5

Application of the methods for stack and system characterization

By finishing the method development and validation, there were the following outstanding points regarding stack and system's RedOx behavior at EK and its subsidiary New Enerday:

- What is the dominant operation phase for oxidation - the start up or shutdown phase of the system?
- What is the main reason for oxidation - air from the system components or from the stack itself?

5.1 Experimental plan

To answer these questions, system as well as close-to-system testing is necessary. This section presents the experimental planing of both experiments. The system experiment begins with building up a new, intact stack. To be sure about the stack's performance and tightness it was tested at a close-to-system test bench and thus without propane. Consequently, the stack were fully reduced before the first start up in the system. Figure 5.1 shows both set-ups. On the left the stack is mounted in the insulating box for close-to-system testing, whearas the right picture shows the stack together with the gas burner and the reformer for system testing. The white cables in both boxes are for cell voltage measurement during operation. The details of the operation principle of the system are already explained according to figure 1.1 in chapter 1.

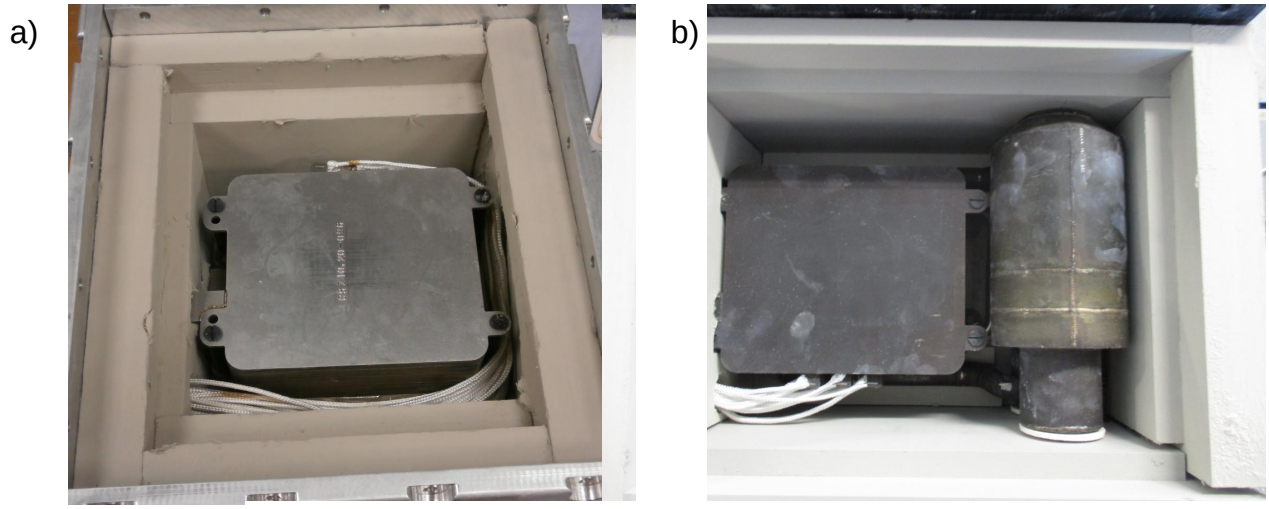

Figure 5. 1: a) Insulating box for close-to-system testing only mounted with the stack. b) Insulating box for system testing mounted with the stack and system components.

Since the functional test at EK (Box-A) was successful, the system components were added and the insulating box (Box-B) was built on a special test bench at New Enerday as illustrated in figure 5. 2. For the determination of the DoO the reduction method should be used. To separate start up and shutdown oxidation the strategy from chapter 4.2 is used:
By finishing the initial test on the close-to-system test bench the stack is fully reduced. Following, the system test should start up without any protective gas by subsequent reduction with accompanying measurement of the reduction time. Of course, that time only represents the oxidation during that start up. After operation the stack will be cooled down without protection and will be started again without any protection. By measuring the reduction time again, start up and shutdown oxidation are captured.
Even if the oxidation behavior of the entire system will be captured by these measurements, there still remains - to what extent does the stack itself lead to the measured DoO/reduction time. For this reason a close-to-system test with a new stack needs to be conducted. Of course, the separation strategy for start up and shutdown will be the same. By comparing the reduction times from both experiments, the influence of the stack and the system on the oxidation behavior will be known.

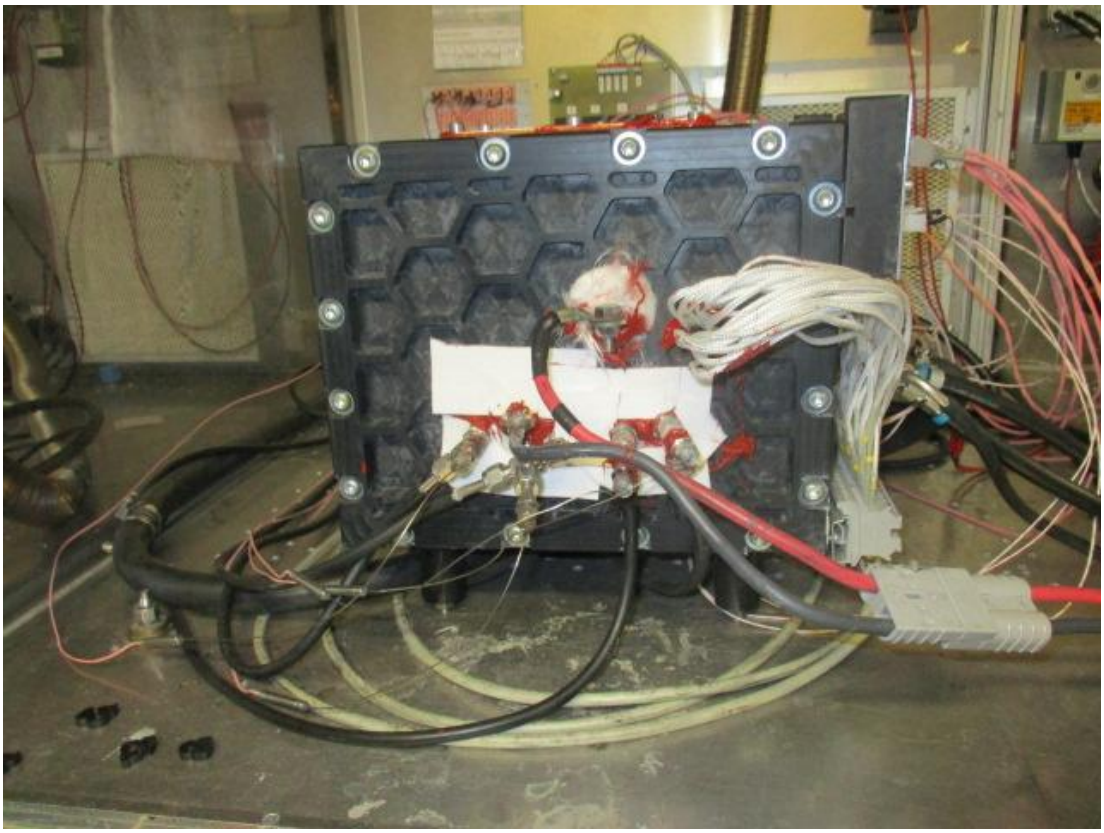

Figure 5. 2: Insulating box including stack and system components for system testing at New Enerday.

5.2 Experimental results

Figure 5. 3 shows the average stack voltage and the cathode temperatures during the first start and stop cycle of the system. The system needs to be heated up to at least 750 °C (cathode outlet temperature) to prevent the formation of soot. In terms of oxidation, the heat up time should be as short as possible. The heat up ramp strongly depends on the air inlet temperature, because the difference of air inlet and outlet is the amount of energy remaining in the stack for heat up. However, a higher inlet temperature leads to higher temperature differences within the stack, inducing thermomechanical stresses. EK has a very high competence level in this area due to doctoral theses from Pausch and Freundt [16, 70]. From these studies a maximum inlet temperature of 780 °C is well-known to enable high stack lifetime. However, the degradation due to RedOx is not considered, so there is a conflict between thermomechanical stresses and degradation by cell oxidation. Based on the thermo-mechanical stack models from [16, 70], the

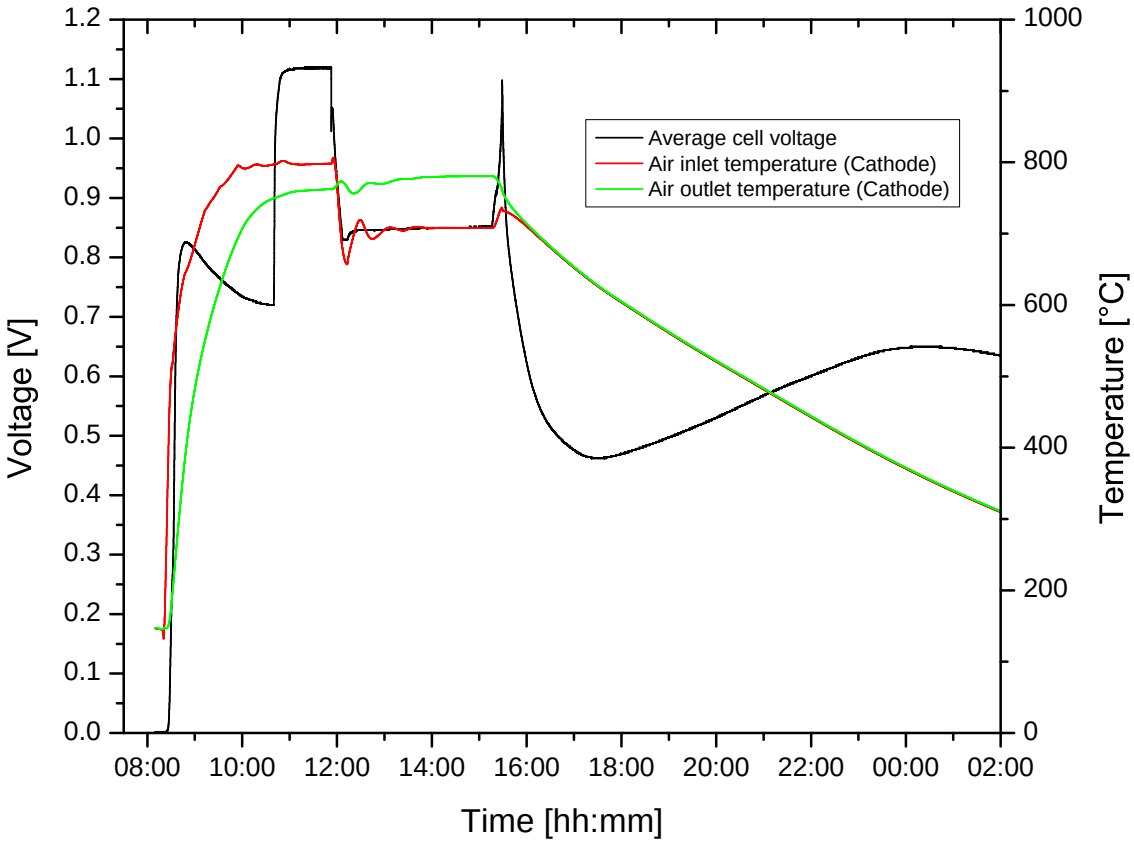

Figure 5. 3: Average cell voltage and cathode in- and outlet temperature of the system start- and stop cycle.

maximum inlet temperature was raised to 800 °C with the effect of a start time reduction from 3 to 2.5 hours as can be seen in the figure. It is important to understand that this reduction of time takes place at high temperatures. Consequently, by this measure the time of oxidation at around 700 °C could be reduced by 30 minutes.

After breaking the 750 °C inlet temperature, the stack is reduced by forming gas to get the time of reduction for start up oxidation. Following, there were several hours of operation until the stack was stopped by turning off the fuel and air supply. By stopping, the average cell voltage immediately drops down, which is well-known from the experiments in the previous chapters. However, the following voltage behavior does not fit the data observed from the experiments during the method development. To get information in more detail, figure 5. 4 shows the single cell voltages over time. In general, cell voltages behave quite differently. Some of them show well-known behavior as they drop down to their RedOx potential and remain there until the

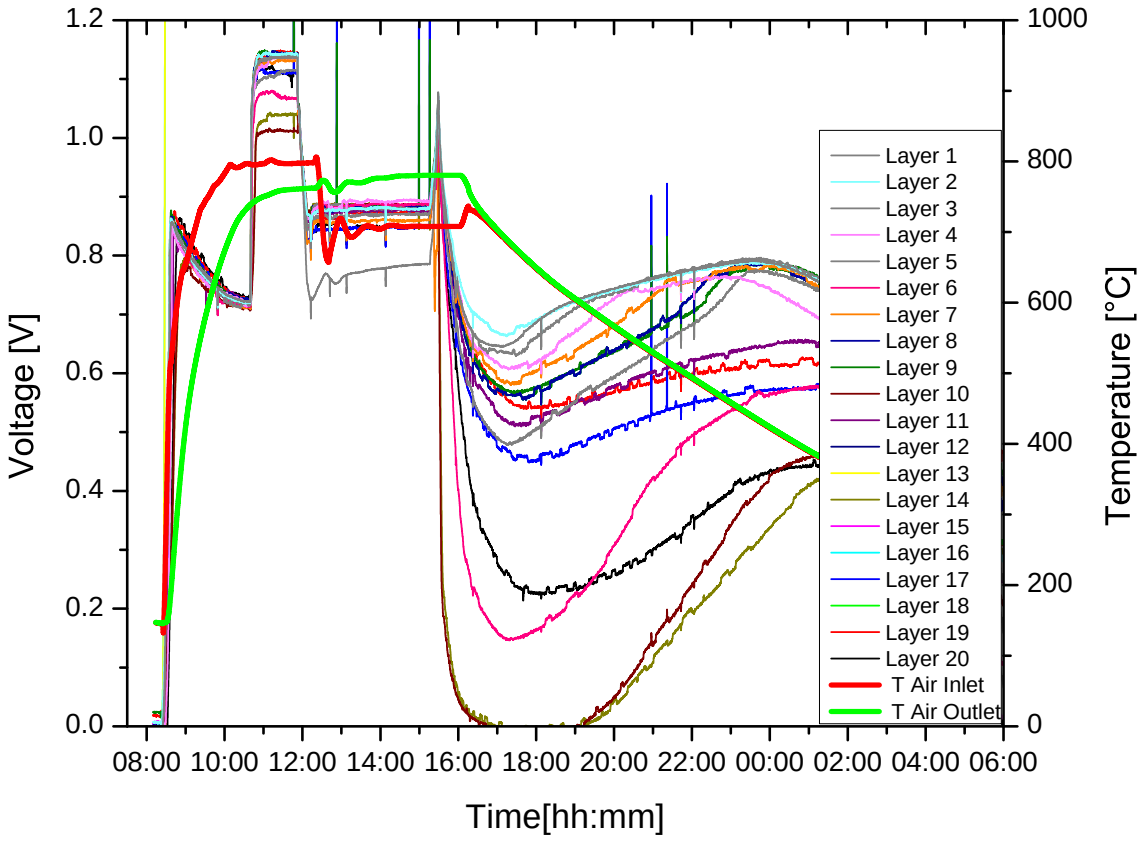

Figure 5. 4: Single cell voltages and cathode in- and outlet temperature of the system start- and stop cycle.

temperature falls below 400 °C. Others even fall to zero indicating a fast oxidation such as the experiment in the validation chapter with the leaky stack. However, in this case the voltage of those cells begin to rise after a while, although there is no change in the conditions. Following the water-pump theory, there are only two possible reasons for such a drop down. Firstly, there is a short-circuit or secondly there is no or too little oxidation. The first reason can be rejected, because the OCVs after reduction were at a normal value. The second reason can be caused either by a high DoO and even complete oxidation, respectively or by a deficiency of oxygen. The renewed increase of the voltage contradicts the assumption of a complete oxidation, so only a very small amount of oxygen can be the reason. It is likely that the air needs some time to diffuse from the exhaust to the cells. There is also a second small detail supporting this explanation. In previous system experiments, the voltage behavior during cooling down under oxidizing conditions corresponded very well to the RedOx potential curve. The difference

between those experiments and the actual one lies in the connection between stack and gas panel, which is located under the stack and is responsible for gas distribution. In previous experiments the connection was sealed by a mica gasket, which as known from the single layer experiments is never completely tight. In order to improve the system's RedOx stability, the actual connection is sealed by welding as this is 100 % tight.

The measurement of the reduction time during the second start up, illustrated in figure 5.5 confirms the first indications from the voltage behavior during the cool down. The graphic

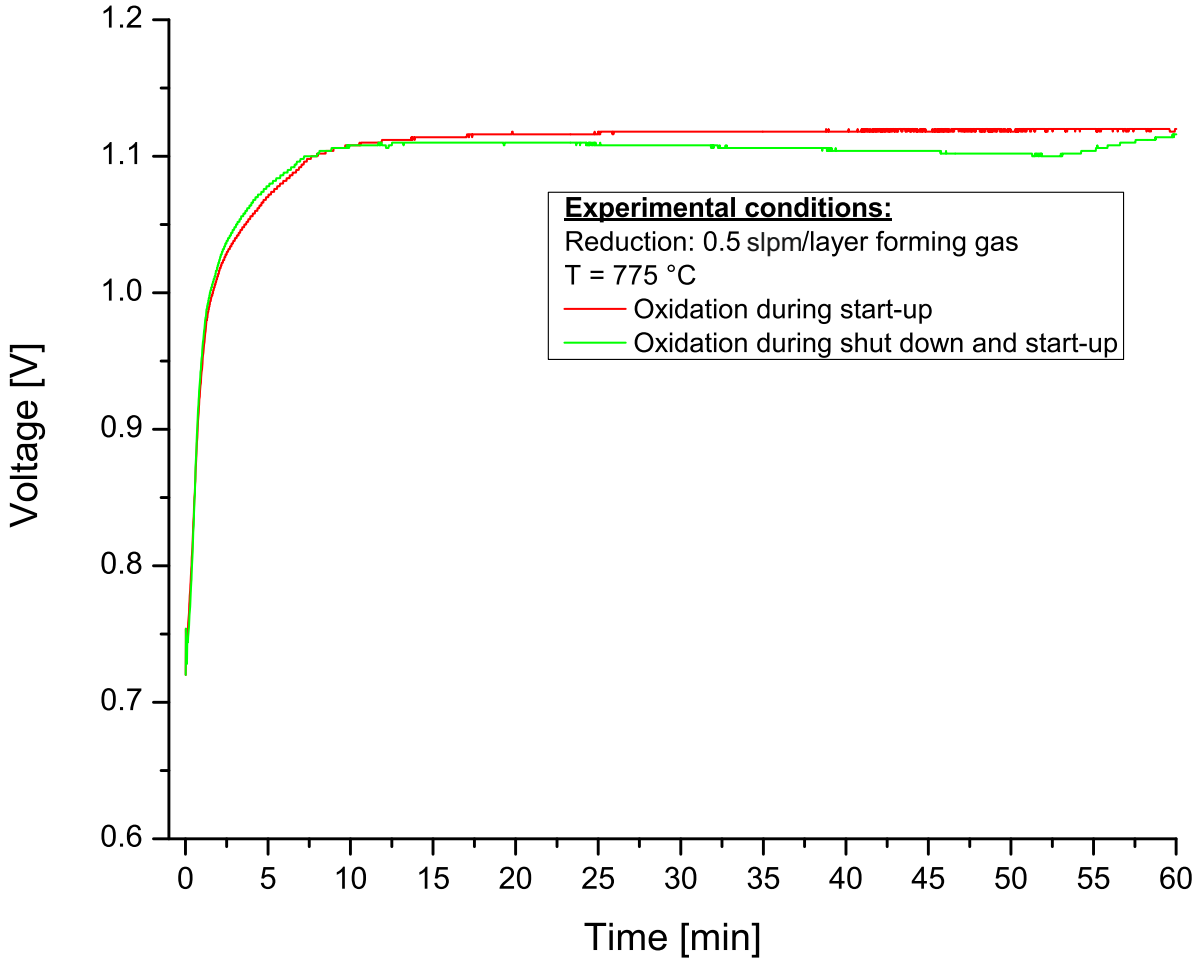

Figure 5.5: Average cell voltage during reduction from two different states of oxidation: Red line: Only start up oxidation, Green line: Start up and cool down oxidation.

shows the voltage versus time. The red line represents the start up oxidation and the green line the oxidation of the entire cycle. From this diagram it can be seen that there is no actual difference in the reduction time. This means that there seems to be no oxidation during the shutdown, which is hard to believe. For this reason the start up times of both cycles should

be investigated in more detail. Figure 5. 6 shows the temperature curves over the time during the heat up of the first and the second cycle. At the time the experiment was conducted, only

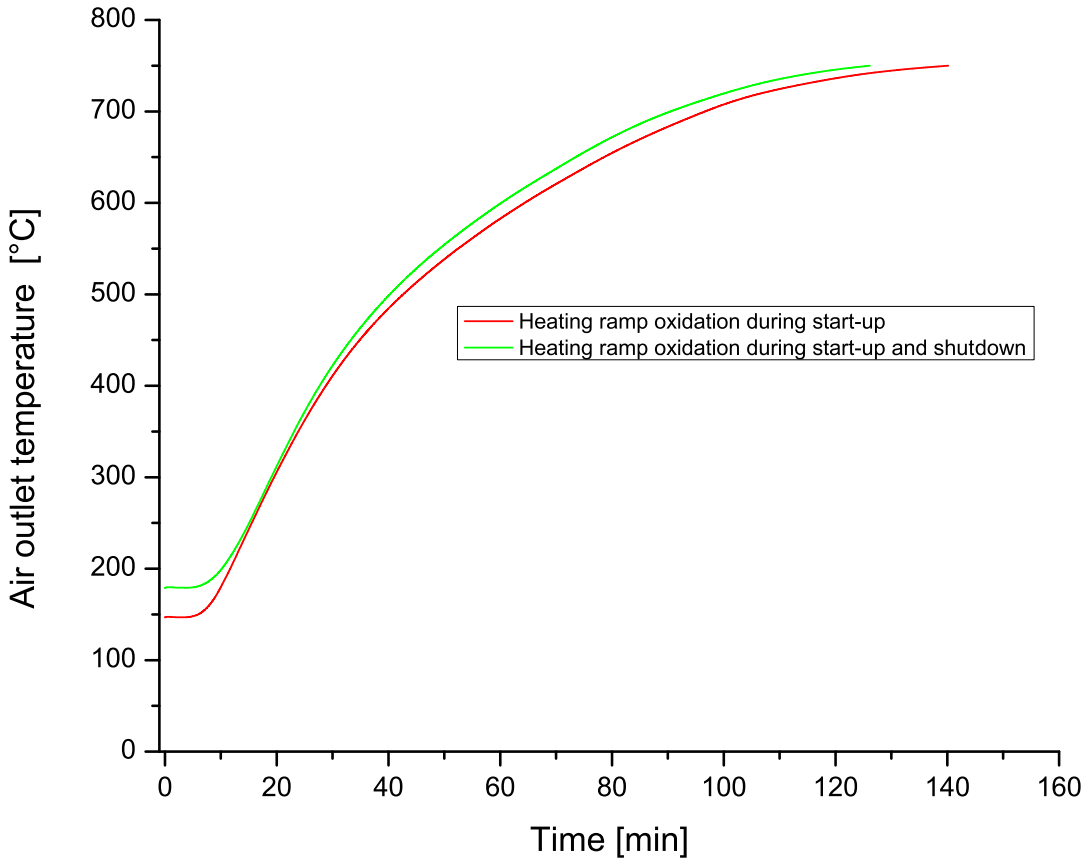

Figure 5. 6: Temperatures curves during the first and second heat up. Red line: Curve during start up oxidation, Green line: Curve during second start up with start up and cool down oxidation.

manual control of the system was possible. This means that the burner is switched on with a specific power input. By passing the 800 °C temperature limit, the power is lowered manually. With rising temperature, the power input needs to be adapted several times. For this reason, it is almost impossible to repeat the same heat up exactly. However, it can be seen from the graphic that the manual control worked very well. Unfortunately there is still a time difference of almost 15 minutes the first start up took longer, which is equal to around 15 % of the time in oxidizing conditions. This means that the influence of the cool down period is equal to 15 minutes difference in start time or 15 %. To sum up, RedOx is mainly a problem during the system start. This result makes sense, because the stack is heated up by air at the cathode side leading to overpressure. Moreover, after flowing through the stack, the air arrives at the

burner, which is directly connected to the anode side. In general the results are quite promising, because the reduction time is equal to DoO of only 6 %. Unfortunately no automatic run was available to check the RedOx cyclability.

Fortunately , there was still the close-to-system test available with the capability of automatic test runs, aiming to answer the second question from the introduction of this chapter. Of course, a stack of the same tightness was chosen for this experiment measured by OCV. Essential for good results is a very close cyclic design, which aims for exact replication from the system cycle regarding heat up and shutdown. Following, the differences should be discussed:

The main limitation is the heat ramp. The burner of the system has a ramp close to infinity, because in the moment of ignition, there is immediately a very high temperature, whereas the electric preheaters are limited by 25 K/min. Moreover, the preheaters need a bit more air flow compared to the system leading to a higher overpressure on the cathode. To make the heating more powerful, additional heating elements were placed at the pipes between stack and test rig. Moreover, the heaters are limited at 820 °C, which is lower compared to burning propane. Nevertheless, the results are quite close to the system as can be seen from figure 5. 7, where the cell voltages and the gas/air in- and outlet temperatures are plotted versus time. The lower heating power can result either in lower outlet temperature when starting the reduction, or significant longer heat up times at high temperatures. In this case there was the decision to choose the heat up time from the system with the result of a lower temperature at 730 °C instead of 750 °C for the cathode outlet. It can be assumed that this is closer to reality than waiting several hours at high temperature to achieve the same temperatures. The following reduction conditions are the same apart from the missing 20 °C.

The temperature characteristic during subsequent cool down is very close to the system due to the use of the same insulating box design. However, there must be a small remaining air flow at the cathode for overheating protection of the electric preheaters. To solve this problem, the preheaters were shut down just before the air flow was set to zero. This way the preheaters were protected and a shut down without air flowing over the cathode side could be realized.

To exclude oxidation by any external air, the exhaust is closed by a valve and the connection between stack and gas panel is ensured by welding. Consequently, all oxidation comes from internal stack leakages. To keep an overview of the differences, they are summed up in the following. ↑ means higher oxidation and ↓ reduced oxidation compared to the system:

- More air flow during heat up and shutdown ↑

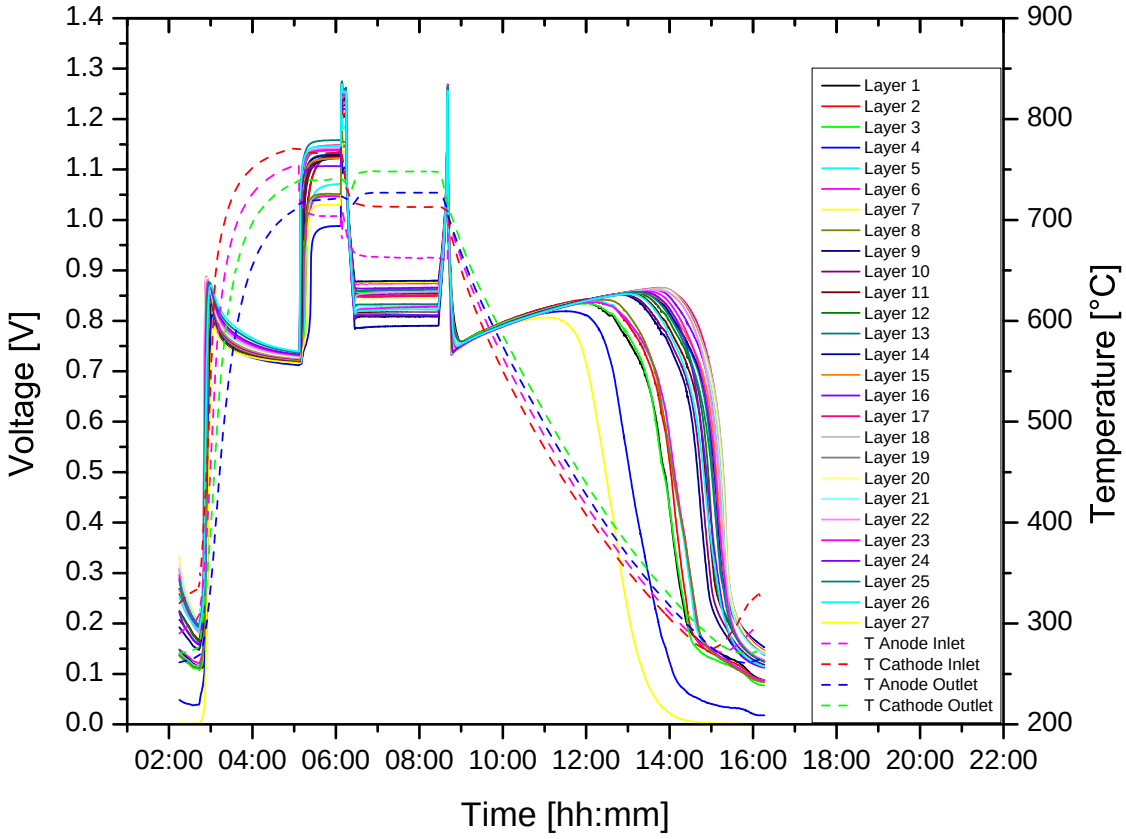

Figure 5. 7: Start up and shutdown cycle without forming gas as close-to-system test: Single cell voltages and gas/air in- and outlet temperatures.

- 20 °C less temperature until reduction ↓
- Closed exhaust - No air from the system components ↓

Figure 5. 8 shows the results from the reduction time measurement for both experiments. The reduction time for the close-to-system experiment is twice that of the system and this is only caused by air coming through internal leakages of the stack. The ratio between start up and shutdown oxidation is equal to the system - meaning almost the entire oxidation comes from the start up in both cases. Looking at the items above, this means the higher air flow during start up has a higher influence on the oxidation than the air flowing back through the system components.

Even if the oxidation is higher than in the system, the stack lifetime should be investigated. For this reason the cycle from figure 5. 7 was repeated several times until the stack was defective.

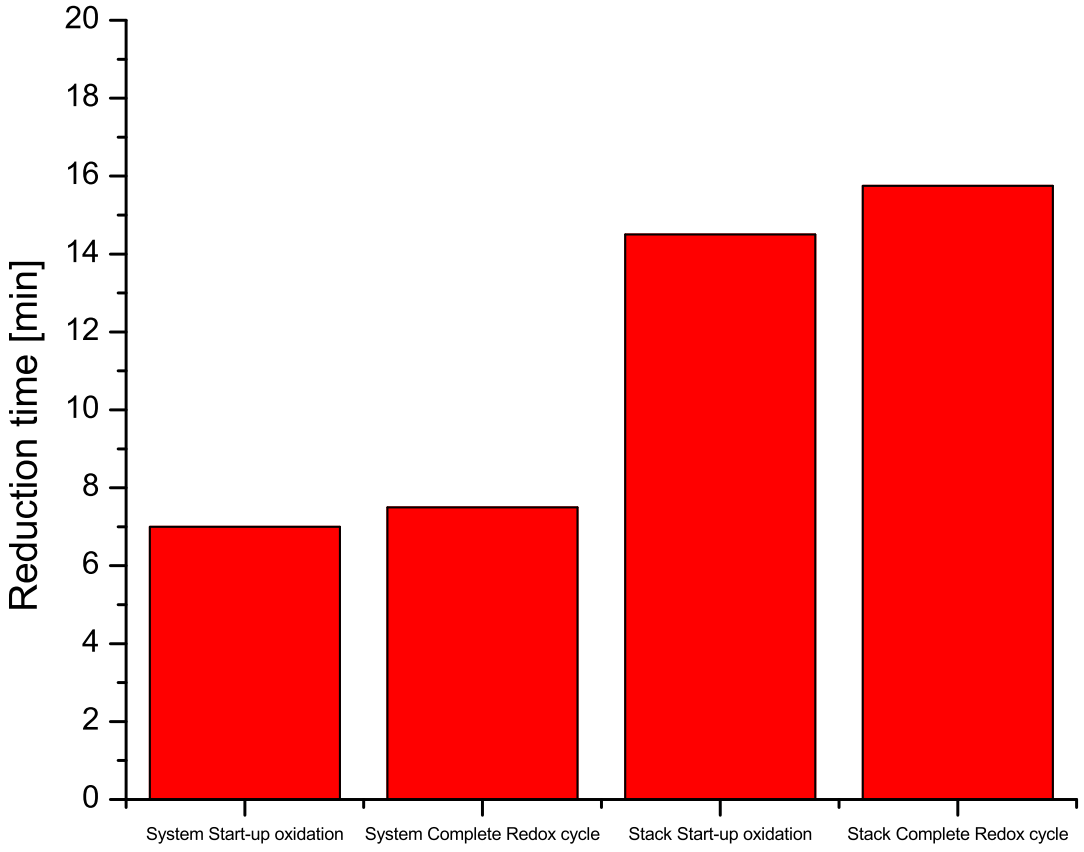

Figure 5. 8: Comparison of close-to-system and system's start up and shutdown oxidation.

Figure 5. 9 and figure 5. 10 show the results. Figure 5. 9 shows the OCV values after full reduction and just before the operation phase against the cycle number. Furtheremore, the gas/air in- and outlet temperatures are plotted. The second diagram shows the stack power, because this is the decisive value for a potential customer. After 15 cycles, the experiment is stopped due to the enormous loss in power and tightness/OCV. From the single cell voltages it can be seen that the good layers remain constant for the first 10 cycles, whereas bad layers begin to fall by the first cycle. The loss in tightness leads to mixing of fuel and air, which causes the increase of temperature.

The results from this chapter can be summed up as double-edged. On the one hand the method application worked very well as the two introducing questions could be answered:

- The system/stack start up phase is clearly dominant in terms of oxidation
- Air from the stack itself without system effect is sufficient to destroy the entire stack within 15 cycles

On the other hand the resulting RedOx behavior puts the SOFC far away from a successful

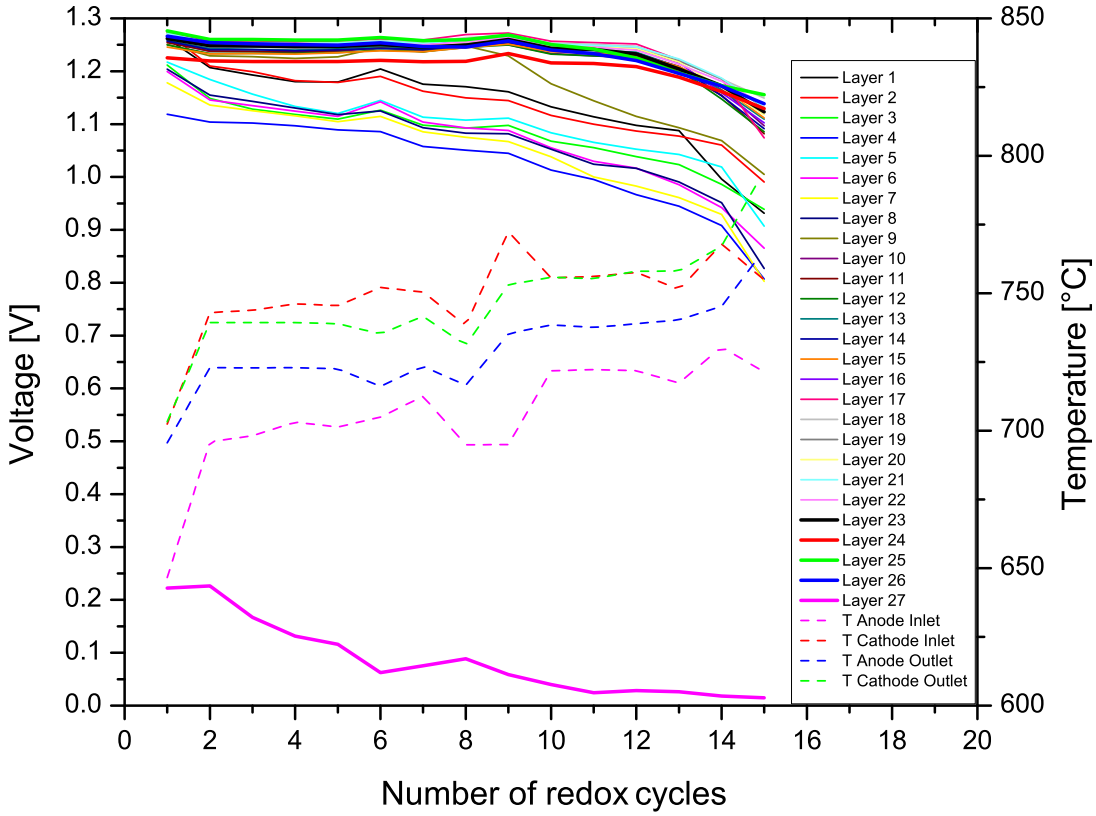

Figure 5. 9: Single cell voltages and gas-/air in- and outlet temperatures versus the cycle number for the close-to-system test without forming gas.

product launch. For this reason the next chapter discusses possible measures, which the author of this work identifies as necessary to make the system ready for the market.

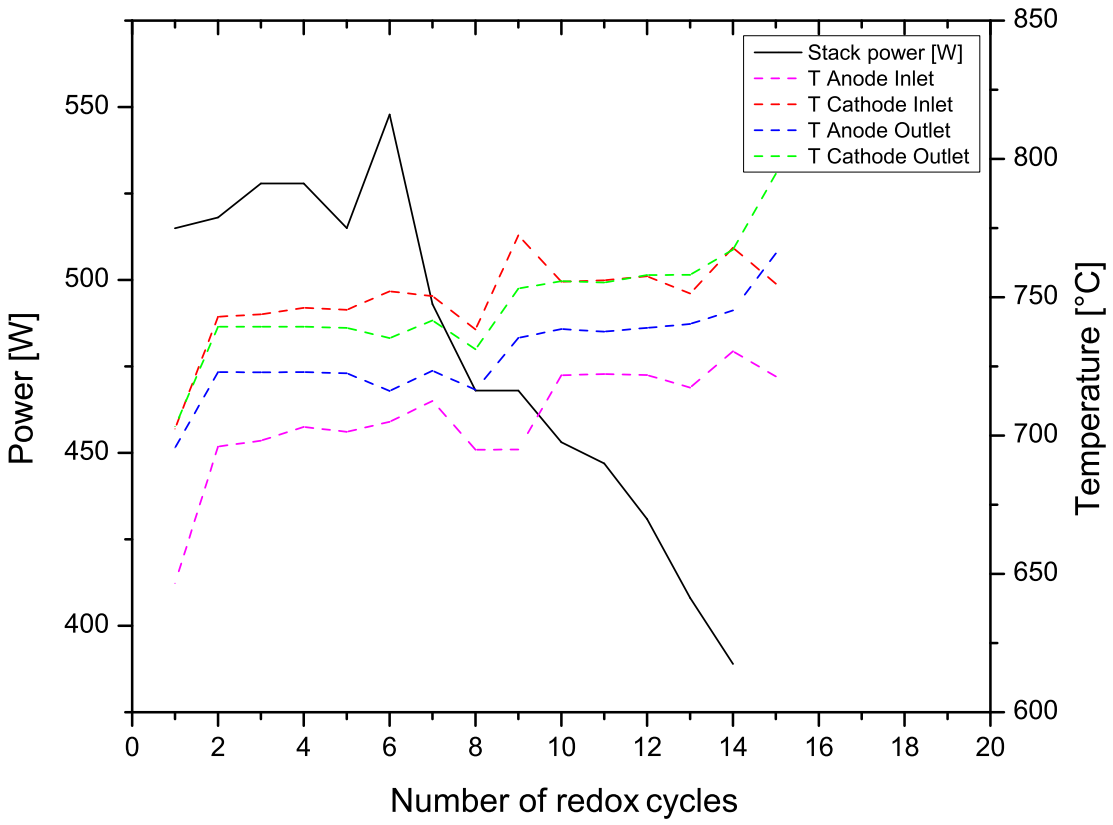

Figure 5. 10: Stack power and gas-/air in- and outlet temperatures versus the cycle number for the close-to-system test without forming gas

Chapter 6

Discussion with focus on a marketable solution

Assuming one start up per week and a 5 year system lifetime means around 250 cycles that the system has to withstand to be a reliable product. This can only be achieved by a significant reduction of the cell oxidation or by RedOx tolerant cells. The second option is already state of the art as there are ESC-cells as described in chapter 2. However, the ESC solution needs higher operation temperatures to achieve the same power densities, which requires a different and not economical stack design. Furthermore, even the ESC has RedOx induced degradation. To overcome the RedOx problem, this chapter discusses a practicable solution and also shows the first experimental results. In general, the solution comprises two elements - use of protective gas and a new 'hybrid cell', which is a mixture of an ASC and ESC. Starting with the first approach it must be said that the use of protective gas is not a new solution. However, even if the stack is still leaking, the tightness was significantly improved over the last few years i.e. by the development of glass-ceramic sealing. This fact leads to the idea of this chapter - to use an adaptive amount of forming gas, which is as little as possible to prevent oxidation, but saves gas as much as possible. Consequently, it must be found out how much forming gas must be used and if that amount is still economically practicable. Since the amount of forming gas depends on the tightness of the stack, it is difficult to define a fixed value. For this reason a voltage limit should be found where no oxidation takes place. This limit should be determined by single layer testing. Following that, the amount of forming gas used at the single layer test bench is used to check the economical efficiency of this solution. By passing this check, a stack test will be conducted showing the possible lifetime by using that voltage limit.

Figure 6. 1 shows two experiments at the single layer test bench investigating the voltage limit. Theoretically, the voltage must be kept above the RedOx potential to prevent oxidation, which

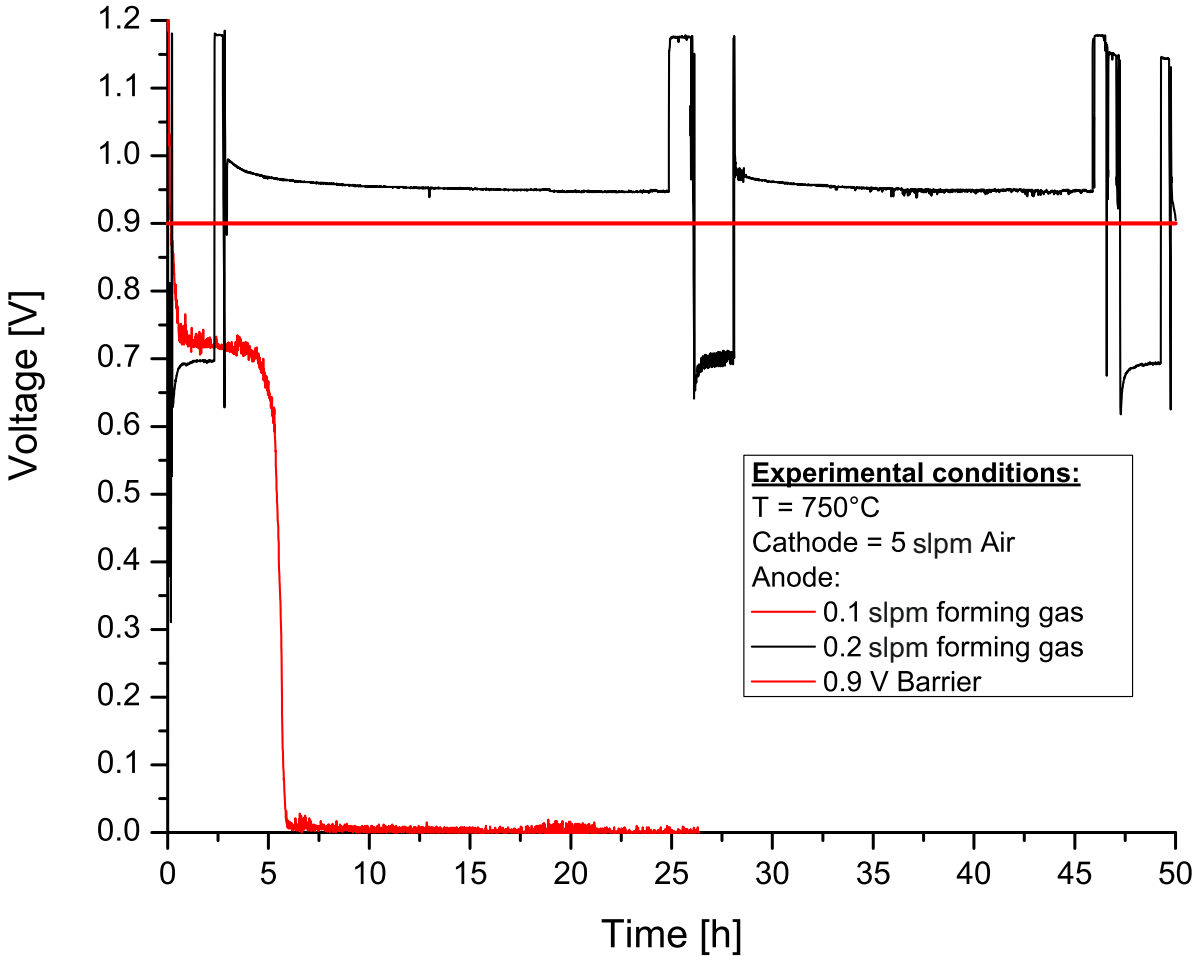

Figure 6. 1: Evaluation of the minimal voltage for RedOx free operation at the single layer test bench. Voltage is controlled by a low amount of forming gas.

was tried in the first experiment represented by the red line. It starts with fuel and air supply at 750 °C. Next, the forming gas was lowered to 0.1 slpm, while the air flow was kept at 5 slpm. Consequently, the voltage dropped, but was still slightly higher than the calculated RedOx potential at this temperature. However, the voltage dropped to zero within 6 hours. Since the voltage was very close to the RedOx potential and the gas distribution is not entirely perfect, there might be areas of oxidation at the cell. The resulting potential is a mixed potential consisting of the RedOx potential and a low OCV value. To be successful the second time, the forming gas flow was doubled to 0.2 slpm and the experiment was started with a new single layer represented by the black line. Before, after and in the middle of the experiment a current-

voltage plot was recorded to check if there was any degradation due to the low flow of forming gas. After the initial performance test, 0.2 slpm were supplied to the layer resulting in an OCV of 0.95 V constant for 40 hours, interrupted once for the intermediate performance test. Figure 6. 2 shows the three current voltage plots, where there is no change in power after 40 hours at 0.2 slpm forming gas.

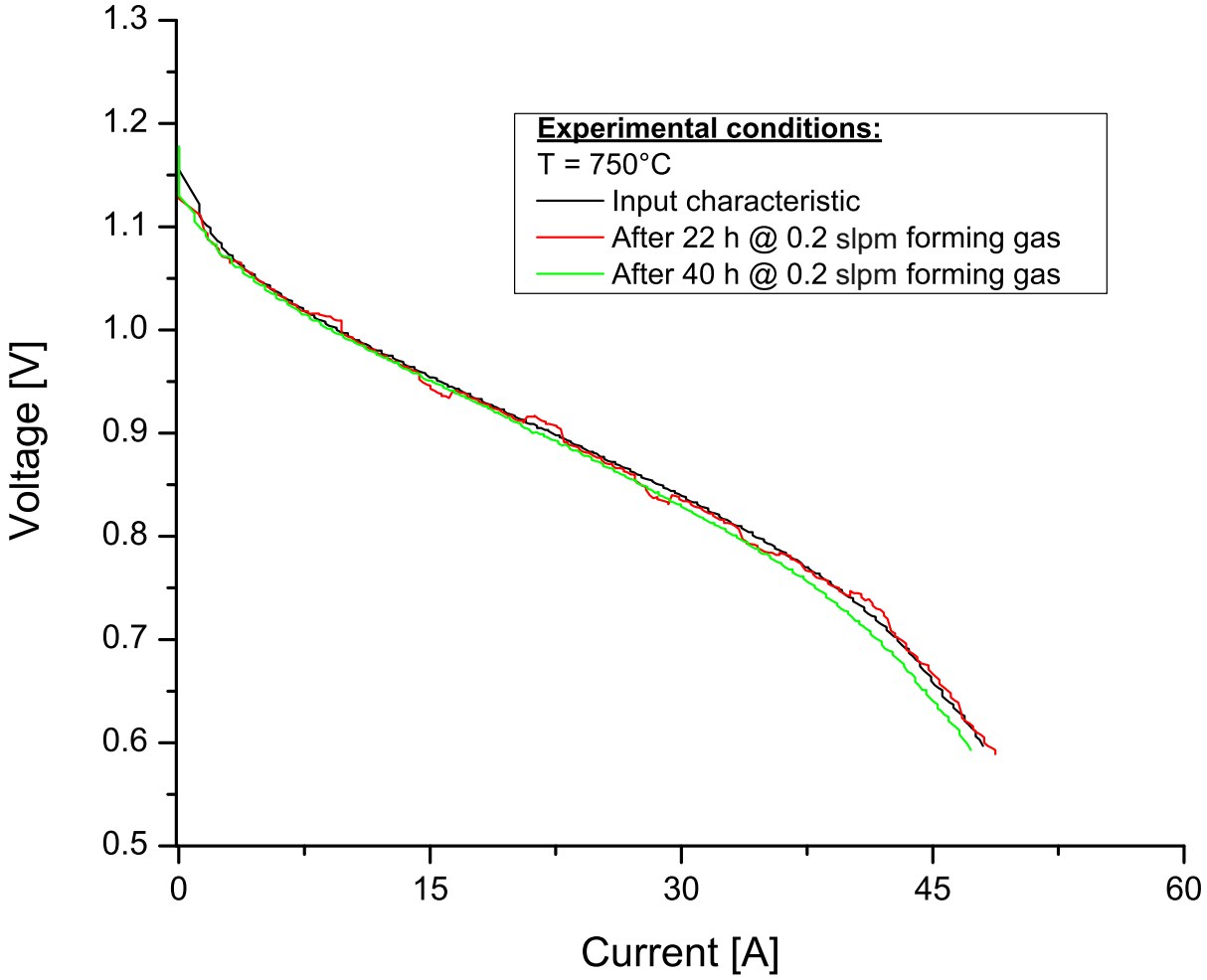

Figure 6. 2: Performance assessment after 40 hours operation with a low amount of forming gas at the single layer test bench.

The single layer testing has shown that a voltage of 0.75 V is not sufficient to protect the cell, whereas at 0.95 V there is absolutely no degradation. For this reason the limit was defined to be 0.9 V represented by the red horizontal line in figure 6. 1. In the following, the economical efficiency as well as the practicability for the customer must be checked. First, the amount of forming gas needed for a system has to be evaluated by transforming the result from the single layer test bench to the stack in the system:

As known from the method development, the glass ceramic sealing of the stack is better than the mica seals of the single layer test bench. Furthermore, the cell area of the system's stack is only half of the one tested in the single layer test bench. For this reason the flow can be cut down to 0.1 slpm/layer, so there is still the safety factor of the better glass ceramic seal. As the stack has 20 layers, 2 slpm are needed. Taking the start time, which essentially causes the cell oxidation, 240 sl forming gas are needed for each cycle. Taking a type 50 gas bottle, which contains 10.000 l gas, 41 cycles would be possible. Depending on the application type this means almost one year of operation. By requesting the gas price at different suppliers, the total cost over lifetime could be calculated to be €100 based on the gas price and the assumption that the customer changes the bottle. Similar services and change/refuel of liquids respectively are already well-known and accepted by the customers in other fields of technology such as in the automotive industry:

- Engine oil change approximately each year depending on the daily mileage
- Refuel of AdBlue for exhaust gas treatment
- WaterBoost technology in series for BMW M4 GTS, water needs to refueled every 3000 km [71]

To validate the forming gas solution, a close-to-system test was conducted as illustrated in figure 6. 3. The graph shows the cell voltages as well as the in- and outlet temperatures versus the time for one complete cycle. In general, the cycle consists of heating up with protective gas followed by turning on the fuel supply, operation phase, operation stop and shutdown. The weakest cell stays above the 0.9 V limit during start up and shutdown. Unfortunately the spread in layer quality was not the best for this stack, so 4 slpm forming gas needed to be used.
Figure 6. 4 illustrates the subsequent cycling test, where the cell voltages and temperatures are plotted versus the number of cycles. This test was very successful as the stack was in operation for three months, equal to 140 cycles. Over the three months there were two errors caused by the test rig and not by the stack. The first one at cycle 49 was due to a local blackout, which fortunately had no influence on the stack due to good safety functions of the test rig. Only the automatic data evaluation did not work correctly as can be seen from the lower temperatures in the graph. The second failure was detrimental for the stack as the test rig put a current to the stack without fuel - an unplanned no fuel current experiment though. Surprisingly, the stack's degradation was very low as only the weakest layer, 19, was lowered in its power density

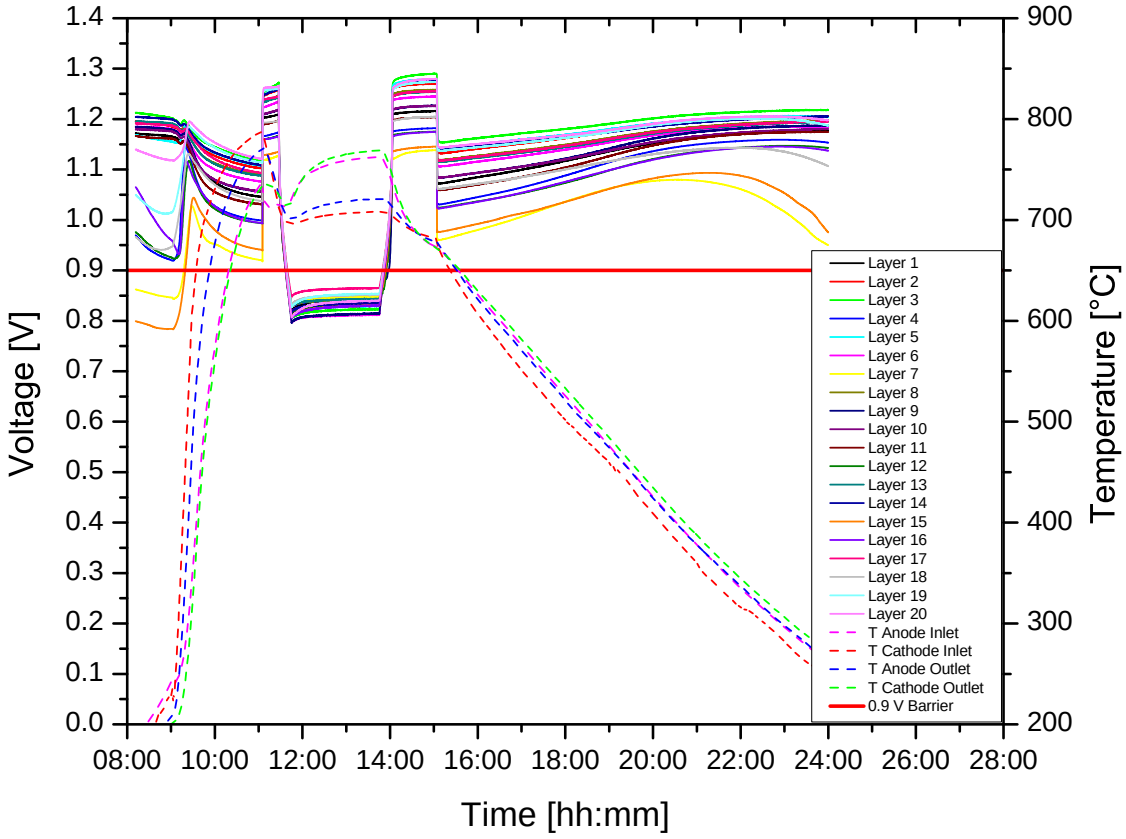

Figure 6. 3: Close to system test showing the start up and shutdown cycle, where the lowest cell voltage is hold above the 0.9 V barrier indicated by the red horizontal line.

and OCV. Unfortunately, the degradation in tightness of this layer worsened from this point of time. However, this degradation was very slow, since around 80 cycles could be added until this layer leaded to the failure of the stack.

Since the absolute power is the value needed to convince the customer, it is illustrated in figure 6. 5 versus the cycle number. To get reliable values, the power data were always taken at the same temperature, which can be seen from the constant temperatures with rising cycle number. Although there was the no fuel current situation, the overall degradation was only at 4 % from 570 W to 550 W, which is quite promising in terms of a marketable product. However, there is still work to do. Comparing the OCV value shows that there is a wide spread in sealing quality. Developments must be made on improvement of the sealing, as well as the process stability to get only the best layers aiming for a lowering of protective gas. By taking this result into account as well as the problem of testing and the development planned for the next months

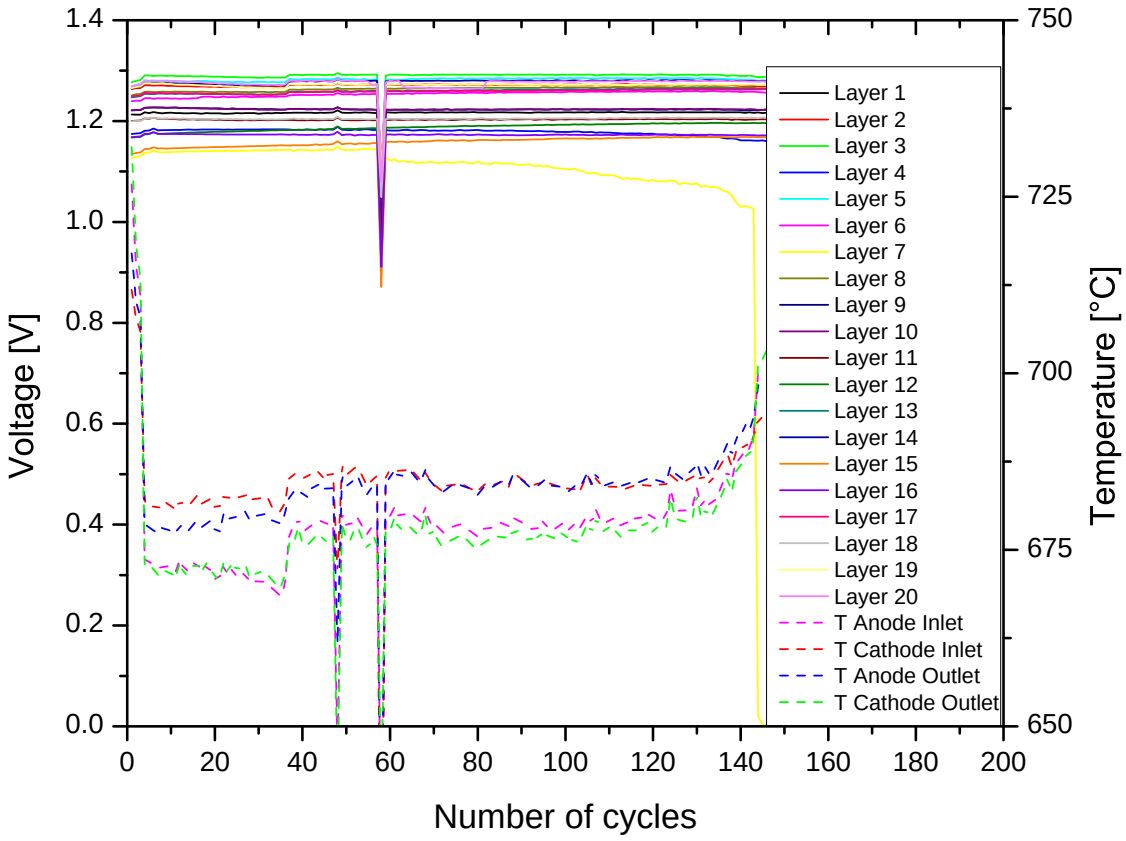

Figure 6. 4: Single cell voltages and gas-/air in- and outlet temperatures versus the cycle number for the close-to-system test, where the minimum cell voltage is hold above 0.9 V within the cycle.

and years, the aim of 250 cycles seems to be realistic. Later on the solution can be taken to the next level by continuously controlling the amount of protective gas with the cell voltages as an input variable. This way the amount can be adapted perfectly to the quality of each stack as well as the decrease in tightness with lifetime.

Even if the protective gas solution works well, it would be good to have cells within the system, which are a bit more RedOx tolerant than the current ones. There can always be system/software failures where the protective gas supply is disturbed. For this reason, it is important to have a second level of safety.

As already shown, ASCs as well as ESCs are not suitable, which leads to the idea to combine the positive properties of both cell types and thus to create a new 'hybrid-cell'. Essentially, the idea is to rethink the ratio of anode and electrolyte layer thickness to develop an optimum of

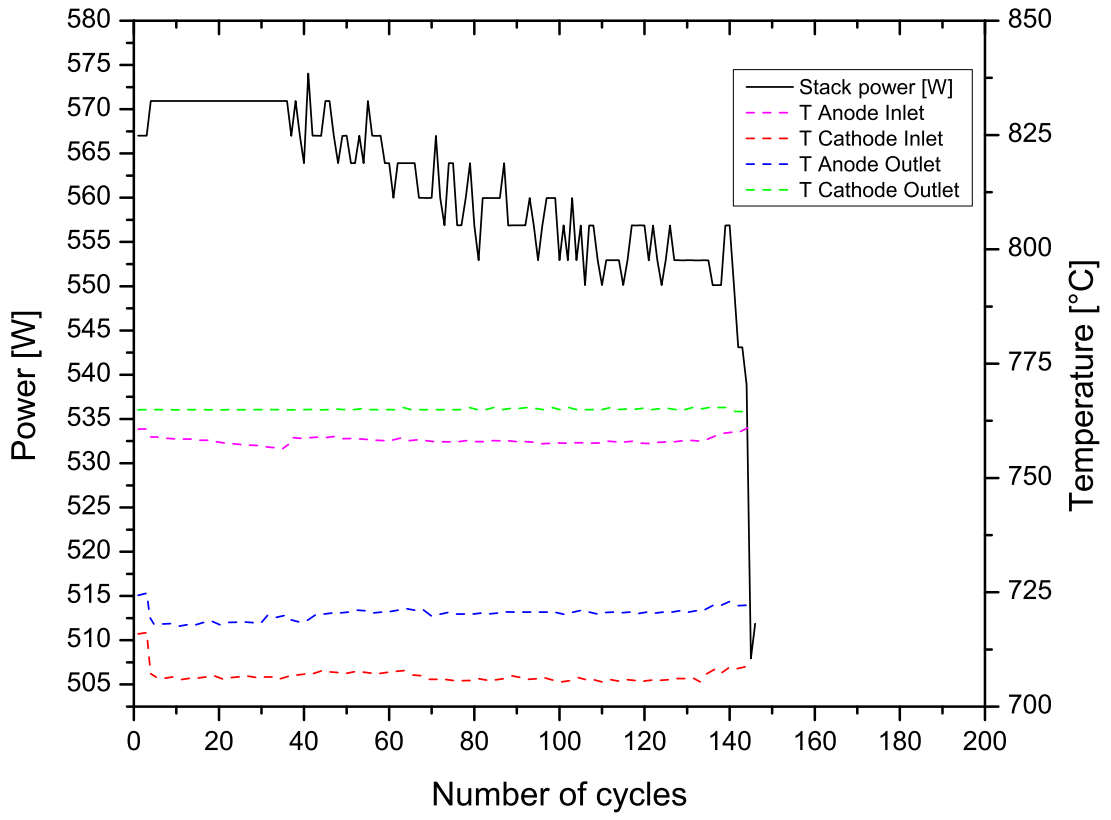

Figure 6. 5: Stack performance and gas-/air in- and outlet temperatures versus the cycle number for the close-to-system test, where the minimum cell voltage is held above 0.9 V within the cycle.

sufficient power density and strength of the electrolyte. For this reason a finite element analysis (FEA) study for several thickness combinations was conducted by PAUSCH [16, 72]. The results are presented in figure 6. 6.

The graph shows the tensile stress of the electrolyte versus the strain of the anode. The strain corresponds to the DoO, which is plotted on the second horizontal axis. The red horizontal line corresponds to the maximum tensile stress the 8YSZ-electrolyte can withstand. All input data for the simulation is taken from the literature as presented in chapter 2. Due to the fabrication process, there are negative stresses in the electrolyte in the reduced state [16]. By starting oxidation, the anode material expands, which puts the electrolyte under tensile stress. Consequently, this stress increases with rising DoO and strain of the anode material. Degradation in terms of tightness of the electrolyte happens if the maximum tensile stress of the 8YSZ material is exceeded. For the same DoO, the value of the electrolyte tensile stress depends on the thickness of the electrolyte and anode layer as illustrated in the graph. The red dotted

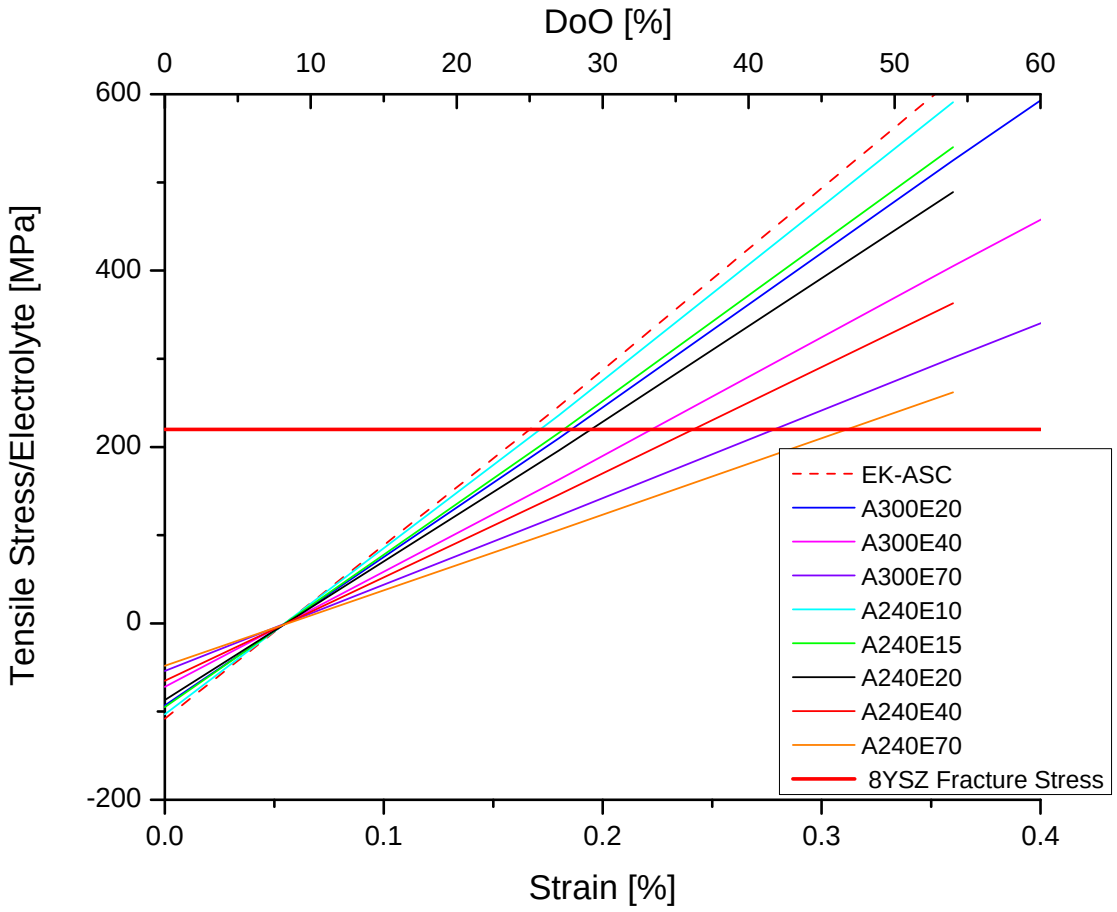

Figure 6. 6: Simulated strain within the electrolyte for different anode/electrolyte thicknesses as a function of the anode strain and the DoO. Red line = Fracture stress of the 8YSZ-electrolyte

line represents the current EK-cell used in this work. Based on the results from the simulation, the fracture stress of that cell is exceeded at a DoO of 25 %. The DoO measurement of the system resulted in a DoO of only 6 %. However, the local DoO can be significantly higher as measured in chapter 4. By changing the thickness of anode and electrolyte layer, the maximum possible strain moves to higher values. In general, a lower anode thickness leads to a lower force affecting the electrolyte, and a higher electrolyte thickness leads to lower stresses based on the stress definition force per area. Based on the graph the best combination is A240E70, which is, however, an ESC. Consequently, something in-between will be the combination of choice, which needs to be evaluated in future work. Performance, improvement of RedOx stability, fabrication issues and cost must be considered.

Chapter 7

Conclusion and future work

Currently SOFC systems do not fulfill the required lifetime for a successful product launch. A life cycle of a SOFC system is characterized by constant operation combined with start and stop cycles. The latter is one of the major technical challenges for successful commercialization. The main difficulties lie in the stress-induced failure of the electrolyte due to repeating oxidation and reduction (RedOx) of the anode material. The most common anode material is fabricated from a precursor composed of a powder mixture of ceramic nickel oxide (NiO) and Yttria Stabilized Zirconia (YSZ). When hydrogen fuel gas is supplied to the cell, NiO is reduced to Ni, so that the precursor is converted into a Ni-YSZ ceramic-metal-composite (cermet)[3]. Once the fuel flow is interrupted (start and stop-phase), oxygen will enter the anode side. This leads to oxidation since nickel is not stable in air at temperatures above 300 °C. This insufficient stability in combination with the tendency towards soot formation forms the core of the RedOx issues for SOFCs.

A key factor indicating the extent of cell damage is the degree of oxidation (DoO), where 100 % is the initial state of the precursor and 0 % is the reduced state during operation. The simplest way to determine the DoO is to measure the weight gain during oxidation. However, weight measurement of cells is only possible after destructive disassembling of the stack.

In this research a new non-destructive method was developed which describes the RedOx behavior of SOFC cells in stacks and systems within operation. Scientific investigations into this topic are very time- and cost-consuming, because of the RedOx-induced cell damage and thus the failure of the entire stack. To simplify the research on such topics, a special test has been developed at the beginning of this investigation. This test bench is supposed to facilitate testing of single stack layers, which goes hand in hand with quick and cheap cell exchange.

The method development is based on the typical voltage curve during a RedOx cycle according to figure 7. 1. At the beginning the fuel supply is turned off. Since the system is not completely

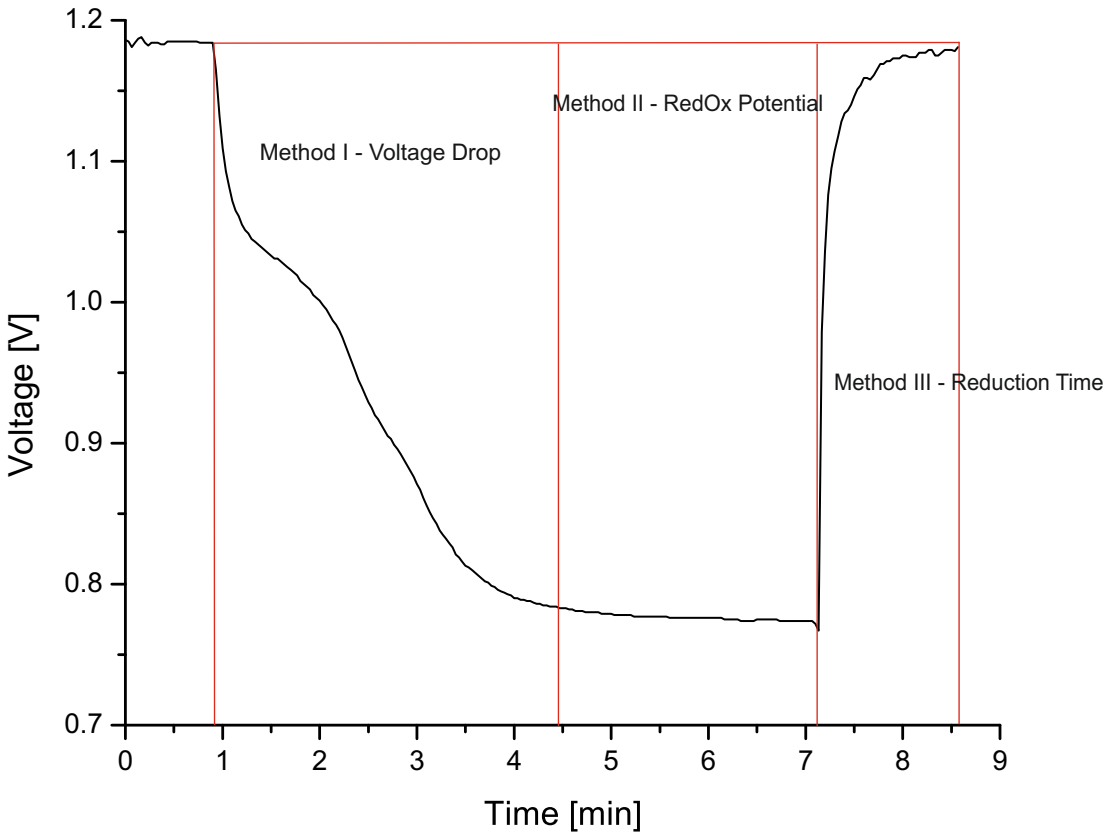

Figure 7. 1: Voltage characteristic during a RedOx cycle and relation to the measurement methods developed in this work.

tight, oxygen flows to the anode area and "burns" directly to water. Furthermore, there can be a low parasitic current, which consumes the fuel. For this reason the water content rises over time and thus the open cell voltage falls. When the hydrogen is fully utilized, oxidation begins and thus the voltage has to be at the value for the calculated RedOx potential. Once hydrogen is supplied to the cell, reduction takes place. If the cell is fully reduced as well as dried of any water (product of the reduction process), the voltage corresponds to the initial value - assuming no cell damage due to the oxidation. In this work additional oxygen was supplied to the cell during the three phases to investigate the influence of the RedOx state on the voltage curve resulting in three measurement methods named after the phase of the cycle, so there is the voltage drop, the RedOx potential and the reduction time method.

First, the voltage drop as a function of the additional air flow on anode side was characterized. It was found, that the voltage drop is quite short. It was possible to characterize to what extent

a layer/stack leaks. Additional air flowing to the cell after the drop down was not captured by this method, but led to further oxidation. To sum up, no additional information could be captured compared to the OCV value, which is well-known as leading criterion for tightness.
During the drop down experiments, it was also observed, that untight layers show not only a fast drop to RedOx potential but also drop below the RedOx potential after a short while. Based on that observation, the RedOx potential method was developed. Therefore the voltage curve was plotted over several hours with different air flows on the anode side. These experiments showed a clear relation between air flow and voltage drop: the higher the air flow at the anode and thus the oxidation state, the faster the drop. Since not only the air flow influences the oxidation state, but also the temperature, the experiment was repeated at different temperatures with a surprising result: The higher the temperature, the slower the drop. This behavior could be explained by using the basics of electrochemical oxidation. Additional non fuel current experiments have been conducted to prove the theory behind the temperature drop relation. During those experiments a current was supplied to the cell without fuel. This way, the power of oxidation could be measured. To conclude, the RedOx potential method can be used to compare different systems concerning their oxidation behavior during start up and shutdown. A big advantage lies in the simple measurement procedure. Every start up and shutdown without forming gas generates characteristic voltage plots. For this reason, the measurement comes without any additional effort. However, this method does not provide quantitative results such as an exact value for the DoO. If this is needed, there is the option to construct calibration curves, where a voltage level is directly referred to a DoO. Moreover, a database can be created providing the information of which voltage plot during start up and shutdown of different system setups leads to which lifetime. To get closer to a direct measurement of the DoO, the reduction time method was developed.
Every RedOx cycle ends with the resupply of fuel leading to a reduction of the anode cermet. Only the nickel particles oxidized before can be reduced - thus the higher the DoO, the more reduction takes place, the longer it takes. Based on that theory, cells were oxidized with different amounts of oxygen. Afterwards the time of reduction was measured showing a linear correlation between oxidation time/DoO and reduction time. The reduction time method is based on the simple relation: The higher the DoO is, the more time is needed for reduction. The time of reduction is a quantitative value, which could be converted to the DoO by using the stoichiometry of the chemical reaction.
After the method development on the single layer test bench, the methods were validated by

stack testing to prove they are scalable and integrable into a standard system cycle without any negative effects. In subsequent system and stack tests, the methods were used to separate the oxidation occurring during start up from oxidation during the shutdown phase. The measurement showed that the start up phase has the more major contribution caused by the hot air flowing through the stack and the system when it heats up. Furthermore, the influence from system components such as oxygen diffusion through the exhaust were separated from leakages of the stack itself. It came out that the internal leakage without additional system influence is sufficient to destroy the stack within a few start- and stop cycles. This work ends with the elaboration of a possible solution. First, the minimal cell voltage for a safe operation was determined on the single layer test bench. Subsequently a stack test was conducted, where the required cell voltage was hold during start and stop-phase by using forming gas. Within this test no negative effect from the low amount of forming gas could be seen. In future this solution must be improved by continuously controlling the amount of protective gas with the cell voltages as an input variable. This way, the amount can be adapted perfectly to the sealing quality of each stack as well as the decrease in tightness over lifetime. This enables the use of forming gas under economically feasible conditions, since it is used as little as possible. For further improvement regarding system failures (no usage of forming gas for some reason) a "hybrid cell" was proposed based on a finite element simulation. Aim of this "hybrid cell" was to combine the benefits of electrolyte and anode supported cells.

Literature

[1] Federal Ministry of Education and Research, https://www.bmbf.de/en/energy-and-economy-2318.html (05.03.2015).

[2] Federal Environmental Agency, http://www.umweltbundesamt.de/daten/klimawandel/treibhausgas-emissionen-in-deutschland.html (05.03.2015).

[3] Radovic, M.; Lara-Curzio, E.: Elastic Properties of Nickel-Based Anodes for Solid Oxide Fuel Cells as a Function of the Fraction of Reduced NiO. Journal of the American Ceramic Society 87 (2004) 12, p. 2242–2246.

[4] O'hayre, R.; Cha, S.; Prinz, F.; Colella, W.: Fuel cell fundamentals. John Wiley & Sons (2016).

[5] new enerday GmbH, http://www.new-enerday.com/pics/funktionsgrafik2en.jpg (10.11.2016).

[6] Larminie, J.; Dicks, A.: Fuel cell systems explained. J. Wiley, Chichester and West Sussex (2003).

[7] Carrette, L.; Friedrich, K.A.; Stimming, U.: Fuel cells–fundamentals and applications. Fuel cells 1 (2001) 1, p. 5–39.

[8] Kurzweil, P.: Thermodynamik und Kinetik der Brennstoffzelle. In Brennstoffzellentechnik, p. 17–52. Springer (2013).

[9] Bujalski, W., University of Birmingham, Solid Oxide Fuel Cells, http://www.durablepower.eu/images/downloads/hoe/02_01_03_REALSOFC_3Review+testing+project.pdf (07.02.2017).

[10] Kettering University, http://orgs.kettering.edu/altfuel/fcback.htm (08.02.2017).

[11] Ivers-Tiffée, E.: Brennstoffzellen und Batterien. In Brennstoffzellentechnik. Universität Karlsruhe, Institut für Elektrotechnik (2006).

[12] Zhu, W.; Deevi, S.: A review on the status of anode materials for solid oxide fuel cells. Materials Science and Engineering: A 362 (2003) 1, p. 228–239.

[13] Kakac, S.; Pramuanjaroenkij, A.; Zhou, X. Y.: A review of numerical modeling of solid oxide fuel cells. International journal of hydrogen energy 32 (2007) 7, p. 761–786.

[14] Faes, A.; Hessler-Wyser, A.; Zryd, A. et al.: A review of redox cycling of solid oxide fuel cells anode. Membranes 2 (2012) 3, p. 585–664.

[15] Forschungszentrum Jülich, http://www.fz-juelich.de/portal/EN/Research/Energy Environment/Fuelcells/SOFC/_anode.html (17.02.2017).

[16] Pausch, M.: Strukturmechanische FEM-Simulation des thermozyklischen Verhaltens planarer SOFC Stacks. Dissertation, RWTH Aachen (02.07.2012).

[17] Hilpert, K.; Quadakkers, W.; Singheiser, L.: Interconnects. Handbook of Fuel Cells (2003).

[18] VDM, ThyssenKrupp: Material Data Sheet No. 4046 for Crofer 22 APU (2010).

[19] Kiefer, T.: Entwicklung neuer Schutz- und Kontaktierungsschichten für Hochtemperatur-Brennstoffzellen. Dissertation, Forschungszentrum Jülich (2008).

[20] Reitz, E.: Dissertation regarding glass ceramic sealings - not yet completed. Dissertation, Karlsruher Institut für Technologie (2017).

[21] Morandi, A.; Fu, Q.; Marrony, M.; Bassat, J.-M.; Joubert, O.: Integration of Innovative Oxide Materials in an Intermediate Temperature Solid Oxide Fuel Cell. ECS Transactions 57 (2013) 1, p. 733–742.

[22] Stevens, R.: An introduction to zirconia: Zirconia and zirconia ceramics. Magnesium Electrum, Twickenham (1986).

[23] Minh, N. Q.; Takahashi, T.: Science and technology of ceramic fuel cells. Elsevier (1995).

[24] Badwal, S.; Drennan, J.: Yttria-zirconia: effect of microstructure on conductivity. Journal of materials science 22 (1987) 9, p. 3231–3239.

[25] Setoguchi, T.; Okamoto, K.; Eguchi, K.; Arai, H.: Effects of anode material and fuel on anodic reaction of solid oxide fuel cells. Journal of The Electrochemical Society 139 (1992) 10, p. 2875–2880.

[26] Ivers-Tiffée, E.; Wersing, W.; Schiessl, M.; Greiner, H.: Ceramic and metallic components for a planar SOFC. Berichte der Bunsengesellschaft für physikalische Chemie 94 (1990) 9, p. 978–981.

[27] Jiang, S.-P.; Chan, S.-H.: A review of anode materials development in solid oxide fuel cells. Journal of Materials Science 39 (2004) 14, p. 4405–4439.

[28] Atkinson, A.; Barnett, S.; Gorte, R. J.; Irvine, J.; McEvoy, A.; Mogensen, M.; Singhal, S.; Vohs, J.: Advanced anodes for high-temperature fuel cells. Nature materials 3 (2004) 1, p. 17–27.

[29] Steele, B.: Materials for IT-SOFC stacks: 35 years R&D: the inevitability of gradualness. Solid state ionics 134 (2000) 1, p. 3–20.

[30] Mori, M.; Yamamoto, T.; Itoh, H.; Inaba, H.; Tagawa, H.: Thermal Expansion of Nickel-Zirconia Anodes in Solid Oxide Fuel Cells during Fabrication and Operation. Journal of the Electrochemical Society 145 (1998) 4, p. 1374–1381.

[31] Hu, W.; Guan, H.; Sun, X.; Li, S.; Fukumoto, M.; Okane, I.: Electrical and Thermal Conductivities of Nickel-Zirconia Cermets. Journal of the American Ceramic Society 81 (1998) 8, p. 2209–2212.

[32] Singhal, S.-C.; Dokiya, M.: Solid Oxide Fuel Cells (SOFC VI): Proceedings of the Sixth International Symposium. The Electrochemical Society (1999).

[33] Lee, J.-H.; Moon, H.; Lee, H.-W.; Kim, J.; Kim, J.-D.; Yoon, K.-H.: Quantitative analysis of microstructure and its related electrical property of SOFC anode, Ni-YSZ cermet. Solid State Ionics 148 (2002) 1-2, p. 15–26.

[34] Müller, A.: Mehrschicht-Anode für die Hochtemperatur-Brennstoffzelle (SOFC). Dissertation, Karlsruher Institut für Technologie (2004).

[35] Itoh, H.; Yamamoto, T.; Mori, M.; Horita, T.; Sakai, N.; Yokokawa, H.; Dokiya, M.: Configurational and electrical behavior of Ni-YSZ cermet with novel microstructure for solid oxide fuel cell anodes. Journal of The Electrochemical Society 144 (1997) 2, p. 641–646.

[36] Ettler, M.: Einfluss von Reoxidationszyklen auf die Betriebsfestigkeit von anodengestützten Festoxid-Brennstoffzellen. Dissertation, Forschungszentrum Jülich (2009).

[37] Hauler, F.: Public funded project SMART II, AP330 Stackintegration: Stacks mit modifizierten Zellen, "Internal Presentation".

[38] Jordan, N.; Assenmacher, W.; Uhlenbruck, S.; Haanappel, V.; Buchkremer, H.; Stöver, D.; Mader, W.: $Ce_{0.8}Gd_{0.2}O_{2-\delta}$ protecting layers manufactured by physical vapor deposition for IT-SOFC. Solid State Ionics 179 (2008) 21, p. 919–923.

[39] Klemensø, T.: Relationships between structures and performance of SOFC anodes. Dissertation, Technical University of Denmark (DTU) (2005).

[40] Iwanschitz, B.: Degradation von Ni-Cermet-Anoden in keramischen Hochtemperaturbrennstoffzellen. Dissertation, RWTH Aachen (2012).

[41] Ettler, M.; Timmermann, H.; Malzbender, J.; Weber, A.; Menzler, N.: Durability of Ni anodes during reoxidation cycles. Journal of Power Sources 195 (2010) 17, p. 5452–5467.

[42] Sarantaridis, D.; Atkinson, A.: Redox Cycling of Ni-Based Solid Oxide Fuel Cell Anodes: A Review. Fuel cells 7 (2007) 3, p. 246–258.

[43] Richardson, J.-T.; Scates, R.; Twigg, M.: X-ray diffraction study of nickel oxide reduction by hydrogen. Applied Catalysis A: General 246 (2003) 1, p. 137–150.

[44] Utigard, T.; Wu, M.; Plascencia, G.; Marin, T.: Reduction kinetics of Goro nickel oxide using hydrogen. Chemical Engineering Science 60 (2005) 7, p. 2061–2068.

[45] Tikekar, N.-M.; Armstrong, T.-J.; Virkar, A.-V.: Reduction and reoxidation kinetics of nickel-based SOFC anodes. Journal of The Electrochemical Society 153 (2006) 4, p. A654–A663.

[46] http://www.periodensystem.info/ (01.03.2017).

[47] Larrain, D.; Autissier, N.; Wuillemin, Z.; Molinelli, M.; Favrat, D. et al.: Modeling and experimental validation of solid oxide fuel cell materials and stacks. Journal of The European Ceramic Society 25 (2005) 12, p. 2627–2632.

[48] Wuillemin, Z.; Autissier, N.; Luong, M.-T.; Favrat, D. et al.: Modeling and study of the influence of sealing on a solid oxide fuel cell. In Proceedings of EFC2005, Vol. 5, p. 130–136 (2005).

[49] Neidhardt, J.-P.: Nickel oxidation in solid oxide cells: modeling and simulation of multi-phase electrochemistry and multi-scale transport. Dissertation, Universität Stuttgart (2013).

[50] Feßmann, J.; Orth, H.: Angewandte Chemie und Umwelttechnik für Ingenieure: Handbuch für Studium und betriebliche Praxis. ecomed-Storck GmbH (2002).

[51] Wang, C.-H.; Lee, M.-C.; Huang, T.-J.; Chang, Y.-C.; Kao, W.-X.; Lin, T.-N.: Breeding phenomenon of nickel in anode of solid oxide fuel cell via electrochemical reaction. Electrochemistry Communications 11 (2009) 7, p. 1381–1384.

[52] Wagner, C.: Oxidation of alloys involving noble metals. Journal of The Electrochemical Society 103 (1956) 10, p. 571–580.

[53] Moore, W.-J.; Lee, J.-K.: Kinetics of the formation of oxide films on nickel foil. Transactions of the Faraday Society 48 (1952), p. 916–920.

[54] Atkinson, A.; Taylor, R.; Goode, P.: Transport processes in the oxidation of Ni studied using tracers in growing NiO scales. Oxidation of metals 13 (1979) 6, p. 519–543.

[55] Fouquet, D.; Müller, A.; Weber, A.; Ivers-Tiffée, E.: Kinetics of oxidation and reduction of Ni/YSZ cermets. Ionics 9 (2003) 1-2, p. 103–108.

[56] Iwanschitz, B.; Sfeir, J.; Mai, A.; Schütze, M.: Degradation of SOFC anodes upon redox cycling: a comparison between Ni/YSZ and Ni/CGO. Journal of The Electrochemical Society 157 (2010) 2, p. B269–B278.

[57] Stehlík, K.: Zur Degradation oxidkeramischer Brennstoffzellen. Dissertation, Universität München (2009).

[58] Faes, A.; Nakajo, A.; Hessler-Wyser, A.; Dubois, D.; Brisse, A.; Modena, S. et al.: Redox study of anode-supported solid oxide fuel cell. Journal of Power sources 193 (2009) 1, p. 55–64.

[59] Sarantaridis, D.; Chater, R.; Atkinson, A.: Changes in physical and mechanical properties of SOFC Ni–YSZ composites caused by redox cycling. Journal of The Electrochemical Society 155 (2008) 5, p. B467–B472.

[60] Laurencin, J.; Delette, G.; Lefebvre-Joud, F.; Dupeux, M.: A numerical tool to estimate SOFC mechanical degradation: case of the planar cell configuration. Journal of the European Ceramic Society 28 (2008) 9, p. 1857–1869.

[61] Vasechko, V.; Roehrens, D.; Malzbender, J.: Oxidation studies of anodes layer microstructures in metal supported solid oxide fuel cells. Ceramics International 41 (2015) 4, p. 5852–5856.

[62] Waldbillig, D.; Wood, A.; Ivey, D.-G.: Electrochemical and microstructural characterization of the redox tolerance of solid oxide fuel cell anodes. Journal of Power Sources 145 (2005) 2, p. 206–215.

[63] Malzbender, J.; Steinbrech, R.; Singheiser, L.: Failure probability of solid oxide fuel cells. In Ceramic engineering and science proceedings, Vol. 26, p. 293–298 (2009).

[64] Garche, J.; Dyer, C.-K.; Moseley, P.-T.; Ogumi, Z.; Rand, D.; Scrosati, B.: Encyclopedia of electrochemical power sources. Newnes (2013).

[65] Moore, W. J.: Der feste Zustand: Eine Einführung in die Festkörperchemie anhand sieben ausgewählter Beispiele. Springer-Verlag (2013).

[66] Waldbillig, D.; Wood, A.; Ivey, D.: Enhancing the redox tolerance of anode supported solid oxide fuel cells by microstructural modification. ECS Proceedings Volumes 2005 (2005), p. 1244–1256.

[67] Robert, G.; Kaiser, A.; Honegger, K.; Batawi, E.: Anode supported solide oxide fuel cells with a thick anode substrate. In Proceedings of 5th European Solid Oxide Fuel Cell Forum, p. 116. EFCF: Lucerne, Switzerland (2002).

[68] Brandenberg, J.: Compression tests with mica gaskets, Forschungszentrum Jülich, "Internal document".

[69] http://grund-wissen.de/physik/elektrizitaet-und-magnetismus/stromstaerke-spannung-widerstand.html (24.04.2017).

[70] Freundt, P.: Systemnahe thermische Charakterisierung eines oxidkeramischen Brennstoffzellen-Stacks für die mobile Anwendung. Dissertation, Universität Stuttgart (2015).

[71] http://www.bosch-mobility-solutions.com/en/highlights/powertrain-and-electrified-mobility/water-injection/ (04.06.2017).

[72] Pausch, M.: "Internal presentation".

Supervised theses

Boch, A.: Entwicklung einer Testvorrichtung für SOFC-Kontaktierungssysteme. Bachelor thesis (2016)